

Radiative sky cooling: Fundamental principles, materials, and applications

Cite as: Appl. Phys. Rev. **6**, 021306 (2019); <https://doi.org/10.1063/1.5087281>

Submitted: 31 December 2018 . Accepted: 05 March 2019 . Published Online: 16 April 2019

Dongliang Zhao , Ablimit Aili, Yao Zhai , Shaoyu Xu, Gang Tan , Xiaobo Yin, and Ronggui Yang 

COLLECTIONS

 This paper was selected as an Editor's Pick



[View Online](#)



[Export Citation](#)



[CrossMark](#)



Applied Physics Reviews
Now accepting original research

2017 Journal
Impact Factor:
12.894



Radiative sky cooling: Fundamental principles, materials, and applications

Cite as: Appl. Phys. Rev. **6**, 021306 (2019); doi: 10.1063/1.5087281

Submitted: 31 December 2018 · Accepted: 5 March 2019 ·

Published Online: 16 April 2019



Dongliang Zhao,^{1,2} Ablimit Aili,¹ Yao Zhai,¹ Shaoyu Xu,³ Gang Tan,⁴ Xiaobo Yin,^{1,5} and Ronggui Yang^{1,5,a)}

AFFILIATIONS

¹Department of Mechanical Engineering, University of Colorado, Boulder, Colorado 80309, USA

²School of Energy and Environment, Southeast University, Nanjing 210096, China

³Ruiling Institute of Advanced Energy and Environmental Solutions, Ningbo 315000, China

⁴Department of Civil and Architectural Engineering, University of Wyoming, Laramie, Wyoming 82071, USA

⁵Materials Science and Engineering Program, University of Colorado, Boulder, Colorado 80309, USA

^{a)}Author to whom correspondence should be addressed: Ronggui.Yang@colorado.edu

ABSTRACT

Radiative sky cooling cools an object on the earth by emitting thermal infrared radiation to the cold universe through the atmospheric window (8–13 μm). It consumes no electricity and has great potential to be explored for cooling of buildings, vehicles, solar cells, and even thermal power plants. Radiative sky cooling has been explored in the past few decades but limited to nighttime use only. Very recently, owing to the progress in nanophotonics and metamaterials, daytime radiative sky cooling to achieve subambient temperatures under direct sunlight has been experimentally demonstrated. More excitingly, the manufacturing of the daytime radiative sky cooling material by the roll-to-roll process makes large-scale deployment of the technology possible. This work reviews the fundamental principles of radiative sky cooling as well as the recent advances, from both materials and systems point of view. Potential applications in different scenarios are reviewed with special attention to technology viability and benefits. As the energy situation and environmental issues become more and more severe in the 21st century, radiative sky cooling can be explored for energy saving in buildings and vehicles, mitigating the urban heat island effect, resolving water and environmental issues, achieving more efficient power generation, and even fighting against the global warming problem.

Published under license by AIP Publishing. <https://doi.org/10.1063/1.5087281>

TABLE OF CONTENTS

I. INTRODUCTION	1	7. Structure design to enhance radiative sky cooling	13
II. FUNDAMENTALS OF RADIATIVE SKY COOLING..	2	III. RADIATIVE SKY COOLING MATERIALS.....	13
A. Introduction to atmospheric radiation	3	A. Nighttime radiative sky cooling materials	13
B. Absorption of solar irradiation	4	B. Daytime radiative sky cooling materials	14
C. Absorption of atmospheric radiation.....	4	IV. APPLICATIONS OF RADIATIVE SKY COOLING ..	19
1. Characteristics of atmospheric emissivity.....	5	A. Buildings.....	19
2. Prediction of atmospheric emissivity.....	6	1. Passive applications	20
D. Thermal radiation from a solid surface	7	2. Active applications.....	25
E. Characteristics of radiative sky cooling	8	B. Solar cells	27
1. Ideal emissivity curves.....	8	C. Dew water harvesting.....	29
2. Thermal measurement methods and devices..	8	D. Cooling of power plant condensers.....	30
3. Broadband and selective radiative sky cooling surfaces.....	9	E. Other applications.....	31
4. Effect of surface temperature on the net radiative cooling power	10	V. SUMMARY	32
5. Nonradiative heat transfer	11		
6. Subambient temperature reduction vs net cooling power	12		
		I. INTRODUCTION	
		The world-wide energy demand for cooling and air conditioning is increasing dramatically in the 21st century due to the global warming effect, population growth, industrial development, and the	

improvement of living standards in the emerging and developing economies, especially those in hot climates.¹ The current predominant vapor compression-based cooling technologies are facing problems such as massive energy consumption and the global warming effect due to the refrigerants used, e.g., hydrofluorocarbons (HFCs), which in turn causes environmental concerns.^{2,3} In addition, with cooling and refrigeration overwhelmingly produced through thermodynamic cycles by consuming nonrenewable fossil resources, cooling actually makes the earth hotter.⁴ The growing awareness of the energy situation and environmental concerns has led to much more interest in improving the efficiency of existing cooling systems and pursuing new alternative cooling technologies. It is well-known that all forms of matters emit radiation, and according to the Stefan-Boltzmann law, the higher the temperature of an object, the stronger its emissive power. Radiative cooling is a ubiquitous process by which a surface loses heat through thermal radiation. Considering that the earth has a surface temperature at around 300 K, while the cosmic microwave background of the universe has a thermal blackbody radiation spectrum at a temperature of 2.7 K,⁵ the large temperature difference between the earth and the universe can potentially be utilized to cool the earth surface by emitting thermal infrared radiation to the universe through the atmosphere. Unlike conventional cooling technologies that dump waste heat into the surroundings, including the local atmosphere and water bodies on the earth, radiative sky cooling sends excessive heat to the outer space without any energy consumption, making it truly appealing.^{6–12}

The significance of radiative sky cooling has been long recognized due to its “free” nature and the applications of radiative sky cooling can be traced back several centuries ago.^{13,14} However, it was not until the 1960s that this phenomenon was investigated systematically. Research studies on radiative sky cooling can generally be grouped into two categories, promoting the understanding of this phenomenon and applying the technique for real-world applications.¹⁵ The first category investigates the fundamental principles, e.g., emissivity properties of radiative cooling surfaces,^{16,17} spectral radiance of the atmosphere, and the dependence of radiative cooling on the wavelength,^{18–20} incident angle,^{21–23} and geographic locations.^{24–27} The second category focuses on finding new materials with desirable radiative properties and exploring radiative sky cooling for different application scenarios,^{28–33} e.g., cooling of residential and commercial buildings,^{34–39} cooling of solar cells,^{35,40–43} dew harvesting,^{44–48} outdoor personal thermal management,⁴⁹ and supplemental cooling for condensers of air conditioners and power plants.^{50–53} The purpose of this work is to present a comprehensive review on radiative sky cooling, from the fundamental principles to materials development and applications in the terrestrial environment. Recent progresses on daytime radiative sky cooling are highlighted. This work will show that radiative sky cooling provides a potential pathway to approach energy saving, water saving, and more efficient power generation in various real-world applications.

Earlier research studies on radiative sky cooling have been limited to nighttime (i.e., nocturnal) use because even a few percent of solar absorption (solar intensity around 1000 W/m²) during the day could balance out the outgoing radiative cooling power (100–150 W/m² depending on the surface temperature). There has been very active research on nighttime radiative sky cooling materials and devices in the 1970s and 1980s. Cooling of a surface at night to 10–15 °C below ambient in delicate devices has been experimentally demonstrated.^{54,55} However, the intrinsically low-energy-density of radiative sky cooling

prohibits the widespread adoption of this technology. In general, radiative sky cooling can provide on average 40–80 W/m² of net cooling power at night with clear sky conditions,^{36,37,56} which suggests that relatively large surface area is needed in order to deliver a meaningful cooling power, e.g., a few kilowatts (kWs) or larger. The need of a large surface area for radiative sky cooling in building applications is associated with the inevitably high installation and maintenance cost. Smith and Granqvist⁶ mentioned that the radiative sky cooling field has fallen short of its potential by a wide margin since few scientists are active in this technical area and the diverse technological scope is not well understood. To date, the most appealing radiative sky cooling application is high-albedo (i.e., high solar reflection) paints for cool roofs, which requires zero energy input and very limited maintenance but the energy savings can be very attractive.⁵⁷

For several decades, daytime (i.e., diurnal) radiative sky cooling remains to be a grand challenge due to the stringent requirements on materials, which should possess extremely low absorptivity in the high intensive solar spectrum (0.3–2.5 μm), while having high emissivity in other wavelengths, preferably within the atmospheric window (8–13 μm), which is the spectrum range that majority of thermal radiation from the earth’s surface passing through the atmosphere to the universe. The recent demonstration of daytime radiative sky cooling has attracted great interest worldwide and revived the radiative sky cooling research field.^{31,32,58} Achieving subambient temperatures under the sun during the day is not only a significant scientific achievement in materials science, but also a meaningful milestone in engineering applications. The cooling energy harnessed during the day matches well with the cooling load profile because most end-users, e.g., buildings, have their peak cooling load taking place during the day. In addition, with the daytime radiative sky cooling demonstrated, a radiative sky cooling system can be built to run 24 h continuously, which renders even larger energy savings from the system.

In this review article, we begin our discussion by introducing the fundamental physics of radiative sky cooling in Sec. II. In Sec. III, radiative sky cooling materials for both nighttime and daytime are reviewed. Detailed technical constraints and prospects for each research area are discussed. Section IV reviews some exploration for real-world applications, along with the associated challenges.

II. FUNDAMENTALS OF RADIATIVE SKY COOLING

Solar irradiation and emitted infrared radiation from the earth’s surface comprise what is commonly termed environmental radiation.⁵⁹ The interaction of environmental radiation with the earth’s atmosphere maintains the energy balance and determines the temperature of the earth’s surface [see Fig. 1(a)]. The incoming short wavelength (0.3–2.5 μm) solar irradiation can be reflected, absorbed, or scattered by air molecules and clouds in the atmosphere. In addition to solar irradiation, the atmosphere is also irradiated by the earth’s surface, which is the terrestrial emission. Assuming a temperature of 300 K at the earth’s surface, this upward terrestrial radiation is concentrated at wavelengths ranges from 2.5 to 50 μm according to the Planck’s law. Similar to the downward solar irradiation, the upward radiation also experiences absorption and scattering when propagating through the atmosphere. Figure 1(b) is a simplified description of the energy flows at the earth’s surface. For a surface on the ground that is exposed to the atmosphere, the net radiation effect is a combination of

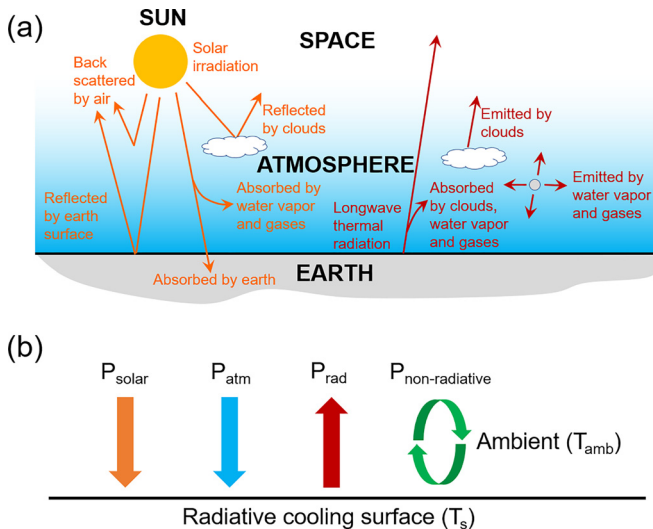


FIG. 1. Fundamentals of radiative sky cooling. (a) On a global scale, the earth gains energy from the sun and radiates the same amount of thermal energy to the universe to maintain its energy balance. (b) Heat transfer processes on a radiative cooling surface. P_{solar} (orange arrow) is the absorbed solar irradiation power on the surface. P_{atm} (light blue arrow) is the absorbed atmospheric radiation power on the surface. P_{rad} (dark red arrow) is the thermal radiation power from the surface. $P_{\text{non-radiative}}$ (green circle arrow) denotes the nonradiative heat transfer (convection and conduction) between the radiative cooling surface and the ambient.

absorption of solar irradiation (during the day) and terrestrial thermal radiation. The net radiative cooling power ($P_{\text{net}}^{\text{rad}}$) can be expressed as

$$P_{\text{net}}^{\text{rad}} = P_{\text{rad}} - P_{\text{atm}} - P_{\text{solar}}, \quad (1)$$

where P_{rad} is the thermal radiation power from the surface. P_{atm} is the absorbed atmospheric radiation power on the surface. P_{solar} is the absorbed solar irradiation power on the surface. These three parameters shown in the right-hand-side of Eq. (1) will be discussed in detail in Secs. II B–II D. Section II A gives an introduction to atmospheric radiation in the wavelength range between 0.3 and 50 μm . Section II B focuses on the short wavelength range between 0.3 μm and 2.5 μm , and how the atmosphere affects the absorption of solar irradiation (P_{solar}) at the ground level. Section II C discusses the absorbed atmospheric radiation in the wavelength range between 3 μm and 50 μm (P_{atm}). Section II D introduces thermal radiation from a solid surface (P_{rad}).

It is important to note that the radiative heat exchange in Fig. 1(b) and Eq. (1) is only between the radiative cooling surface, the atmosphere, and the sun, while neglecting the effect of the surrounding buildings, trees, and the ground. This usually applies to those surfaces that are placed horizontally or with a small tilt angle (e.g., a low-slope roof). For radiative sky cooling applications, the assumption of a horizontal surface toward the atmosphere is generally acceptable. However, in cases where the surface has a large tilt angle or vertically mounted, radiative heat exchange with the surrounding objects should be taken into consideration.^{37,60}

When considering the nonradiative heat transfer processes from the surrounding, such as convection and conduction, the net cooling power (P_{net}) can be expressed as

$$P_{\text{net}} = P_{\text{net}}^{\text{rad}} - P_{\text{non-radiative}}, \quad (2)$$

where $P_{\text{non-radiative}}$ denotes the nonradiative heat transfer, i.e., conduction and convection, between the radiative cooling surface and the ambient, which will be discussed in detail in Sec. II E 5.

A. Introduction to atmospheric radiation

The study of atmospheric radiation (i.e., sky radiation) can be dated back to the early 19th century and is still very active today due to its importance in meteorology,⁶¹ remote sensing,⁶² and climate studies,⁶³ to name a few. Pioneering studies on atmospheric radiation have been performed by researchers including Angstrom,⁶⁴ Brunt,⁶⁵ Bennett,⁶⁶ Goody,⁶⁷ Bell *et al.*,²⁰ Bliss,⁶⁸ Swinbank,⁶⁹ Idso and Jackson,⁷⁰ Brutsaert,⁷¹ and Martin and Berdahl.²³

Under clear sky conditions, the atmospheric radiation is a combined effect from different radiative sources, primarily different gas molecules and aerosol particles. Though the major components of the atmosphere are nitrogen (N_2) and oxygen (O_2), they have much less absorptivity/emissivity in the infrared spectra comparing to the major contributors of atmospheric absorption such as water vapor (H_2O), carbon dioxide (CO_2), and ozone (O_3). Figure 2(a) shows the spectral emissivity of the atmosphere for the wavelengths from 0.3 to 50 μm . It is observed that the atmosphere has a low emissivity in the visible spectra (0.38–0.74 μm), but has several emission bands in the infrared spectra. Figures 2(b), 2(c), and 2(d) show that O_3 emission has a relatively narrow band at a wavelength around 9.6 μm , CO_2 has a broad emission band centered at wavelengths around 15 μm , and water

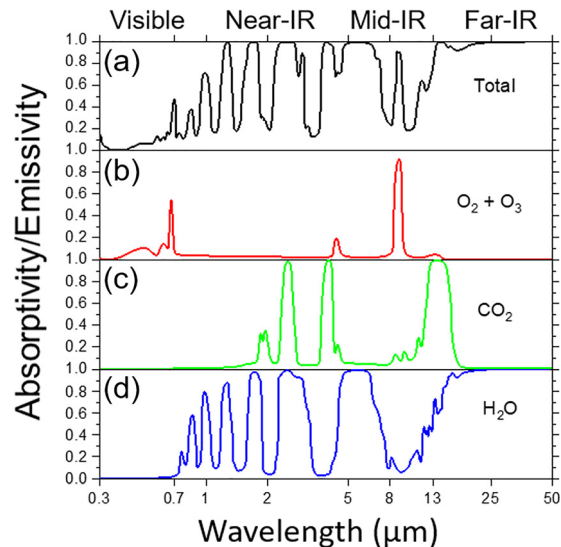


FIG. 2. Emissivity of various gases in the atmosphere at wavelengths ranging from 0.3 μm to 50 μm . (a) Total atmospheric emissivity. (b) Ozone emission has a relatively narrow band at wavelengths around 9.6 μm . (c) Carbon dioxide has three large emissivity bands in the infrared region at about 2.7, 4.3, and 15 μm . (d) Water vapor has several emissivity bands between 0.7 μm and 8 μm wavelengths and for wavelengths larger than 13 μm . Adapted with permission from Cold Facts on Global Warming, <http://www.randombio.com/co2.html> for absorption of ultraviolet, visible, and infrared radiation by various gases in the atmosphere; accessed 7 August 2018. Copyright 2018 American Institute of Physics.⁷² From *Physics of Climate*. Copyright 1992 American Institute of Physics. Adapted with permission from AIP-Press.⁷³

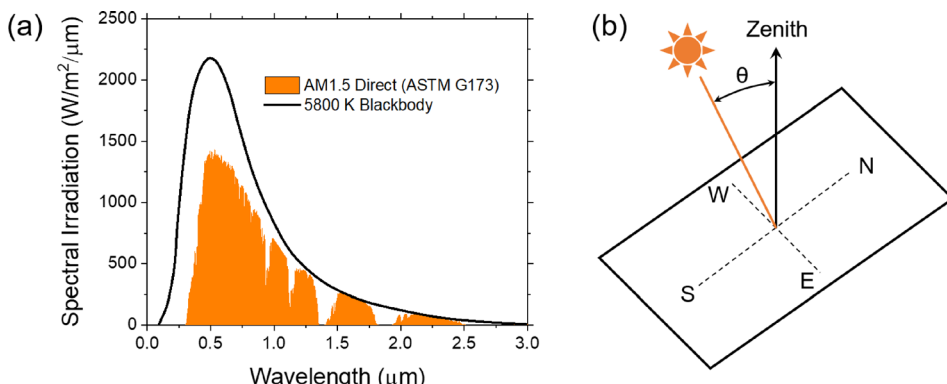


FIG. 3. Absorption of solar irradiance on a horizontal radiative cooling surface. (a) Air mass (AM) 1.5 direct solar spectrum (highlighted in orange) and ⁷⁷ blackbody spectrum at a temperature of 5800 K (solid black curve). After sunlight travels through the atmosphere, sunlight is attenuated due to the scattering and absorption by atmospheric constituents. (b) Illustration of solar absorption on a horizontal surface.

vapor has a strong split band centered at a wavelength of $6.3\text{ }\mu\text{m}$ and has substantial emission at a wavelength greater than $20\text{ }\mu\text{m}$, respectively.⁷⁴ It is estimated that the percentage contribution to the greenhouse effect from water vapor and clouds, CO_2 , CH_4 , and O_3 are 36%–72%, 9%–26%, 4%–9%, and 3%–7%, respectively.⁷⁵ The absorptivity of the atmosphere in the wavelength range between $0.3\text{ }\mu\text{m}$ and $2.5\text{ }\mu\text{m}$ affects the absorption of solar irradiation at the ground level, while the absorptivity of the atmosphere in the wavelength range between $2.5\text{ }\mu\text{m}$ and $50\text{ }\mu\text{m}$ affects ground thermal radiation passing through the atmosphere to the universe.

B. Absorption of solar irradiation

The sun emits approximately as a blackbody with an effective temperature of 5800 K. After sunlight rays travel through the atmosphere, sunlight is attenuated due to the scattering and absorption by atmospheric constituents, aerosols, and clouds. For a specific wavelength, the higher the absorptivity/emissivity of the atmosphere [see Fig. 2(a)], the greater the attenuation of the sunlight. In addition, the more atmosphere through which the sunlight passes, the greater the attenuation. The air mass (AM) coefficient⁷⁶ can be used to characterize the solar spectrum after the sunlight has traveled through the atmosphere, which is defined as the direct optical path length through the atmosphere and expressed as a ratio relative to the path length vertically upward, i.e., the zenith. Figure 3 illustrates the spectral distribution of AM1.5 solar irradiation, which corresponds to a solar zenith angle of 48.2° . It can be observed that the solar irradiation is mostly concentrated in the short wavelength region (0.3 – $2.5\text{ }\mu\text{m}$) with the peak occurring at approximately $0.5\text{ }\mu\text{m}$ in the visible range.

The absorbed solar power is given by

$$P_{\text{solar}} = \cos \theta \int \varepsilon_s(\theta, \lambda) I_{\text{solar}}(\lambda) d\lambda, \quad (3)$$

where θ is the angle between the incident direction of solar irradiation and the normal direction of the surface, $\varepsilon_s(\theta, \lambda)$ is the emissivity of the surface as a function of direction and wavelength, and $I_{\text{solar}}(\lambda)$ is the direct spectral solar irradiance.

For a long time, absorption of solar irradiation was not a concern in radiative sky cooling applications because they have been focused on nighttime use only. However, for application of radiative sky cooling during daytime under direct sunlight, solar absorption on a surface must be considered. Fortunately, the solar irradiation has been extremely well studied. Figure 3(a) shows that the wavelength of solar

irradiation has a very small overlap with blackbody radiation at 300 K (black curve in Fig. 4). It is thus possible to develop a spectrally-selective surface that possess low emissivity close to zero (highly reflective) in the solar spectrum, while maintaining high emissivity in the infrared region for daytime radiative sky cooling.

C. Absorption of atmospheric radiation

For radiative sky cooling applications, one usually has particular interest in the atmospheric emissivity (or transmittance) in the mid- and far-infrared regions (3 – $50\text{ }\mu\text{m}$ wavelength) because this is the emission spectrum of a blackbody at around 300 K (close to the ground temperature), as shown in Fig. 4. Also shown in Fig. 4 is the clear sky atmospheric transmittance in the mid- and far-infrared regions. The combined effects from all atmospheric components result in a minimum atmospheric radiation wavelength interval between $8\text{ }\mu\text{m}$ and $13\text{ }\mu\text{m}$, i.e., the “atmospheric window.” Most of the terrestrial thermal radiation that can propagate through the atmosphere is in this wavelength range, where the atmosphere is highly transparent. Interestingly, the spectrum of the

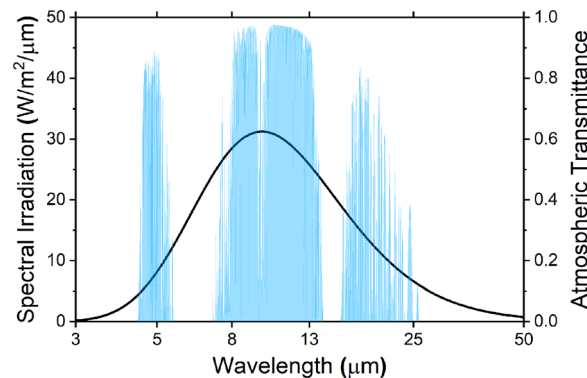


FIG. 4. The spectrum of a blackbody surface with a temperature of 300 K (solid black curve) and the atmospheric transmittance in the mid- and far-infrared regions (highlighted in blue). The wavelength range between $8\text{ }\mu\text{m}$ and $13\text{ }\mu\text{m}$ is usually termed as the atmospheric window due to the high transmittance. Coincidentally, the spectrum of atmospheric window matches well with the blackbody radiation curve from an object that has a temperature at around 300 K . For a clear sky with a low humidity level, the net radiative cooling power given by Eq. (1) could be as high as 140 W/m^2 at ambient temperature (300 K).⁷² In addition, there exists a secondary atmospheric transmission window between $16\text{ }\mu\text{m}$ and $25\text{ }\mu\text{m}$.⁷³ The presence of the secondary transmission window has the potential to generate an extra of 10 – 20 W/m^2 radiative cooling power.⁷⁹

atmospheric window coincides with the wavelength range of thermal radiation from terrestrial objects. This indeed tells well how the earth keeps its surface temperature relatively stable throughout the year. It absorbs the sunlight but releases the thermal energy to the universe mostly by thermal radiation through the atmospheric window.

The absorption of atmospheric radiation on a horizontal surface facing toward the sky comes primarily from those wavelengths outside of the atmospheric window. According to the Kirchhoff's law of thermal radiation,⁵⁹ under thermal equilibrium the emissivity value at a given wavelength and in a given direction equals to the absorptivity value in the same wavelength and direction, that is $\varepsilon_s(\lambda, \theta) = \alpha_s(\lambda, \theta)$. The total absorbed atmospheric radiation on a ground-level radiative cooling surface can be expressed as

$$P_{atm}(T_{amb}) = \int \cos \theta d\Omega \int_0^\infty I_{bb}(\lambda, T_{amb}) \varepsilon_s(\Omega, \lambda) \varepsilon_{atm}(\Omega, \lambda) d\lambda, \quad (4)$$

where $\int d\Omega = \int_0^{\pi/2} d\theta \sin \theta \int_0^{2\pi} d\phi$ is the angular integral over a hemisphere, $\varepsilon_{atm}(\Omega, \lambda)$ is the emissivity of atmosphere as a function of direction and wavelength, which is the ratio of the actual atmospheric radiation to the corresponding blackbody radiance at a certain angle and wavelength. $I_{bb}(\lambda, T_{amb})$ is the blackbody spectral radiance for a temperature T_{amb} , which can be further expressed as $\frac{2hc^2}{\lambda^5} [\exp(hc/\lambda kT_{amb}) - 1]$ according to Planck's law, where $h = 6.626 \times 10^{-34}$ J s and $k = 1.381 \times 10^{-23}$ J/K are the universal Planck and Boltzmann constants, respectively, $c = 2.998 \times 10^8$ m/s is the speed of light in vacuum, and λ is the wavelength. T_{amb} is the absolute air temperature near the ground. It is important to note that most of the atmospheric thermal radiation comes from the lowest few hundred meters of the atmosphere for those wavelengths where water vapor and carbon dioxide are strongly absorbing.⁵⁴ Therefore, T_{amb} is usually used to characterize atmospheric radiation, which is a common practice in estimating downward (toward the ground) atmospheric radiation power.^{31,52}

1. Characteristics of atmospheric emissivity

It is rather clear that atmospheric emissivity has spectral dependence as depicted in Fig. 2. Atmospheric emissivity is also dependent

on several other factors such as the zenith angle,^{80,81} air humidity,⁸² cloud cover,⁸³ aerosol,⁸⁴ latitude,⁸⁵ day-night effect,^{86,87} and seasonal effect.^{61,88} Here, we focus on introducing the dependence of atmospheric emissivity on the zenith angle and air humidity, which are the two most important factors. Figure 5(a) shows the atmospheric emissivity at three different zenith angles (0° , 60° , and 75°) in the wavelength range between $5 \mu\text{m}$ and $25 \mu\text{m}$. Essentially, higher emissivity can be expected at larger zenith angles. A few earlier researchers have worked on expressing atmospheric emissivity as a function of zenith angle.^{22,23,74} For example, if atmospheric emissivity in the zenith angle $\varepsilon_{atm}(0, \lambda)$ is known, atmospheric emissivity in other angles can be deduced by using a "box model,"⁵⁴ which is given by $\varepsilon_{atm}(\theta, \lambda) = 1 - (1 - \varepsilon_{atm}(0, \lambda))^{1/\cos \theta}$. Figure 5(b) shows the spectral emissivity as a function of the zenith angle and effective atmospheric emissivity (from 0.57 to 0.93). The emissivity values are not sensitive to zenith angle when zenith angles are small, and the emissivity values become unity (close to 1) when zenith angles are large.

The level of water content in the atmosphere also greatly influences atmospheric emissivity in the atmospheric window ($8\text{--}13 \mu\text{m}$). Grant⁹⁰ presented a critical review on the water vapor absorption coefficient in the $8\text{--}13 \mu\text{m}$ spectral region. Usually, the level of water content in the atmosphere is characterized as "precipitable water (PW, unit: millimeter or centimeter)," which is defined as the depth of water in a column assuming that all the water in that column is precipitated as rain.⁹¹ Figure 6(a) shows the atmospheric emissivity under three different precipitable water levels, 1.5 cm, 3 cm, and 6 cm, respectively. Figure 6(b) gives the relationship between precipitable water and relative humidity at various ambient temperatures. It can be found that atmospheric emissivity increases with the precipitable water, and the presence of water vapor reduces the radiative cooling power.⁹² By using a similar setup as Raman *et al.*,³¹ who has obtained 40.1 W/m^2 daytime radiative cooling power at Stanford, California, Tso *et al.*⁹³ conducted a field test in Hong Kong and showed that radiative sky cooling does not perform as well under a humid and cloudy climate. The researchers found that the maximum nighttime cooling power was only 38 W/m^2 with a clear sky and did not observe any daytime cooling effect. Suichi *et al.*⁹⁴ conducted tests in Okayama, Japan

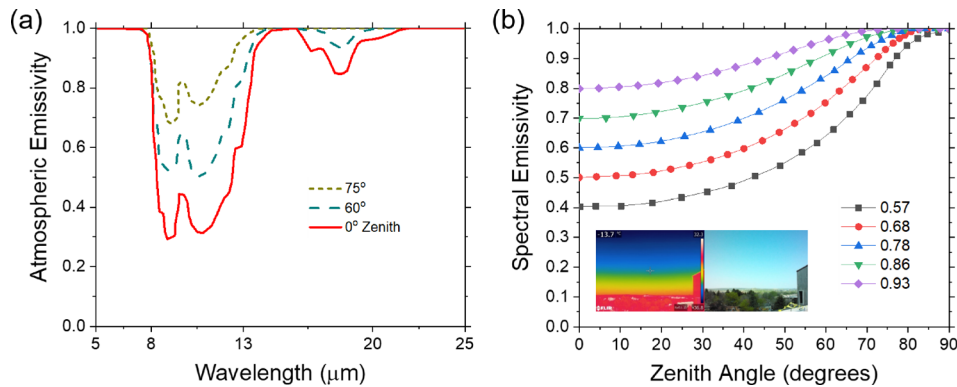


FIG. 5. Angular dependence of atmospheric emissivity. (a) The atmosphere gradually becomes more emissive as the zenith angle increases from 0° to 75° .⁵⁴ Adapted with permission from J. Appl. Phys. **52**, 4205 (1981). Copyright 1981 American Institute of Physics. (b) The spectral emissivity as a function of the zenith angle and total emissivity (from 0.57 to 0.93).⁸¹ Adapted with permission from X. Berger and J. Bathiebo, Renewable Energy **28**, 1925–1933 (2003). Copyright 2003 Elsevier. The insets show an infrared image and an optical image that depict large spectral emissivity change at large zenith angles, which provide some insights into the angular dependence of radiative effects. The images were taken at the rooftop of Engineering Center, University of Colorado Boulder, USA.

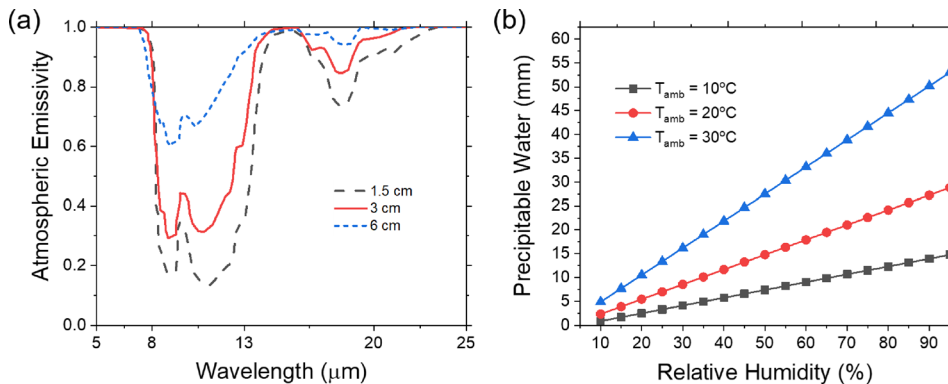


FIG. 6. The dependence of atmospheric emissivity on humidity. (a) The atmosphere becomes more emissive as the precipitable water vapor content increases from 1.5 cm to 6 cm.⁵⁴ The red solid curve corresponds to the red solid curve in Fig. 5(a). Adapted with permission from J. Appl. Phys. **52**, 4205 (1981). Copyright 1981 American Institute of Physics. (b) Precipitable water as a function of relative humidity at various ambient temperatures. Results calculated using equations from Ref. 89.

(warm and humid) by using alternating layers of SiO_2 and poly(methyl methacrylate) on an aluminum mirror. It was shown that the device is 2.8 °C higher than the ambient temperature of 35 °C during the day. With water vapor being the most important source of infrared absorption, the atmospheric emissivity depends strongly on the geographic location and climate conditions.

2. Prediction of atmospheric emissivity

Spectral atmospheric emissivity [$\varepsilon_{atm}(\lambda, \theta)$] is very complicated due to the different constituents of the atmosphere, along with the varying weather and climate conditions. Atmospheric emissivity for a particular location can be obtained either from direct radiance measurements by using a spectral radiometer,^{18,22,95,96} or more commonly, can be obtained by modeling methods based on ground-level meteorological data.^{19,27,97,98} Under clear sky conditions, the atmospheric spectral transmittance [$1 - \varepsilon_{atm}(\lambda, \theta)$] can be calculated using several computational tools such as LOWTRAN (LOWTRAN 1–3,^{99–101} LOWTRAN 4,^{19,102} LOWTRAN 5,^{103,104} LOWTRAN 6,^{85,105} LOWTRAN 7,^{106,107}), MODTRAN,^{108,109} and ATRAN.^{110,111} Note that both MODTRAN and ATRAN were developed and improved based on LOWTRAN.

In practice, a lumped “effective atmospheric emissivity”^{61,112} ($\bar{\varepsilon}_{atm}$, sometimes also named as sky emissivity,^{95,113,114} global sky emissivity,²² total atmosphere emissivity,⁸¹ total sky emissivity,¹⁰⁵ integrated sky emissivity,¹¹⁵ or average atmosphere emissivity⁵⁵) concept is usually defined based on the absolute air temperature near the ground, which assumes a continuous spectrum disregarding the actual spectral distribution of the outgoing and incoming radiation

$$\bar{\varepsilon}_{atm} = \frac{\int \cos \theta d\Omega \int_0^\infty I_{bb}(\lambda, T_{amb}) \varepsilon_s(\Omega, \lambda) \varepsilon_{atm}(\Omega, \lambda) d\lambda}{A \sigma T_{amb}^4}, \quad (5)$$

when expressed in terms of a lumped effective atmospheric emissivity [defined in Eq. (5)], which is usually described by a linear or quadratic equation as a function of dew point temperature and/or ambient temperature,^{65,116} the effective atmospheric emissivity value can be used to describe the full spectrum, or a particular spectrum range of interest, for example, 8–13 μm ($\bar{\varepsilon}_{atm, 8–13 \mu\text{m}}$).¹¹⁷ A list of these correlations can be found in earlier review papers.^{34,118–122} However, when using these simple correlations, one has to carefully consider their validity conditions. For example, some of the equations are developed for specific conditions such as arid regions, at sea level, clear sky, or specific

wavelength range, while others may consider one or more of the following conditions such as day-night effect,²² seasonal effect,⁸⁸ and water vapor pressure,^{27,106} as summarized in Table I. In general, effective atmospheric emissivity values are sufficient to be used to calculate radiative cooling power in most scenarios. However, it is important to note that when using the effective atmospheric emissivity ($\bar{\varepsilon}_{atm}$) and effective emissivity of a radiative cooling surface ($\bar{\varepsilon}_s$) to calculate the absorbed atmospheric radiation on the surface, that is $P_{atm} = \bar{\varepsilon}_s \bar{\varepsilon}_{atm} \sigma T_{amb}^4$, the $\bar{\varepsilon}_{atm}$ could be ill-defined in some cases. The reason is that even if two surfaces have the same lumped emissivity but different spectral emissivity characteristics, they might not absorb the same amount of the atmospheric radiation. In these cases, spectral-dependent atmospheric emissivity is preferred.

The above discussion only considers clear sky conditions (though humidity level can be different). Yet, the sky could be covered by clouds for a significant amount of time during the day and throughout the year. Therefore, the effect of clouds on downward atmospheric radiation has also been investigated extensively.^{129–133} Unfortunately, the effect of cloud cover has very complicated impacts on the atmospheric radiation due to the different types of clouds (e.g., cirrus, stratus), different altitude of clouds, different thickness of clouds, different constitution of clouds, different droplet size distribution, different observation angle from the radiative cooling surface, and the constantly changing of cloud behaviors over time and space.^{129,134,135} Since the major composition of clouds is condensate water droplets and ice crystals that have an average emissivity of 0.92–0.98,^{51,136} the emissivity of thick clouds may be considered as 1 over the whole infrared spectrum, including the atmospheric window.¹³⁵

Experimental results show that the decrease in radiative cooling power could be proportional to the increase in cloud cover fraction, compared to clear sky, as shown in Fig. 7. However, the experiments shown in Fig. 7 only presents the effect of cloud cover fraction, while neglecting other factors such as cloud height, cloud thickness, and observation angle from the radiative cooling surface. This is the reason why net radiative cooling powers have a minor difference between cases “few” and “clear” in Fig. 7(a). A more quantitative study on the effect of cloud is still in the need. Usually, a sky clearness index (i.e., cloud cover fraction) can be obtained from meteorological data.^{137,138} Then, for a cloud cover fraction of f , the power of absorbed atmospheric radiation may be calculated as the sum of two terms respectively associated with clear and cloudy skies

TABLE I. List of correlations that predict the effective atmospheric emissivity. T_{dp} is the dewpoint temperature (Kelvin); T_{amb} is the ambient temperature (Kelvin); \bar{p}_{pw} is the partial water pressure (millibar); Z is altitude (meter); P_{atm} is atmospheric pressure (hectopascal); RH is relative humidity (percentage); clf is cloud fraction; and PW is precipitable water (millimeter).

Correlation	Validity conditions	Year	Sky	Reference
$\varepsilon_{sky} = a + b \bar{p}_{pw}^{0.5}$	Zenith angle dependent	1932	Clear	Brunt ⁶⁵
$\varepsilon_{sky} = 0.67 \bar{p}_{pw}^{0.08}$	$0.2 < \bar{p}_{pw} < 20 \text{ mb}$	1972	Clear	Staley and Jurica ¹¹²
$\varepsilon_{sky} = 0.1 + 3.53 \times 10^{-8} \bar{p}_{pw}^2 \exp(3000/T_{amb})$	$10.5\text{--}12.5 \mu\text{m}$	1981	Clear	Idso ¹¹⁷
$\varepsilon_{sky} = 0.24 + 2.98 \times 10^{-8} \bar{p}_{pw}^2 \exp(3000/T_{amb})$	$8\text{--}14 \mu\text{m}$	1981	Clear	Idso ¹¹⁷
$\varepsilon_{sky} = 0.601 + 5.95 \times 10^{-8} \bar{p}_{pw}^2 \exp(1500/T_{amb})$	For Antarctic and Arctic	1982	Clear	Andreas and Ackley ¹²³
$\varepsilon_{sky} = [5.7723 + 0.9555 \times (0.6017)^z] \times T_{amb}^{1.893} RH^{0.0665} \times 10^{-4}$	Nighttime and altitude dependent	1982	Clear	Centeno ¹¹³
$\varepsilon_{sky} = 0.741 + 0.0062(T_{dp} - 273.15)$	Nighttime	1982	Clear	Berdahl and Fromberg ²²
$\varepsilon_{sky} = 0.727 + 0.0060(T_{dp} - 273.15)$	Daytime	1982	Clear	Berdahl and Fromberg ²²
$\varepsilon_{sky} = 0.711 + 0.56(T_{dp}/100) + 0.73(T_{dp}/100)^2 + 0.013\cos(2\pi t/24) + 0.00012(P_{atm} - 1000)$	Nighttime and altitude dependent	1984	Clear	Martin and Berdahl ²⁷
$\varepsilon_{sky} = 0.770 + 0.0038 T_{dp}$	Nighttime	1984	Clear	Berger <i>et al.</i> ¹²⁴
$\varepsilon_{sky} = -\exp\{-1.66[2.32 - 1.875(T_{amb}/273.15) + 0.735(PW/25)^{0.5}]\}$		1998	Clear	Dilley and O'Brien ¹²⁵
$\varepsilon_{sky} = 0.72 + 0.009(\bar{p}_{pw} - 2)$	$\bar{p}_{pw} \geq 2$	2001	Clear	Niemelä <i>et al.</i> ¹²⁶
$\varepsilon_{sky} = 0.72 + 0.076(\bar{p}_{pw} - 2)$	$\bar{p}_{pw} < 2$	2001	Clear	Niemelä <i>et al.</i> ¹²⁶
$\varepsilon_{sky} = 0.754 + 0.0044 T_{dp}$	Nighttime, Negev highlands, Israel	2004	Clear	Tang <i>et al.</i> ¹¹⁴
$\varepsilon_{sky} = 1.18(\bar{p}_{pw}/T_{amb})^{0.143}$	For Andean Altiplano, Bolivia	2007	Clear	Lhomme <i>et al.</i> ¹²⁷
$\varepsilon_{sky} = \varepsilon_{sky,clear} + N[1 - (D/T_{amb})^4 - \varepsilon_{sky,clear}]$	Altitude dependent, D is a constant related to altitude	1982	Cloudy	Centeno ¹¹³
$\varepsilon_{sky} = \varepsilon_{sky,clear} + C[1 - \varepsilon_{sky,clear}]$	where C is a constant related to cloud fraction	1984	Cloudy	Martin and Berdahl ²⁷
$\varepsilon_{sky} = clf + (1 - clf)\varepsilon_{sky,clear}$		1999	Cloudy	Crawford and Duchon ⁶¹
$\varepsilon_{sky} = 1.18 \left[-0.34 \left(\frac{P_{solar, real}}{P_{solar, cloud}} \right) + 1.37 \right]$	For Andean Altiplano, Bolivia	2007	Cloudy	Lhomme <i>et al.</i> ¹²⁷
$\varepsilon_{sky} = C(\bar{p}_{pw}/T) \left[1.67 - 0.83 \left(\frac{P_{shortwave}}{P_{extra}} \right) \right]$	For Zongo, Bolivia	2010	Cloudy	Sicart <i>et al.</i> ¹²⁸

$$P_{atm} = \int d\Omega \cos \theta \int [(1-f)I_{BB}(T_{amb}, \lambda) \varepsilon_{atm}(\lambda, \Omega) + fI_{BB}(T_{cloud}, \lambda)] \varepsilon_s(\lambda, \Omega) d\lambda, \quad (6)$$

where T_{cloud} is the cloud base temperature.

It is important to note that even for a completely cloudy sky, the atmospheric window is completely opaque and radiative sky cooling is still possible because the cloud base temperature can be lower than the ground temperature. The cooling power in this case is primarily determined by the base height of the cloud. As the height of the cloud base increases, radiative cooling power also increases. If the cloud base height from the ground is known, the cloud base temperature can be estimated using the lapse rate of atmospheric temperature under humid conditions. The lapse rate varies from 2.5°C/km to 7.5°C/km depending on the ground temperature, season, and geographic

location.¹⁴⁰ If the cloud base height is low and the lapse rate at a specific location or during a specific time period is also low, the cloud temperature may be assumed equal to the ambient temperature. In this case, radiative cooling power would be close to zero.

D. Thermal radiation from a solid surface

The total radiative power per unit area (P_{rad}) from a surface is the rate at which radiation is emitted at all possible wavelengths and in all possible directions, as given in the following equation:

$$P_{rad}(T_s) = \int \cos \theta d\Omega \int_0^\infty I_{bb}(\lambda, T_s) \varepsilon_s(\Omega, \lambda) d\lambda, \quad (7)$$

where T_s is the absolute temperature of the radiative cooling surface, Ω is the solid angle between the direction of radiation and normal to

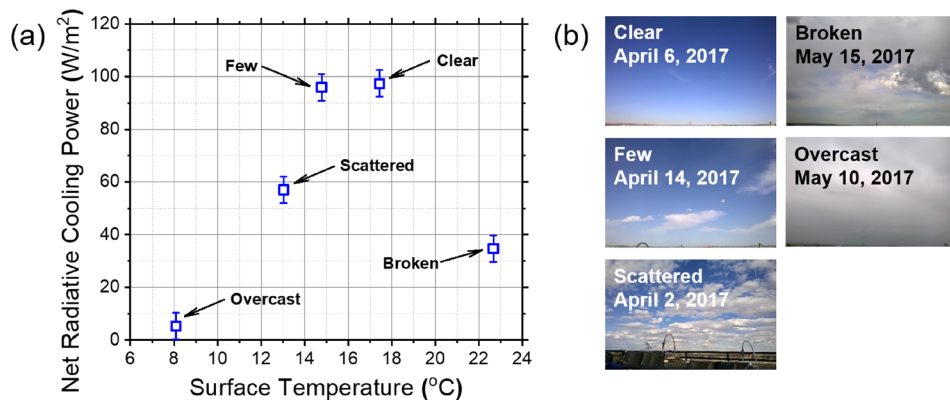


FIG. 7. Measurement of net radiative cooling power on different days with different cloud cover conditions at Boulder, Colorado, USA. (a) The net radiative cooling power at different cloud cover conditions. The cloud conditions are estimated in terms of how many eighths of the sky are covered by the cloud, ranging from 0 (clear sky) to 8 (overcast), which is a common practice in meteorology.¹³⁹ The human observations of the cloud amount are usually reported in five categories: clear (0/8), few (1/8–2/8), scattered (3/8–4/8), broken (5/8–7/8), and overcast (8/8). (b) Pictures show sky conditions during the test days.

the surface [Fig. 8(b)], and $\varepsilon_s(\Omega, \lambda)$ is the emissivity of the surface as a function of wavelength and direction.

The most important parameter in Eq. (7) is the emissivity of the surface $\varepsilon_s(\Omega, \lambda)$, which is usually assumed to be independent of temperature because the variation of surface emissivity in the temperature range of interest for most radiative sky cooling applications is negligible. Thus, it is reasonable to assume that the surface emissivity $\varepsilon_s(\Omega, \lambda)$ has angular and spectral dependence only, as shown in Figs. 8(a) and 8(b). The emissivity for a specific material may have different values at a given wavelength or in a given direction, or in integrated averages over a particular wavelength band and in certain direction. For example, in radiative sky cooling applications, due to the importance of the atmospheric window, particular interest has been paid to the integrated average emissivity in the range $8 < \lambda < 13 \mu\text{m}$ and in the zenith direction. Figure 8(c) shows that a surface has low reflection (i.e., high emission) at a small angle of incidence, and as the angle of incidence approaches 90° , the reflection will become close to unity. For most materials, the emissivities usually remain relatively stable and high for an angle of incidence between 0° and 60° .^{31,141}

Instead of spectral and wavelength dependence emissivity $\varepsilon_s(\Omega, \lambda)$, the total hemispherical emissivity ($\bar{\varepsilon}_s$) is also used, which is defined as the total radiation energy emitted over all wavelengths and in all directions from a surface

$$\bar{\varepsilon}_s = \frac{\int \cos \theta d\Omega \int_0^\infty I_{bb}(\lambda, T_s) \varepsilon_s(\Omega, \lambda) d\lambda}{A \sigma T_s^4}, \quad (8)$$

where σ is the Stefan-Boltzmann constant, $5.67 \times 10^{-8} \text{ W}/(\text{m}^2 \text{ K}^4)$.

Based on the total hemispherical emissivity, Eq. (7) can be rewritten as

$$P_{rad}(T_s) = \bar{\varepsilon}_s A \sigma T_s^4. \quad (9)$$

E. Characteristics of radiative sky cooling

1. Ideal emissivity curves

From what has been discussed above, one can obtain a few ideal surface emissivity curves for radiative sky cooling applications in

different scenarios. Figure 9 shows the ideal emissivity spectrum of radiative sky cooling materials in four different application scenarios: daytime above-ambient, daytime subambient, nighttime above-ambient, and nighttime subambient. Almost all research efforts on radiative sky cooling materials have been devoted to design and synthesize materials with these spectral curves. The wavelength ranges that are of interest are 2.5 – $50 \mu\text{m}$ and 0.3 – $50 \mu\text{m}$ for nighttime and daytime applications, respectively. Subambient applications require emissivity close to unity in the atmospheric window (8 – $13 \mu\text{m}$), and daytime applications require emissivity close to zero in the solar spectrum (0.3 – $2.5 \mu\text{m}$).

2. Thermal measurement methods and devices

While spectroscopic characterization of emissivity, absorptivity, reflectivity, and transmissivity of a material at a specific wavelength is a routine practice in materials sciences (see Sec. III), thermal measurement of a radiative cooling surface is not straightforward. The measurement can be conducted in different ways for different objectives. Figure 10 shows three types of measurement methods with the schematic of their corresponding devices. Figure 10(a) shows a radiative cooling surface that is directly exposed to ambient air. This type of measurement is usually for those applications that need to decrease the temperature of the underlying structure, such as a cool roof (see Sec. IV A).¹⁴³ Typical measurement results from this method are given in Fig. 10(b), where a 2 – 5°C subambient cooling is demonstrated with a glass-polymer hybrid metamaterial³² at noon (11 am–2 pm) under $\sim 800 \text{ W}/\text{m}^2$ solar irradiance. Figure 10(c) shows a measurement device designed for obtaining large subambient temperatures, which is usually employed to demonstrate the effectiveness of a wavelength-selective surface. The convection shield is used to suppress nonradiative heat transfer (conduction and convection loss) between the radiative cooling surface (at subambient temperatures) and ambient. Usually, 10 – 15°C subambient temperatures can be achieved at night with clear sky conditions and low humidity. By using a dedicated vacuum chamber that is shielded from direct sunlight, Chen *et al.*¹⁴⁴ demonstrated an average temperature reduction of 37°C from the ambient through a 24-h day-night cycle, as shown in Fig. 10(d). The

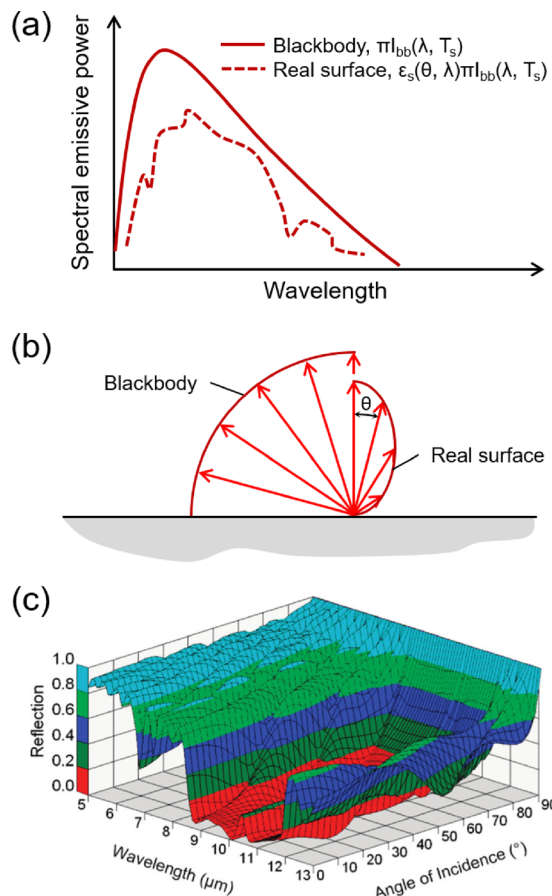


FIG. 8. Fundamentals of thermal radiation from a surface. (a) Spectral distribution of blackbody and real surface emission. (b) Directional distribution of blackbody and real surface emission. (c) An example showing reflectance [$R(\Omega, \lambda) = 1 - \epsilon_s(\Omega, \lambda)$, transmission = 0] of doped polyethylene foil on aluminum as a function of wavelength and angle of incidence.¹⁴² Reproduced with permission from A. R. Gentle and G. B. Smith, *Nano Lett.* **10**, 373–379 (2010). Copyright 2010 American Chemical Society.

devices shown in Figs. 10(a) and 10(c) focuses on demonstrating a temperature difference between the radiative cooling surface and ambient, but with a small thermal mass. In real-world applications, one might be interested in cooling an object with a decent amount of thermal mass. This type of measurement can be conducted using the device shown in Fig. 10(e). By placing the radiative cooling metamaterial surface³² onto a 9-mm-thick water layer, Zhao *et al.*⁵² demonstrated 10.6 °C subambient cooling of water under $\sim 700 \text{ W/m}^2$ solar irradiance, as shown in Fig. 10(f).

3. Broadband and selective radiative sky cooling surfaces

To achieve a large emissive power, a surface should have emissivity close to unity for all wavelengths, i.e., a broadband emitter, and in all directions. However, for a broadband emitter, according to the Kirchhoff's law of thermal radiation,⁵⁹ the spectral absorption equals

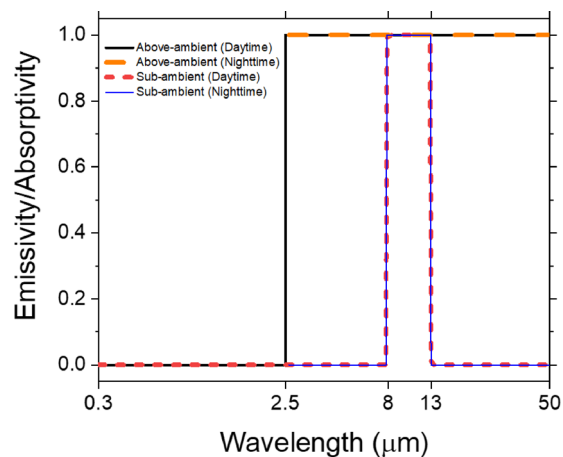


FIG. 9. Ideal emissivity spectrum of radiative sky cooling materials in four different application scenarios, daytime above-ambient (black solid line), daytime subambient (red dashed line), nighttime above-ambient (orange dashed line), and nighttime subambient (blue solid line), respectively.

to the spectral emission at thermodynamic equilibrium. Therefore, for subambient radiative cooling, the radiative cooling surface would also absorb radiation from the surroundings (e.g., ground, buildings, and trees) which are at temperatures much higher than the temperature of atmosphere or the universe. To reduce the incoming radiative flux, radiative cooling surfaces need to be designed to have spectral dependent emissivity (i.e., selective surface), that is, the emissivity at some specific wavelengths is higher than other regions, for example, within the atmospheric window (i.e., 8–13 μm). The effectiveness of a wavelength-selective surface can be defined as⁵⁴

$$\eta = \bar{\epsilon}_{s, 8-13\mu\text{m}} / \bar{\epsilon}_{s, 0-\infty}, \quad (10)$$

where $\bar{\epsilon}_{s, 8-13\mu\text{m}}$ and $\bar{\epsilon}_{s, 0-\infty}$ denote the integral of the emissivity over the atmospheric window and the whole spectrum, respectively.

Since the incoming radiative flux is minimized, a selective surface could achieve a much lower temperature compared to a broadband surface.⁵⁵ Figure 11 shows an example of performance comparison between the broadband and wavelength-selective surfaces. Figure 11(a) shows an ideal broadband surface (emissivity = 1 in the wavelength range between 3 μm and 25 μm), ideal wavelength-selective surface (emissivity = 1 in the wavelength range between 8 μm and 13 μm, and emissivity = 0 elsewhere), real broadband surface, and real wavelength-selective surface, respectively. The real broadband surface is a 0.5-mm-thick polycarbonate sheet, and the real wavelength-selective surface is a 30-μm-thick polyvinylidene fluoride (PVDF) thin film. Figure 11(b) shows the theoretically calculated net cooling power for the 4 surfaces. Clearly, for both ideal and real surfaces, the broadband surfaces have a larger net cooling power when $T_s - T_{amb} > 0$ or $T_{amb} - T_s$ is small, while selective surfaces can achieve a larger subambient temperature drop. The results of theoretical calculation are confirmed by a comparison test between the PVDF thin film and the polycarbonate sheet in Boulder, Colorado, USA, as shown in Fig. 11(c). The two surfaces are controlled to have the same initial temperature. At the beginning, the rate of temperature decrease is faster for the broadband surface, while at the “steady-state,” temperature

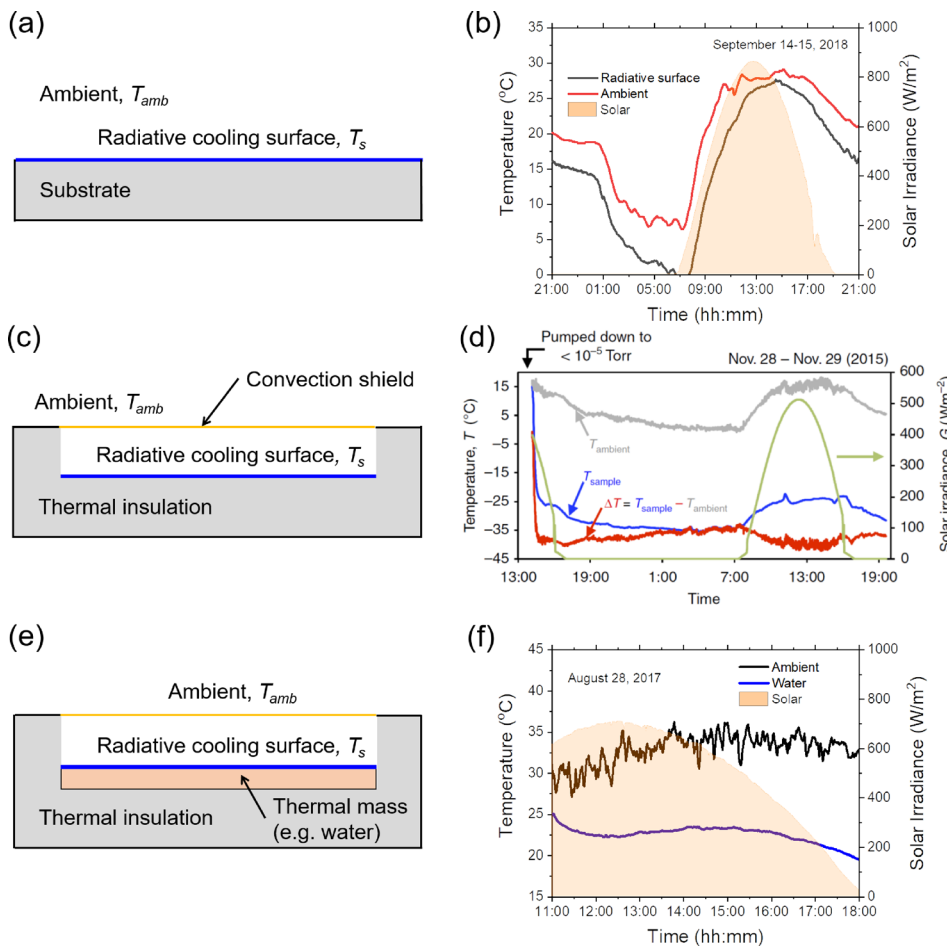


FIG. 10. Schematic drawings of three different thermal measurement devices for radiative sky cooling materials. (a) The radiative cooling surface (solid blue line) is placed on a substrate and directly exposed to the ambient. (b) Results of a typical cool roof measurement conducted at Laramie, Wyoming, USA. The experiment was performed on the roof of a single-space model room ($2.44 \text{ m} \times 1.83 \text{ m} \times 2.44 \text{ m}$, $L \times W \times H$). (c) The radiative cooling surface is placed in a well-insulated enclosure (highlighted in gray). The insulation can be regular polystyrene boards or a dedicated vacuum chamber. A convection shield (solid yellow line) is employed at the top to suppress thermal losses due to convection and conduction heat transfer at subambient conditions. (d) Measurement results obtained using a dedicated vacuum chamber to minimize parasitic heat losses. An average temperature reduction of 37°C from the ambient air temperature is achieved at Stanford, California, USA.¹⁴⁴ (e) Instead of demonstrating a temperature difference between the radiative cooling surface and ambient ($T_{amb} - T_s$), the radiative cooling surface is placed on an object (e.g., water) that has a large thermal mass to generate useful cooling energy. (f) Measurement results obtained from a radiative cooling module ($0.58 \text{ m} \times 0.58 \text{ m}$ surface area) that contains a 9-mm-thick stationary water layer. The measurement was conducted at Boulder, Colorado, USA.

differences $T_{amb} - T_s$ are 16.0°C and 14.7°C for the selective surface and the broadband surface, respectively. The test results clearly confirm that the broadband surface has larger cooling power at temperatures close to the ambient and the selective surface can achieve lower temperature. Figure 11(d) gives the precipitable water and wind speed conditions during the test.

We note here both broadband and selective surfaces are important depending on the applications whether a larger net cooling power or a lower temperature is more favorable. In general, a broadband surface has larger cooling power at temperatures higher than (above-ambient) or close to ambient temperature, e.g., cooling of solar cells, while a selective surface could achieve larger subambient temperature reduction.¹⁴⁵ Granqvist¹⁴⁶ summarized materials for nighttime radiative sky cooling and concluded that for most of the time, a broadband surface works efficiently due to their larger cooling power.

4. Effect of surface temperature on the net radiative cooling power

It is important to understand how the net radiative cooling power changes with the surface temperature. Figure 12 shows the theoretical and experimental results of the net radiative cooling power [given in

Eq. (1)] as a function of surface temperature.⁵² Here, all tests were conducted under the condition that the radiative cooling surface temperature is controlled to be close to the ambient temperature, so the nonradiative heat transfer can be ignored. Essentially, a higher surface temperature gives a higher net radiative cooling power for both day-and night time. This is consistent with the Stefan-Boltzmann's law, the higher the temperature, the larger the emissive power of a surface. At night, when the radiative cooling surface temperature is increased from -1 to 20.5°C , the net radiative cooling power increases from 61.2 to 101.4 W/m^2 . Therefore, over 100 W/m^2 , the net radiative cooling power can be easily expected with a surface temperature higher than 20°C . Daytime experiments were performed at around noon with a direct solar irradiance on the radiative cooling surface between 680 and 730 W/m^2 . When the surface temperature is increased from 10.9 to 31.9°C , the net radiative cooling power increased from 39.7 to 79.0 W/m^2 . For the modeling part, the absorbed solar irradiation power on the surface (P_{solar}), the absorbed atmospheric radiation power on the surface (P_{atm}), and the thermal radiation power from the surface (P_{rad}), are obtained from Eqs. (3), (4), and (7), respectively. These three parameters are then substituted into Eq. (1) to obtain the net radiative cooling power. The calculated net radiative cooling power in Fig. 12 agrees well with the measurement results for both daytime

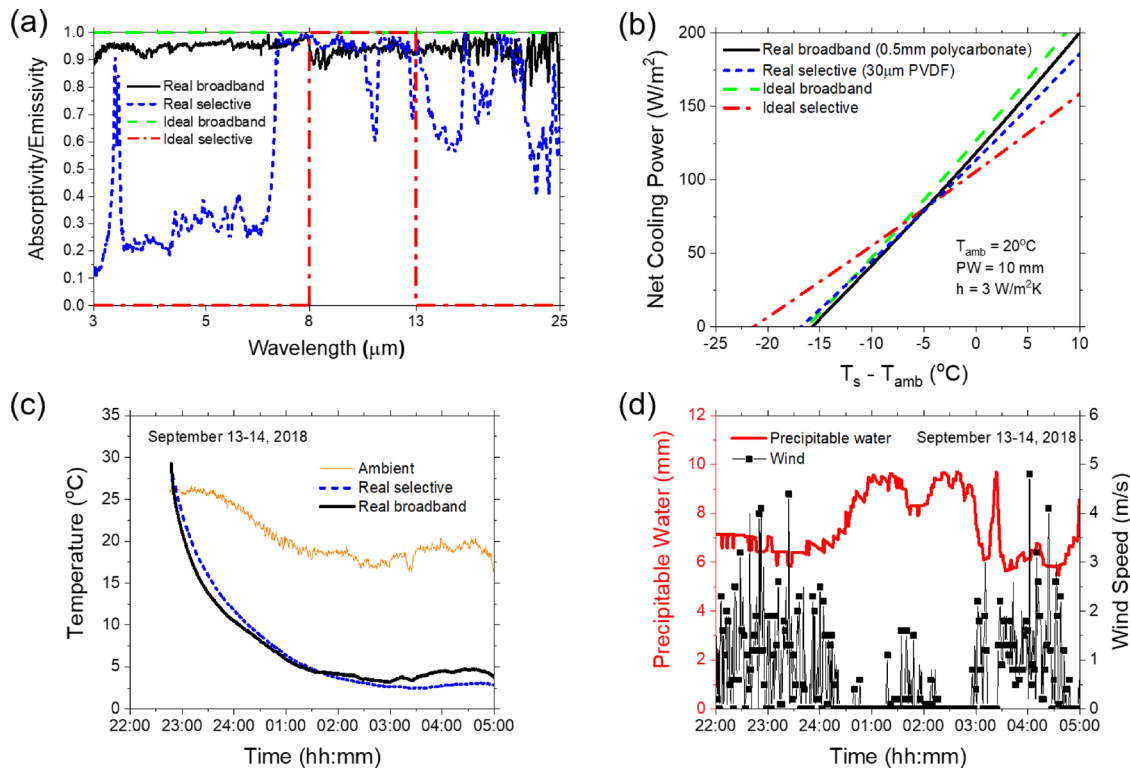


FIG. 11. Broadband blackbody and wavelength-selective radiative cooling surfaces. (a) Emissivity spectrum for ideal broadband, ideal wavelength-selective, real broadband, and real wavelength-selective surfaces. The real broadband surface is a 0.5-mm-thick polycarbonate sheet, and the real wavelength-selective surface is a 30- μm -thick PVDF thin film. (b) Theoretical analysis of the nighttime net cooling power as a function of the temperature difference between radiative cooling surface and ambient ($T_s - T_{\text{amb}}$) for the four types of surfaces. (c) Comparison test of the real broadband and real wavelength-selective surfaces. Temperatures of the two surfaces are plotted as a function of time during September 13–14, 2018, at Boulder, Colorado, USA. The initial temperatures of the two surfaces are controlled to be identical. It is clear that the broadband surface has a larger cooling power when $T_s - T_{\text{amb}}$ is small, but the wavelength-selective surface can reach a lower temperature. The temperature curves are measured using a thermal testing device with the schematic shown in Fig. 10(c). (d) Precipitable water and wind speed conditions for the comparison test.

and nighttime. Therefore, correlations between the net radiative cooling power and surface temperature are developed for daytime and nighttime, respectively: $P_{\text{net}}^{\text{rad}} = 0.0079 \times T_s^2 + 1.27 \times T_s + 31.6$ and $P_{\text{net}}^{\text{rad}} = 0.0079 \times T_s^2 + 1.27 \times T_s + 69.9$ (valid for surface temperatures between -10°C and 40°C).

5. Nonradiative heat transfer

In addition to thermal radiation, the radiative cooling surfaces are also subject to other nonradiative heat transfer processes with the surrounding environment. The nonradiative loss can be lumped together as

$$P_{\text{non-radiative}} = hA(T_{\text{amb}} - T_s), \quad (11)$$

where h is an overall heat transfer coefficient that accounts for convection and conduction heat transfer between the ambient and the radiative cooling surface.

To quantify nonradiative heat transfer, one needs to accurately determine the overall heat transfer coefficient h . Fortunately, wind flow over rectangular plate surfaces such as solar collectors or photovoltaic (PV) panels has been well-studied.^{147,148} However, it is not suggested to directly apply those h values for solar collectors or PV panels in radiative sky cooling applications, especially when the local wind

speed is small (i.e., natural convection dominates). The reason is that solar collectors and PV panels usually have surface temperature much higher than ambient, while radiative cooling surfaces have temperatures close to or lower than the ambient. If without a convection shield, Zhao *et al.*⁵² showed that for a radiative sky cooling device that has a $0.58 \text{ m} \times 0.58 \text{ m}$ surface area, the following equation can be used to quantify the nonradiative thermal loss due to wind:

$$h = 8.3 + 2.5V_{\text{wind}}, \quad (12)$$

where V_{wind} is the zero-incidence wind velocity. This equation is generally valid for local wind speed between 0 m/s and 8 m/s.

In case that there is a convection shield over the radiative cooling surface, the h should be case-specific due to the different convection shield structures and the air gap thickness between the convection shield and the surface. For a radiative sky cooling device ($0.58 \text{ m} \times 0.58 \text{ m}$ surface area) that has a polyethylene (PE) film 1.5-cm above the surface, Zhao *et al.*⁵² suggested the following overall heat transfer coefficient (valid for local wind speed between 0 m/s and 8 m/s):

$$h = 2.5 + 2.0V_{\text{wind}}. \quad (13)$$

The convection and conduction heat transfer can be either beneficial or detrimental to radiative sky cooling, depending on the

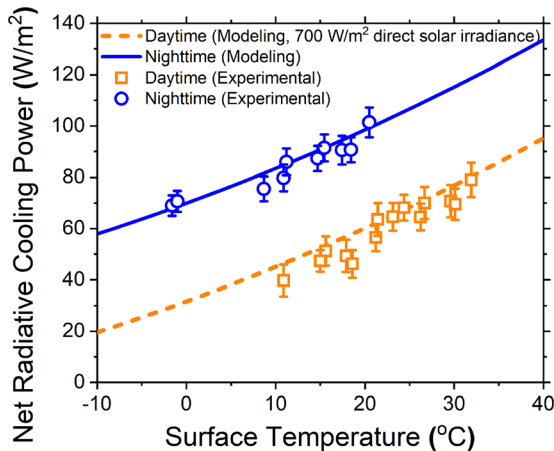


FIG. 12. Net radiative cooling power as a function of surface temperature. All tests were conducted at Boulder, Colorado, under the condition that the surface temperature is close to the ambient temperature to eliminate the nonradiative heat transfer between radiative cooling surface and the ambient. Comparison of experimentally measured net radiative cooling power (dots) to the modeling results (curves) under clear sky conditions, with measured 7.4–10.7 mm precipitable water at night and 12.5–17.0 mm precipitable water during the day. Here, the direct solar irradiance on the surface during the daytime is assumed to be 700 W/m². Reproduced with permission from Zhao *et al.*, Joule 3, 111–123 (2019). Copyright 2018 Elsevier Inc.

operating temperature of a radiative cooling surface (T_s) compared to temperature of ambient (T_{amb}). In general, for above-ambient applications, e.g., cooling of solar cells¹⁴⁹ and supplemental cooling of power plant's condensers,¹⁵⁰ nonradiative heat transfer is beneficial to the cooling process. However, for subambient applications,^{6,51} nonradiative heat transfer must be suppressed.

At subambient operating conditions, the extent of subambient temperature reduction and the cooling power at a certain subambient temperature of the radiative cooling surface is limited by the heat exchange with surrounding warmer air. Figure 13(a) shows that different overall heat transfer coefficients have strong influence on the net cooling power and the lowest achievable temperature. For a typical radiative sky cooling device as shown in Fig. 9(c), the suppression of heat transfer from all sides and the bottom surface are necessary but reasonably straightforward by using highly insulating materials. However, to insulate the top surface that facing the sky where the infrared radiative flux comes out, the covering material (i.e., convection shield) must possess the following characteristics: (1) high transmittance close to unity in the whole infrared region, especially in the atmospheric window (8–13 μ m), (2) high mechanical strength to survive strong winds and even hail, (3) low cost, and (4) long term durability. In some studies,^{151,152} the covering material also needs to have high reflectance in the solar spectrum in order to prevent heating caused by the sun during the day. In these cases, the reflection of solar radiation is done by the covering material, instead of the radiative cooling surface. However, no covering materials have yet been identified with all these desired features, while the best candidate till now is the polyethylene (PE) film that has a thickness usually less than 30 μ m.^{92,115,142,153–155} The PE film is usually installed a few centimeters above the radiative cooling surface as a convection shield where the air is trapped between the PE and the surface to suppress convective and conductive thermal losses.

Figure 13(b) shows the transmittance of PE films at different thicknesses. Clearly, the thinner the PE, the higher the transmittance, which results in a contradictory requirement for the PE film as it has to be thin to be transparent enough in the infrared, and also has to withstand unusual environmental conditions such as wind and hail.¹⁵⁶ Therefore, although almost ideal in terms of infrared transparency, there are concerns in using PE films due to durability and mechanical sustainability.¹⁵⁷ For a relatively large radiative cooling aperture area (in meter scale), a thin PE film will experience up and down movement when the wind blows across the surface, causing the centimeter-thick air layer trapped between the convection shield and the radiative cooling surface to mix and transfer heat through convection. In addition, the PE film can deteriorate under solar ultraviolet (UV) radiation.¹⁵⁸ To make the convection shield resist wind and possible hail, instead of only one layer of PE film, researcher have proposed multiple layers to achieve better performance (double layer,¹⁵⁹ or even triple layers¹⁶⁰).

Researchers have explored several other materials for convection shields. Figure 13(c) shows the transmittance of two other possible candidates in the wavelength range between 5 μ m and 50 μ m, zinc sulfide (ZnS), and zinc selenide (ZnSe).^{144,161} ZnSe has very high transmittance in the atmospheric window, and is mechanically stronger than PE, but much more expensive. The ZnS film is also strong and impervious to damage by solar UV,^{152,162} but infrared transmittance is not as good as PE and ZnSe. Other possible materials include transparent fluorinated ethylene propylene (FEP)¹⁵⁸ and potassium chloride (KCl),⁹³ but KCl transparent is very brittle and can be dissolved in water.⁹³

Usually the convection shield is a planar structure, as shown in Fig. 9(c), but some other structures have also been investigated. Nilsson *et al.*¹⁶³ introduced a design with crossed layers of V-corrugated high-density PE films, as shown in Fig. 13(d). Typical results show that the infrared transmittance over the atmospheric window is up to 0.73 together with a thermal resistance of 1.1 m² K W⁻¹. Golaka and Exell¹⁵⁶ introduced a novel wind shield that can reduce the convection loss through the separation of the main airflow from the radiative cooling surface, as depicted in Fig. 13(e). The simulation results show that the structure can effectively reduce convection loss at wind velocities above 1.5 m/s. Gentle *et al.*¹⁶⁴ introduced a self-supporting PE mesh as a durable infrared transparent convection shield [Fig. 13(f)].

6. Subambient temperature reduction vs net cooling power

With the nonradiative thermal loss significantly suppressed, radiative sky cooling could even achieve cryogenic temperature in deep space,¹⁶⁵ or in a dedicated man-made vacuum (to deep subfreezing temperatures), as shown in Fig. 9(d).¹⁴⁴ In real-world applications, it is the requirement from end-users that determines the target temperature. Radiative sky cooling applications can involve cooling an object to a temperature as low as possible (when $P_{net} = 0$), or continuous cooling at an acceptable net cooling power ($P_{net} > 0$). Figure 14 shows the net cooling power (P_{net}) calculated using Eq. (2) as a function of the targeted subambient temperature reduction at three different ambient temperatures for both daytime and nighttime. Essentially, a larger subambient temperature reduction results in a larger thermal loss to the ambient due to nonradiative heat transfer, and therefore, a smaller net cooling power. At a larger subambient temperature, the

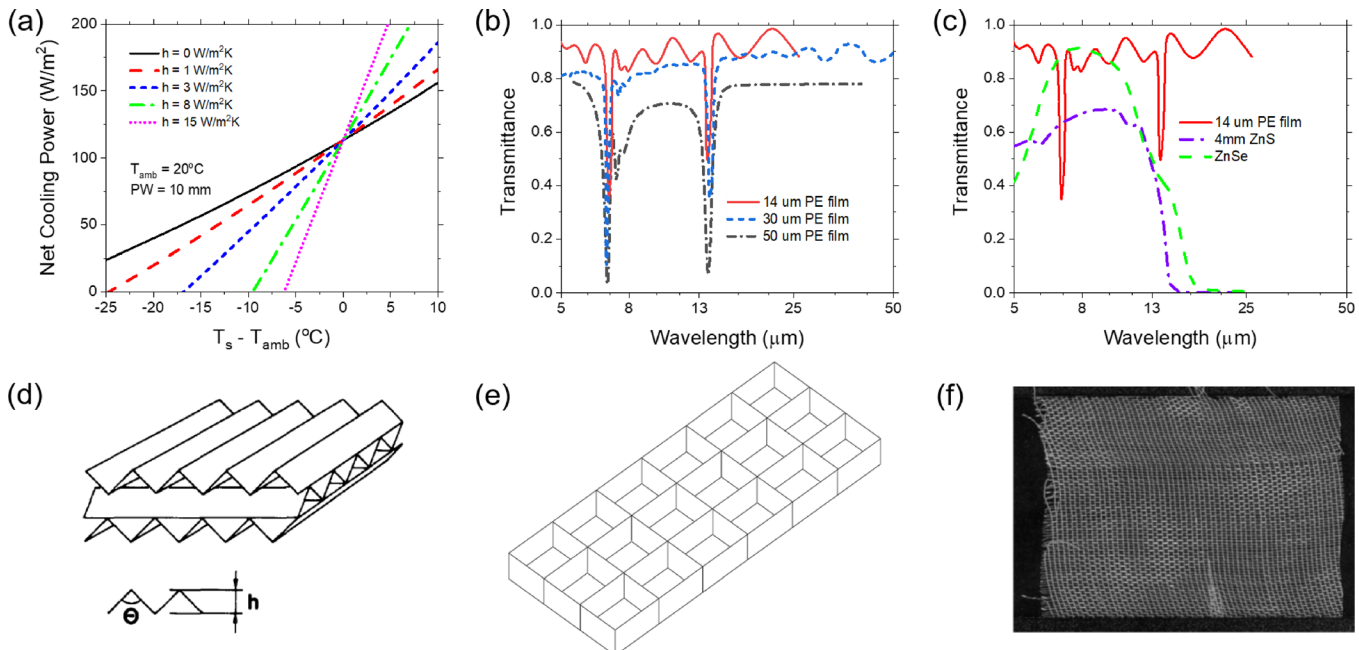


FIG. 13. Convection shield to suppress parasitic thermal losses through convection and conduction to the ambient from a radiative sky cooling device. (a) Net cooling power plotted as a function of subambient temperatures under a variety of overall heat transfer coefficients. The 30- μm -thick PVDF film is employed as a radiative cooling surface. Deep subambient temperature $\geq 25^\circ\text{C}$ can be achieved if h is controlled to be $\leq 1 \text{ W}/(\text{m}^2 \text{ K})$. Results are obtained at ambient temperature 20°C and precipitable water 10 mm. (b) Transmittance of the polyethylene (PE) film with different thicknesses in the wavelength range between 5 μm and 50 μm . Data adapted with permission from J. Appl. Phys. **52**, 4205 (1981). Copyright 1981 American Institute of Physics, Nilsson *et al.*, Sol. Energy Mater. **12**, 327–333 (1985). Copyright 1985 Elsevier, Berdahl *et al.*, Int. J. Heat Mass Transfer **26**(6), 871–880 (1983). Copyright 1983 Pergamon Press Ltd. (c) Transmittance of the PE film, ZnS, and ZnSe in the infrared range. The solid red curve in (b) corresponds to the red solid curve in (c). Data adapted with permission from J. Appl. Phys. **52**, 4205 (1981). Copyright 1981 American Institute of Physics, S. N. Bathgate and S. G. Bosi, Sol. Energy Mater. Sol. Cells **95**, 2778–2785 (2011). Copyright 2011 Elsevier, Chen *et al.*, Nat. Commun. **7**, 13729 (2016). Copyright 2016 The Author(s). (d) A design with crossed layers of V-corrugated high-density polyethylene (HDPE) foils. Reproduced with permission from Nilsson *et al.*, Sol. Energy Mater. **12**, 327–333 (1985). Copyright 1985 Elsevier. (e) A novel wind shield that can reduce the convection loss through the separation of the main airflow from the radiative cooling surface. Reproduced with permission from A. Golaka and R. H. B. Exell, Renewable Energy **32**, 593–608 (2007). Copyright 2006 Elsevier. (f) Image of a UV stabilized high density polyethylene (HDPE) mesh. It has a thread diameter of 0.15 mm and a hole size of approximately 0.8 mm \times 0.4 mm. The HDPE mesh structure is stronger and has a longer life than an impermeable PE film. Reproduced with permission from Gentile *et al.*, Sol. Energy Mater. Sol. Cells **115**, 79–85 (2013). Copyright 2013 Elsevier.

net cooling power drops at a faster rate. On the other hand, a smaller temperature difference might not generate sufficient useful cooling utility for practical applications. There is apparently a need to strategize the operation in radiative cooling systems to balance the net cooling power and the subambient temperature which are dependent on each other.

7. Structure design to enhance radiative sky cooling

As introduced above, both surface emissivity and atmospheric emissivity have angular dependence. For radiative sky cooling, it is more efficient to let thermal radiation take place predominately in those angles that have large surface emissivity and small atmospheric emissivity, e.g., the zenith direction, due to the shortest atmospheric path length.^{30,166} In addition, though the radiative cooling surface usually has the maximum radiation intensity occurs at its normal direction [see Fig. 8(b)], a good radiative cooling surface should have emissivity variation as small as possible from 0° to 90° zenith angles.⁵⁴ The angle dependence of the emissivity can be tuned at both the material level^{167,168} and the device level.¹⁴⁴ Figure 15 shows some structures that can increase radiative sky cooling power by blocking atmospheric

radiation from large zenith angles. Jacobs *et al.*¹⁶⁹ experimentally showed that by changing a radiative cooling surface from a planar structure to inverted pyramid structure, as shown in Fig. 15(b), 20% increase in cooling power is achieved. Chen *et al.*¹⁴⁴ used a highly reflective inverted mirror cone placed on top of the radiative cooling surface to restrict the angular range of the apparatus to around the zenith direction where the sky is most transparent, as shown in Fig. 15(c).

III. RADIATIVE SKY COOLING MATERIALS

In this section, we summarize the daytime and nighttime radiative-cooling materials with an emphasis on the recent progresses on daytime radiative sky cooling materials.

A. Nighttime radiative sky cooling materials

Achieving subambient radiative cooling at nighttime is straightforward. Broadband high emissivity in the infrared range can be easily obtained (orange dashed line in Fig. 9). The majority of research works on nighttime radiative cooling materials have been focused on selective surfaces within the atmospheric window (blue solid line in Fig. 9) to

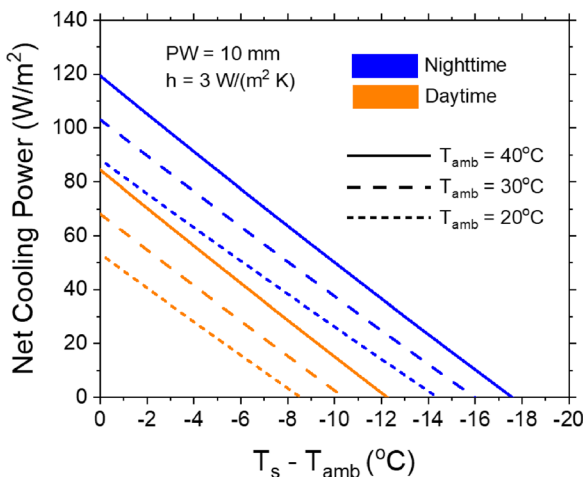


FIG. 14. Modeling results show the net cooling power (P_{net}) calculated using Eq. (2) as a function of the targeted subambient temperature reduction at three different ambient temperatures for both day and night. Nonradiative heat transfer coefficient is kept constant at $3 \text{ W}/(\text{m}^2 \text{ K})$. Precipitable water is 10 mm. Solar irradiance is kept at $700 \text{ W}/\text{m}^2$ for daytime modeling.

achieve larger subambient temperatures. These materials can be generally categorized into the following groups as discussed below: (1) polymer-based materials [polyvinyl chloride (PVC),¹⁷⁰ polymethyl methacrylate (PMMA),¹⁷¹ modified polyphenylenoxid (PPO) resin,³⁷ composite polymer materials¹⁴² and paints based on a polymeric binder with various pigments^{92,172}]; (2) inorganic thin films of coating materials [silicon monoxide (SiO),⁵⁴ silicon dioxide (SiO_2),¹⁷³ silicon oxynitride (SiO_xN_y),^{174–176} SiN ,¹⁷³ white pigmented paints¹⁷²]; (3) gas slab [ammonia (NH_3),⁷⁴ ethylene (C_2H_4),¹⁶⁰ ethylene oxide ($\text{C}_2\text{H}_4\text{O}$),⁹⁷ and mixtures of those].

Polymer-based radiative cooling materials generally consist of a thin layer of polymer and a reflective metal, e.g., aluminum. For example, Catalanotti *et al.*⁵⁵ developed a $12.5\text{-}\mu\text{m}$ -thick polyvinyl-fluoride (PVF) film with aluminum back coating that has strong emissivity within the atmospheric window and high infrared reflectivity out of this region, as shown in Fig. 16(a). This radiative cooler demonstrated 15°C subambient temperature cooling when it was placed in a thermal-insulated box covered with an infrared transparent PE film. Other polymer films, including polymethylpentene (PMP, more commonly called TPX),¹⁷⁷ and polyphenylenoxid (PPO),³⁷ also demonstrated their capability of nighttime cooling.^{170,177} Another type of polymer-based material is composite materials that mix infrared transmitting polymers with nanoparticles (NPs). These nanoparticles usually have narrow absorption bands lying within the atmospheric

window. By adjusting the nanoparticle concentration, the composite material can have absorption spectra lie almost entirely within the atmospheric window. Gentle and Smith¹⁴² developed a composite material that uses amorphous SiC nanoparticles as dopants (20% concentration) into $25\text{ }\mu\text{m}$ thick free-standing polyethylene, as shown in Fig. 16(b). Compared to pure polyethylene film that is highly transparent in the atmospheric window, the sharp spectral tuning by phonon resonant nanoparticles yields much larger absorption in the atmospheric window. Other nanoparticles, such as $\text{Si}_2\text{N}_2\text{O}$,^{178,179} SiO_2 ,¹⁴² as well as other carbon-based nanomaterials,¹⁸⁰ such as nanodiamonds, multiwall carbon nanotubes, and carbon black, have also been used.

Inorganic thin films of silicon-based oxide (SiO), nitride (Si_3N_4), and oxynitride (SiO_xN_y) have been shown to have a high mid-infrared emissivity because Si-O and Si-N bonds are absorptive at $9.5\text{ }\mu\text{m}$ and $11.5\text{ }\mu\text{m}$, respectively.^{54,174,181} In order to improve the emissivity, the SiO film was optimized to be $1\text{-}\mu\text{m}$ -thick to reduce infrared reflection via destructive interference.¹⁶ Bilayer and multiple layer coatings of SiO , Si_3N_4 , and SiO_xN_y feature broadband infrared emissivity compared to a single SiO film.^{173,175} Figure 16(c) shows an example of computed spectral reflectance for a bilayer SiO_2 and $\text{SiO}_{0.25}\text{N}_{1.52}$ on aluminum in the wavelengths between $5\text{ }\mu\text{m}$ and $25\text{ }\mu\text{m}$. Besides the silicon-based thin film, ceramic materials, such as MgO and LiF , also exhibit radiative sky cooling capability when they were backed with an infrared reflective layer.¹⁷ The 1.1-mm -thick MgO film has demonstrated around 20°C subambient cooling temperature during a dry and clear sky night.¹⁷

Spectrally selective infrared emissivity can also be achieved by using a slab of selectively infrared-emitting gas enclosed in an infrared transparent container. Some molecular stretching and rotation modes feature strong infrared absorption within the atmospheric window. For example, the C=C bond has strong light absorption between $10\text{ }\mu\text{m}$ and $12.5\text{ }\mu\text{m}$, C-O and C-N stretching bonds are absorptive from $8\text{ }\mu\text{m}$ to $10\text{ }\mu\text{m}$, deformation vibration of OH group provides IR absorption between $8\text{ }\mu\text{m}$ and $10\text{ }\mu\text{m}$.^{28,97} Granqvist and co-authors studied the possibility of using different confined gas slabs as radiative sky cooling materials, such as NH_3 ,⁷⁴ C_2H_4 ,¹⁶⁰ $\text{C}_2\text{H}_4\text{O}$,⁹⁷ or mixtures of them. With thicknesses of a few centimeters, these gases were reported as good candidates for radiative sky cooling by characterizing their optical transmission spectrum in the mid-infrared region, as shown in Fig. 16(d) for C_2H_4 . Field temperature measurement showed $12\text{--}18^\circ\text{C}$ subambient cooling, and subambient cooling is achieved during the day when the sunlight is shaded.^{28,74,160} The significant advantage to use such gas over a solid radiative cooling surface is that no extra heat transfer fluid is needed to build a cooling device.⁷⁴

B. Daytime radiative sky cooling materials

Compared to nighttime cooling, daytime radiative sky cooling is much more desirable as it matches better with cooling load profile

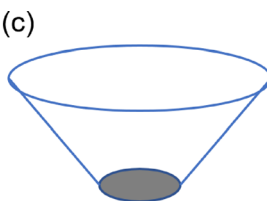
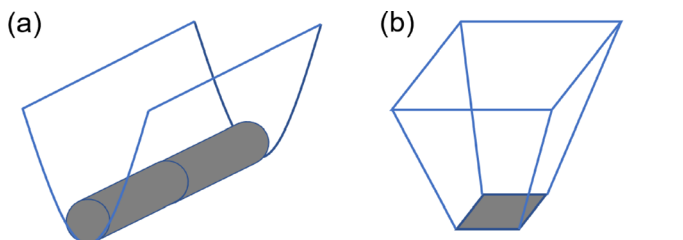


FIG. 15. Structures that can increase radiative sky cooling power by blocking atmospheric radiation from large zenith angles. The bottom areas highlighted in gray are radiative cooling surfaces. The structures that surround the radiative cooling surfaces are highly reflective: (a) parabolic,⁵³ (b) inverted pyramid,¹⁶⁹ and (c) inverted cone structures.¹⁴⁴

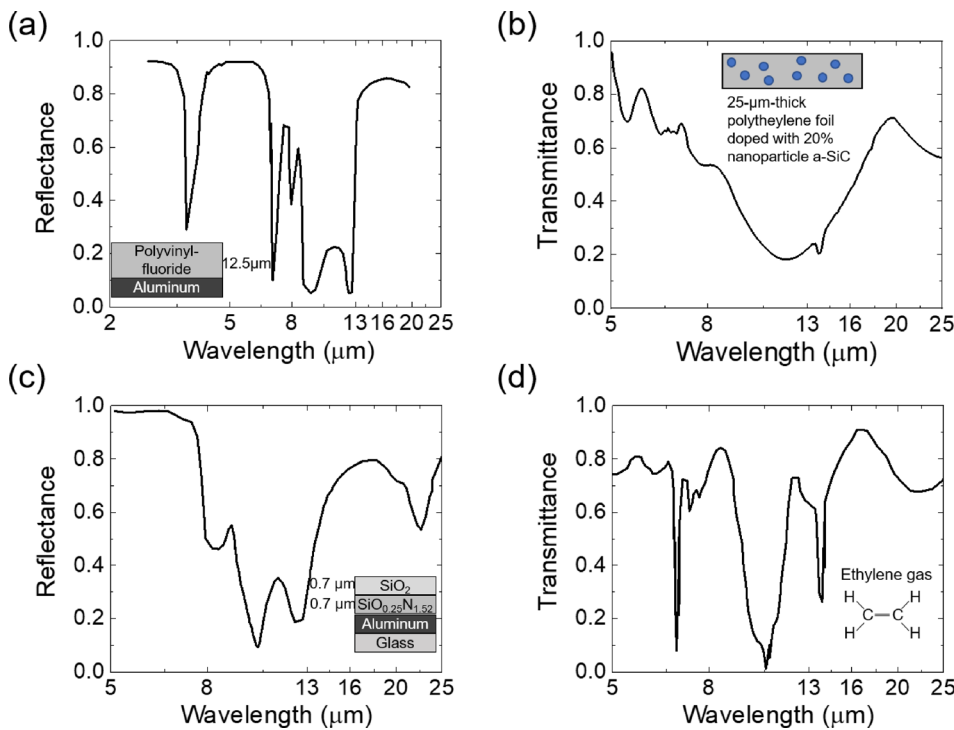


FIG. 16. Infrared transmission/reflection spectrum of some nighttime radiative cooling materials. (a) Metallized polyvinyl-fluoride thin film.⁵⁵ Adapted with permission from Catalanotti *et al.* Solar Energy **17**, 83–89 (1975). Copyright 1975 Pergamon Press. (b) Composite of a polyethylene (PE) thin film with amorphous SiC nanoparticles.¹⁴² Adapted with permission from A. R. Gentle and G. B. Smith, Nano Lett. **10**, 373–379 (2010). Copyright 2010 American Chemical Society. (c) Silicon oxide and nitride film on aluminum. Adapted with permission from Eriksson *et al.*, Sol. Energy Mater. **12**, 319–325 (1985). Copyright 1985 Elsevier. (d) A slab of selectively infrared-emitting ethylene gases.¹⁶⁰ Adapted with permission from Appl. Phys. Lett. **39**(6), 507–509. Copyright 1981 American Institute of Physics.

because most end-users, e.g., buildings, have their peak cooling load during the day. However, for either above-ambient (black solid spectrum line in Fig. 9) or subambient (red dashed spectrum line in Fig. 9) cooling, significant challenge exists to achieve high solar reflectance simultaneously with high emissivity over the atmospheric window. The stringent requirement seems a big challenge in the past few decades,^{152,182,183} with a few attempts in the 1980s and 1990s.^{152,184} The materials being sought after are primarily oxides and carbonates of titanium, aluminum, calcium, and zinc, due to their high reflectivity in the solar spectrum. By testing different pigments, Nilsson and Niklasson¹⁸⁴ found that a ZnS pigmented polyethylene (PE) can achieve a solar reflectance of 0.825,¹⁵² but cannot achieve noon-time radiative sky cooling.¹⁸⁴ Some other researchers also investigated radiative sky cooling during the day. However, the radiative cooling surface was shielded from direct solar radiation, with only diffuse solar radiation falls upon it.^{153,160,185} Since it is not practical to shade the radiative cooling surface from the sunlight in many scenarios, especially for large surfaces. This section focuses on the materials that show a noticeable cooling effect under direct sunlight.

One should not miss the daytime radiative sky cooling effect recently observed in many nature beings. Figure 17 shows reflectivity and absorptivity of some nanostructured biomaterials. Figures 17(a) and 17(b) show that the Saharan silver ant's body are covered by a dense array of hair that is strongly reflective in solar wavelengths between 0.4 μm and 1.7 μm, and emissive in mid-infrared wavelengths between 2.5 μm and 16 μm to maintain a comfortable body temperature in a hot desert.¹⁸⁶ Figure 17(c) shows a Bistonina biston butterfly's scent pad/patch with a unique nanostructure that is very emissive in the mid-infrared (2.5–16 μm) to dissipate heat and has high reflectivity to reduce solar absorption, enabling it to cool the wings.¹⁸⁷ Another

example in nature is the cocoon made by wild silk moths, which is a random structure of fibers, exhibiting high solar reflectivity due to the scattering of light along with high mid-IR emissivity. It can protect moth pupae from overheating under the sun [see Fig. 17(d)].¹⁸⁸ These nanostructured biomaterials could have an inspiration for the development of daytime radiative sky cooling materials.

Nanophotonic structures with structural features at a wavelength or subwavelength scale, can have distinct thermal radiation properties.¹⁸⁹ In 2013, Rephaeli *et al.*⁷⁸ introduced a metal-dielectric nanophotonic structure and predicted theoretically the possibility to achieve daytime radiative sky cooling. The photonic structure is a two-dimensional (2D) periodic pillar array consisting of quartz and SiC as top two layers on a stack of high- and low-index dielectric materials on a silver substrate, as shown in Fig. 18(a). The emissivity is shown to be enhanced across the whole atmospheric window by phonon-polariton resonance from quartz and the SiC layer, with a net cooling power greater than 100 W/m² achievable at ambient temperature under the sun. In 2014, Raman *et al.*³¹ experimentally demonstrated subambient daytime radiative sky cooling with an integrated photonic thermal radiative cooler. This radiative cooler consists of seven layers of silicon dioxide (SiO₂) and hafnium dioxide (HfO₂) with optimized thickness on top of the 200 nm silver (Ag) coated silicon wafer [Fig. 18(b)]. The bottom four layers of SiO₂ and HfO₂ are thinner and primarily responsible for solar reflection, while the top three layers are much thicker and designed for thermal radiation. The structure can reflect 97% of incident sunlight and emitting strongly in the atmospheric window [Figs. 18(c) and 18(d)]. With an apparatus that minimizes nonradiative heat losses on the radiative cooler, a 4.9 °C subambient temperature difference and 40.1 ± 4.1 W/m² cooling power were achieved when the photonic radiator is exposed to direct sunlight exceeding 850 W/m² [Figs. 18(e) and 18(f)].

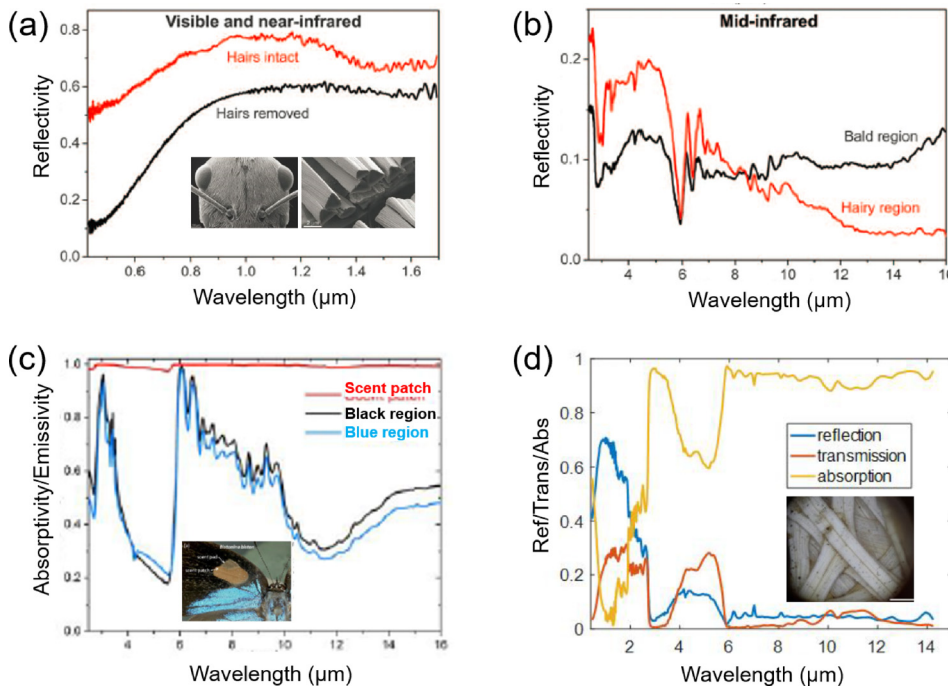


FIG. 17. Daytime radiative sky cooling in nanostructured biomaterials. (a) and (b) The reflectivity spectra of the Saharan silver ant's body surface with and without hair in the visible and near infrared ($0.4\text{--}1.7\,\mu\text{m}$), and mid-infrared region ($2.5\text{--}16\,\mu\text{m}$), respectively.¹⁸⁶ Reflectivity = 1 – Emissivity. Reproduced with permission from Shi *et al.*, Science 349(6245), 298–301. Copyright 2015 The American Association for the Advancement of Science. (c) Infrared absorptivity (emissivity) spectra of scent pad (red), black region (black) and blue region (blue) of Bistonina biston butterfly's wings.¹⁸⁷ Reproduced with permission from Tsai *et al.*, in 2017 Conference on Lasers and Electro-Optics (CLEO) (2017), pp. 1–2. Copyright 2017 Optical Society of America. (d) The hemispherical reflection, transmission and absorption spectra of cocoon shell from $400\,\text{nm}$ to $14\,\mu\text{m}$, showing high solar reflectance and high thermal emittance.¹⁸⁸ Reproduced with permission from Shi *et al.*, in 2017 Conference on Lasers and Electro-Optics (CLEO) (2017), pp. 1–2. Copyright 2017 Optical Society of America.

A few other nanophotonic structures, such as metal-dielectric multilayer conical pillar arrays,¹⁹⁰ metal-loaded dielectric resonator metasurfaces,¹⁹¹ metal-dielectric-metal resonators,¹⁹² multilayer pyramidal nanostructures,¹⁹³ and nanoparticle embedded double-layer coatings¹⁹⁴ have also shown high reflectivity in the solar spectrum and high emissivity over the atmospheric window. Hossain *et al.*¹⁹⁰ introduced a design of a thermal emitter with multilayer conical metamaterial pillar arrays, as shown in Fig. 19(a). Each pillar consists of alternating layers of aluminum and germanium. The thickness of the aluminum layer is 30 nm and the thickness of the germanium layer is 110 nm. Figure 19(b) shows that the structure can achieve very high emissivity within the entire atmospheric window ($8\text{--}13\,\mu\text{m}$) and low emissivity outside the atmospheric window. With a solar reflector that can minimize the total solar power absorption down to 3%, the emitter can possess a radiative cooling power of $116.6\,\text{W/m}^2$ at ambient temperature. Zou *et al.*¹⁹¹ introduced a metal-loaded dielectric resonator metasurface for radiative sky cooling. The designed surface consists of phosphorous-doped n-type silicon and silver, as shown by a false-color scanning electron microscope image in Fig. 19(c). The spectral absorptivity measurement showed a strong absorption/emission band that matches well with the atmospheric window, as shown in Fig. 19(d). This metasurface has the advantage of convenient integration with various silicon-based photonic/electronic platforms. Wu *et al.*¹⁹³ introduced a multilayer all-dielectric micropyramid structure to achieve high mid-infrared selectivity in planar photonic devices, as shown in Fig. 19(e). The optimized structure achieves broadband selective emissivity in the atmospheric window and extremely low absorption in the entire solar spectrum, as shown in Fig. 19(f).

Cost and scalability is always of interest for real-world energy solutions. In 2017, Zhai *et al.*^{32,195,196} reported a ground-breaking approach to make a metamaterial that is scalable and low cost, as

shown in Fig. 20. The “designer metamaterial” consists of a transparent TPX polymer over the solar spectra, encapsulating randomly distributed silicon dioxide (SiO_2) microspheres and backed by a 200-nm-thick silver layer [Fig. 20(a)]. The metamaterial is extremely emissive across the entire atmospheric window ($8\text{--}13\,\mu\text{m}$) due to phonon-enhanced Fröhlich resonances of the embedded microspheres [Fig. 20(b)]. Such a glass-polymer hybrid metamaterial thin film can generate $93\,\text{W/m}^2$ radiative cooling power at noon under direct sunlight, and an average of $110\,\text{W/m}^2$ radiative cooling power for three consecutive days, as shown in Fig. 20(c). The metamaterial can be scalably-manufactured by the mature roll-to-roll extrusion and web coating systems, which makes large-scale application of radiative sky cooling possible [Figs. 20(d) and 20(e)].

The pioneering studies by the Stanford group³¹ and by the Colorado group³² have inspired many researchers and have revived the interest in radiative sky cooling. Table II lists some successful experimental demonstration of daytime subambient radiative sky cooling under direct sunlight. Apparently manufacturing scalability is now an important factor, among which polymers and paints show great advantages.^{58,194,197–202} By coating a commercially available polyester reflector with a 200-nm-thick silver layer [Fig. 21(b)], Gentle and Smith¹⁴³ successfully demonstrated a 2°C subambient cooling under the sun without using a convection shield. The so-called “supercool roof” can be manufactured on a large scale. However, the authors mentioned that refinements are still needed to make the reflectance diffuse to avoid glare. By using a dual-layer structure consisting of a polytetrafluoroethylene (PTFE) sheet on top of a silver film [Fig. 21(c)], Yang *et al.*²⁰³ reported that a record-high solar reflectance (99%) has been achieved from spectrum analysis, as shown in Fig. 21(a).

Paints and coatings can potentially be more cost-effective and applied to almost any surfaces in a relatively easy way. Bao *et al.*²⁰⁴

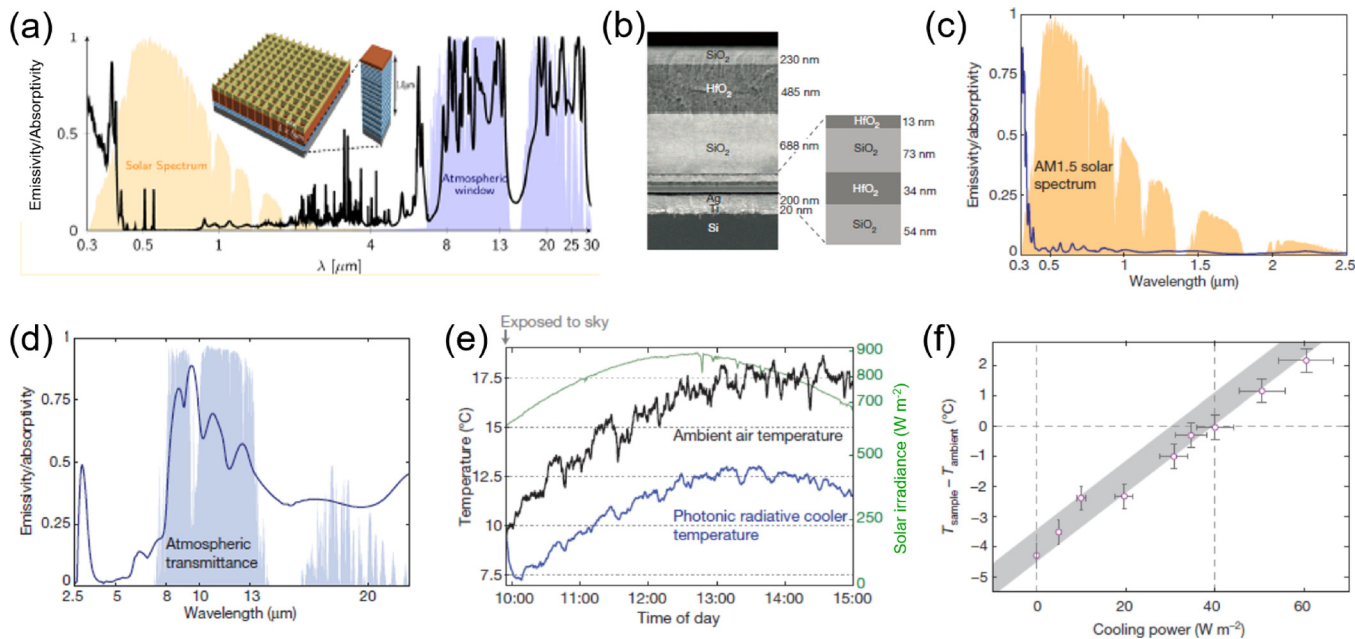


FIG. 18. First experimental demonstration of daytime subambient radiative sky cooling by using a nanophotonic radiative cooler. (a) Absorptivity/emissivity spectra of 2D the periodic pillar array show high solar reflection and infrared emission in the atmospheric window.¹⁸ Reproduced with permission from Rephaeli *et al.*, *Nano Lett.* **13**, 1457–1461 (2013). Copyright 2013 American Chemical Society. (b) The photonic radiative cooler is a multilayer coating structure of SiO_2 and HfO_2 on the Ag coated substrate. (c) Spectral emissivity of the photonic radiative cooler in solar spectra region. (d) Spectral emissivity of the photonic radiative cooler in mid-infrared region. (e) Subambient cooling demonstrated during the day with a maximum temperature difference of 4.9°C. (f) The measured cooling powers at a various of subambient temperatures.³¹ Figures (b)–(f) are reproduced with permission from Raman *et al.*, *Nature* **515**, 540 (2014). Copyright 2014 Macmillan Publishers Limited.

introduced a double-layer nanoparticle-based coatings [Fig. 21(d)], which is composed of a top solar reflection layer and an underlying layer that has high emissivity in the atmospheric window. The material has high selective emissivity in the atmospheric window, but the solar absorption at wavelengths 0.3–0.4 μm is still high, as shown in Fig. 21(a). Atiganyanun *et al.*¹⁹⁹ introduced a paint-format microsphere-based photonic random media. The random media consists of silica microspheres as shown in Fig. 21(e). The size of microspheres and the filling fraction are two important parameters that determine performance. While those two parameters are not optimized, the authors showed that the material outperformed a commercial solar reflective white paint and achieved subambient cooling for most of time during the day. Recently, Mandal *et al.*⁵⁸ introduced hierarchically porous poly(vinylidene fluoride-co-hexafluoropropene) (P(VdF-HFP)_{HP}) coatings for passive daytime radiative sky cooling. The idea is to replace the pigments in the commercial cool-roof paints with light-scattering air voids to eliminate pigments' ultraviolet absorption. A hemispherical solar reflectance of 0.96 ± 0.03 and infrared (7–18 μm) emittances of 0.97 ± 0.02 were reported for this material, along with a subambient temperature reduction of $\sim 6^\circ\text{C}$.

It is important to note that some daytime radiative cooling materials need to be scalably manufactured on an existing substrate, e.g., glass in solar cell cooling application. Lu *et al.*²⁰⁵ introduced ultra-broadband versatile glass textures that exhibit emissivity >0.96 across the atmospheric window and solar transmittance and haze above 0.94 and 0.95 at the wavelengths from 350 to 750 nm, respectively. The authors modified a silica sol-gel imprinting process to transfer the

pyramidal textures from textured crystalline silicon wafers with a desirable feature size (between 1.2 and 2.5 μm) to low iron glass substrates. Figure 22 shows the modified sol-gel imprinting process. A crystalline silicon wafer with a desired feature size was used as an original master template. The original master was used to shape an intermediate PDMS mold, which was later imprinted onto a sol-gel silica layer to replicate the pyramidal textures. By applying the ultrabroadband imprinted glass to silicon PV modules as an encapsulant cover, the short-circuit current and energy conversion efficiency were increased relatively by 5.12% and 3.13%, respectively. The authors claimed that the fabrication of such textures is photolithography-free, scalable, and compatible with the PV industry.

Polymer-based radiative sky cooling metamaterials are likely to be commonly used in the future due to their significant advantage over other nonpolymer nanophotonic materials in terms of manufacturability and cost.²⁰⁶ However, several challenges still remain unsolved with reliability being the most critical one. Maintaining high infrared emissivity in the atmospheric window may not be a challenge. However, maintaining high solar reflectivity turns out to be much more difficult due to the degradation of the polymer itself and the metal solar-reflective layer, e.g., the silver layer in Figs. 21(b) and 21(c). Oxidation of the metal layer by oxygen and moisture permeating from the front and back surfaces causes a major threat to the long-term solar reflectivity. Several approaches can be taken to tackle this problem. For example, increasing the thickness of the emissive polymer layer and/or the metal layer slows and delays oxygen and moisture permeation, while using a barrier polymer, such as polyvinylidene

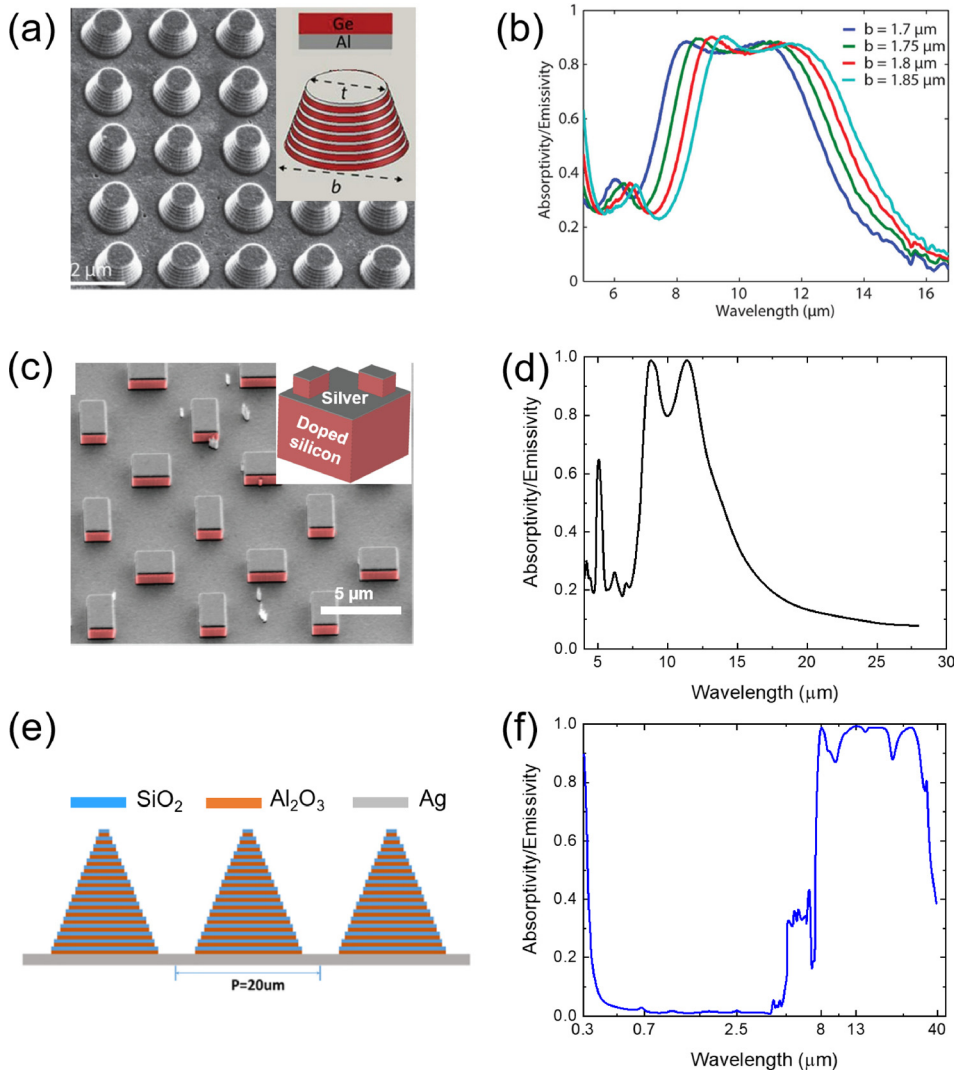


FIG. 19. Nanophotonic structures for daytime radiative sky cooling. (a) Radiative emitter with multilayer conical metamaterial pillar arrays. (b) Absorptivity/emissivity of the multilayer conical metamaterial pillar arrays between 5 μm and 17 μm .¹⁹⁰ Adapted with permission from Hossain *et al.*, *Adv. Opt. Mater.* **3**, 1047–1051 (2015). Copyright 2015 Wiley. (c) Radiative cooler with a metal-loaded dielectric resonator metasurface. (d) Absorptivity/emissivity of the metal-loaded dielectric resonator metasurface.¹⁹¹ Adapted with permission from Zou *et al.*, *Adv. Opt. Mater.* **5**, 1700460 (2017). Copyright 2017 Wiley. (e) Radiative cooling with a multilayer all-dielectric micropyramid structure. (f) Absorptivity/emissivity of the multilayer all-dielectric micropyramid structure.¹⁹³ Adapted with permission from Wu *et al.*, *Mater. Des.* **139**, 104–111 (2018). Copyright 2017 Elsevier.

chloride (PVDC) and polychlorotrifluoroethylene (PCTFE), against water and oxygen, can be another solution. Alternatively, a thin layer of barrier material can be coated onto the polymer and metal layers. It is worth noting that the recent study by Mandal *et al.*⁵⁸ shows that it is possible to achieve high solar reflectivity without backing the polymer layer with a reflective metal layer. Through a phase inversion method, micro- and nanoscale pores are generated in polymers, which strongly scatter and reflect light in all directions. Although this type of radiative sky cooling polymers without the metal layer could be a good alternative to metal-backed radiative sky cooling polymeric metamaterials, the reliability needs to be thoroughly investigated, for example, whether the porous structures are prone to dust and moisture accumulation. Another aspect of long-term reliability is the prevention of the polymer layer from UV and chemical degradation. UV degradation of polymers is a well-known phenomenon. There are polymers such as PET and PTFE that are not easily affected by UV. Anti-UV additives may be added to increase the lifetime.

Integrating functionality with radiative sky cooling materials is also of interest. A great example is the demonstration of self-adaptive/switchable radiative sky cooling based on phase change materials for active temperature control.^{207–209} Since ambient temperature varies during the day and throughout the year, radiative sky cooling may not be needed at night and in the winter season. It is thus desirable to design a switchable radiative cooling material that can adapt itself according to different ambient temperatures. Ono *et al.*²⁰⁷ designed a photonic structure to realize self-adaptive radiative cooling. The structure consists of a spectrally-selective filter (11 layers of Ge/MgF₂) as the top layer and a three-layer VO₂/MgF₂/W structure as the bottom radiative cooler, as shown in Fig. 23(a). When VO₂ experiences phase transition from the insulating to metallic state, absorptivity/emissivity does not have too much change in the solar spectrum as shown in Fig. 23(b), but there is significant change in the mid-infrared wavelength range (8–13 μm) as shown in Fig. 23(c). Another study by Wu *et al.*²⁰⁸ proposed a structure consisting of a VO₂/SO₂ multilayer metasurface for radiative sky cooling

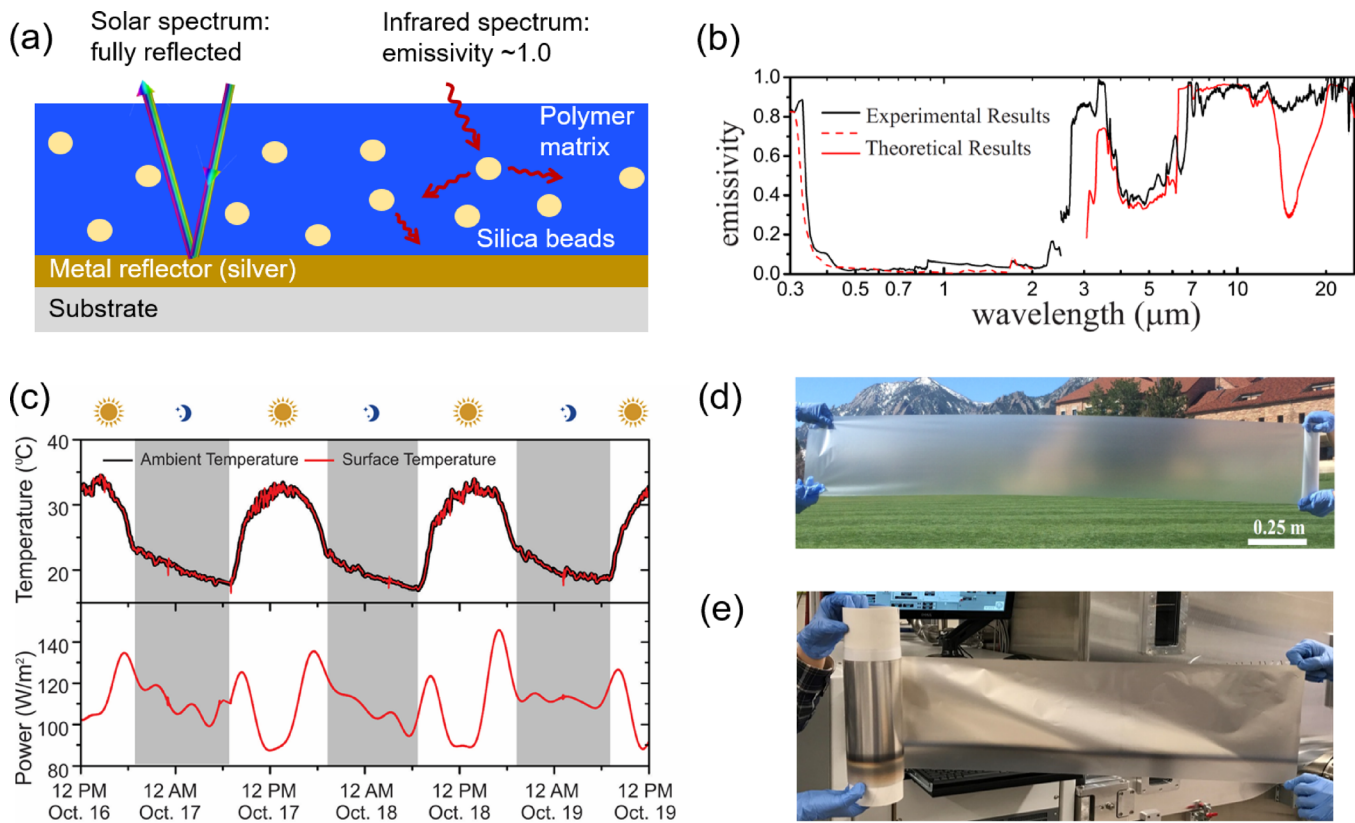


FIG. 20. Scalable-manufactured daytime radiative sky cooling metamaterial developed at the University of Colorado Boulder.^{32,196} (a) Schematic of the glass-polymer hybrid metamaterial backed with a thin silver film. The silver film reflects most of the incident solar irradiance and is highly emissive in the atmospheric window. (b) The full spectroscopic performance of the glass-polymer hybrid metamaterial. The metamaterial reflects $\sim 96\%$ solar irradiation while possessing emissivity >0.93 in the atmospheric window. (c) The continuous measurement of cooling power over three days shows an average cooling power $>110 \text{ W/m}^2$ and a noon-time cooling power of 93 W/m^2 between 11 am–2 pm. (d) A photo showing the 300-mm-wide hybrid metamaterial thin film that was produced in a roll-to-roll manner, at a speed of 5 m/min. The film is $50 \mu\text{m}$ in thickness and not yet coated with silver. (e) A photo showing the 300-mm-wide hybrid metamaterial thin film that has been coated with silver by roll-to-roll web coating. Figures (a)–(d) are reproduced with permission from Zhai *et al.*, Science **355**, 1062–1066 (2017). Copyright 2017 The American Association for the Advancement of Science.

as shown in Fig. 23(d), where a distinct change in cooling power can be seen when experiencing a phase-change [Fig. 23(e)].

IV. APPLICATIONS OF RADIATIVE SKY COOLING

Though many radiative cooling materials have been developed with very appealing spectroscopic properties, not many reliable cooling systems are available yet due to another set of challenges beyond materials. The intrinsically low energy density of radiative sky cooling represents one of the most important challenges for the practical use of this technology for either large scale systems such as power plant cooling or the interest in electronics cooling which in general has a power density on the order of 100 W/cm^2 . Other issues that need to be considered when building radiative sky cooling devices and systems include the system configuration and controls, cooling load profiles from end-users, the impact of weather conditions, as well as the system cost and payback period.

The use of nighttime radiative sky cooling can be traced back to 400 BC when Persians made ice during a clear cold winter night, even though mechanisms of this phenomena was completely not

understood yet.^{14,210} In 1700s, the water desalination system was built by freezing to purify sea water and impure water.²¹¹ In this section, we review existing applications of radiative sky cooling as well as those that are currently been explored. A few potential application areas, such as cooling of buildings and solar cells, dew water harvesting, and supplemental cooling for power plants are discussed in detail. The use of daytime radiative sky cooling is highlighted as it represents an exciting new direction over the last few years.

A. Buildings

Buildings consume approximately 40% of total energy use in the United States, and most of energy consumption is for heating, ventilation, and air conditioning (HVAC) systems.^{212,213} More specifically, space cooling accounts for about 12% of building energy consumption in the United States.²¹⁴ The integration of radiative sky cooling technology with buildings, which consumes no or very little energy, could have tremendous impact on world energy saving and CO_2 emission reduction. Earlier works on radiative sky cooling in buildings were summarized in review articles by Lu *et al.*,³⁴ Vall and Castell,¹¹⁸ and

TABLE II. List of successful demonstration of daytime radiative sky cooling under direct sunlight in field thermal measurement.

Materials	Fabrication Process	Cooling performance	Year	Location	Reference
Seven layers of alternating silicon dioxide (SiO_2) and hafnium dioxide (HfO_2) thermal emitter backed by a silver (Ag) solar reflector	The thermal emitter was deposited using electron beam evaporation on top of a silicon wafer. A 20-nm-thick adhesion layer of Ti was first deposited, followed by 200 nm of Ag, and the seven alternating dielectric layers of HfO_2 and SiO_2 at desired thicknesses	Producing cooling power of 40 W/m^2 and a temperature reduction of nearly 5°C below ambient	2014	Stanford, California	Raman <i>et al.</i> ³¹
Vikuiti Enhanced Specular Reflector (ESR) film with a 200-nm-thick silver coating at the bottom	The material was fabricated by adding a silver coating to the Vikuiti Enhanced Specular Reflector (ESR) film. The coating method was not mentioned	Achieving 2°C subambient cooling under 1060 W/m^2 solar irradiance with no convection shield	2015	Sydney, Australia	Gentle and Smith ¹⁴³
Randomized SiO_2 microparticles dispersed in TPX polymers	The selectively emissive polymer layer was fabricated through roll-to-roll extrusion, followed by roll-to-roll deposition of the reflective metal layer via plasma-enhanced magnetron sputtering	Average cooling power of 93 W/m^2 at noon and $>110 \text{ W/m}^2$ over a continuous 72-h day-nighttime measurement	2017	Cave Creek, Arizona	Zhai <i>et al.</i> ³²
A fused silica coated by polydimethylsiloxane (PDMS) and Ag on the top and bottom sides, respectively	The silver film was deposited by electron beam evaporation under high vacuum. The PDMS film was spin-coated for 60 s followed by degassing for 10 min and curing for 1 h at 80°C	Temperature reduction of 8.2°C at noon time under direct sunlight	2017	Pasadena, California	Kou <i>et al.</i> ²⁰²
A visibly-reflective extruded copolymer mirror (3 M Vikuiti ESR film), on top of an enhanced silver reflective surface	Visibly-reflective extruded copolymer mirror (3M Vikuiti ESR film) was placed on top of an enhanced silver reflective surface	Cool water up to 5°C below the ambient air temperature at water flow rates of $0.2 \text{ l min}^{-1} \text{ m}^{-2}$, corresponding to an effective heat rejection flux of up to 70 W/m^2	2017	Stanford, California	Goldstein <i>et al.</i> ⁵¹
Hierarchically porous poly(vinylidene fluoride-co-hexafluoropropene) ($\text{P(VdF-HFP)}_{\text{HP}}$)	Phase-inversion-based method was used to prepare a precursor solution of P(VdF-HFP) (polymer) and water (nonsolvent) in acetone (solvent) to achieve hierarchically porous polymers	Subambient temperature reduction of $\sim 6^\circ\text{C}$ and cooling powers of $\sim 96 \text{ W/m}^2$ under solar intensities of 890 and 750 W m^{-2} , respectively	2018	Phoenix, Arizona	Mandal <i>et al.</i> ⁵⁸

Zhao *et al.*¹²⁰ In general, the use of radiative sky cooling can be achieved either in a passive way such as cool roof (with no energy input), or in a more active way such as cooling of a heat transfer fluid and then use the heat transfer fluid for building cooling (requiring a small percentage of energy input for pumping). Passive systems have the advantage of system simplicity, but suffer from possibly excessive cooling when cooling is not needed, especially during the winter or the nighttime. Active systems can be better controlled, and thus are more feasible for those applications where cooling power needs to be regulated, but the systems are much more complex. The efficiency of a radiative sky cooling system in a building depends on the availability of exposed flat (or low slope) roof area and the cooling potential that can be explored in single floor buildings or in the top floor of multi-floor buildings.²¹⁵ This section presents an overview of radiative sky

cooling for buildings, and more importantly, the opportunities and challenges in deploying this technology. Note that when using the term “passive,” some researchers highlight the use of a natural cooling source and does not exclude the use of a fan or pump to enhance system performance.^{34,216} In this work, the term passive refers to the technology with zero energy input. Those systems with a fan or a pump are described as an active system in Sec. IV A 2.

1. Passive applications

Passive cooling of buildings with a large rooftop is an effective way to reduce building energy consumption, especially considering that the cooling load of most buildings are on the order of 100 W/m^2 of building area.^{216,217} Nahar *et al.*²¹⁸ experimentally

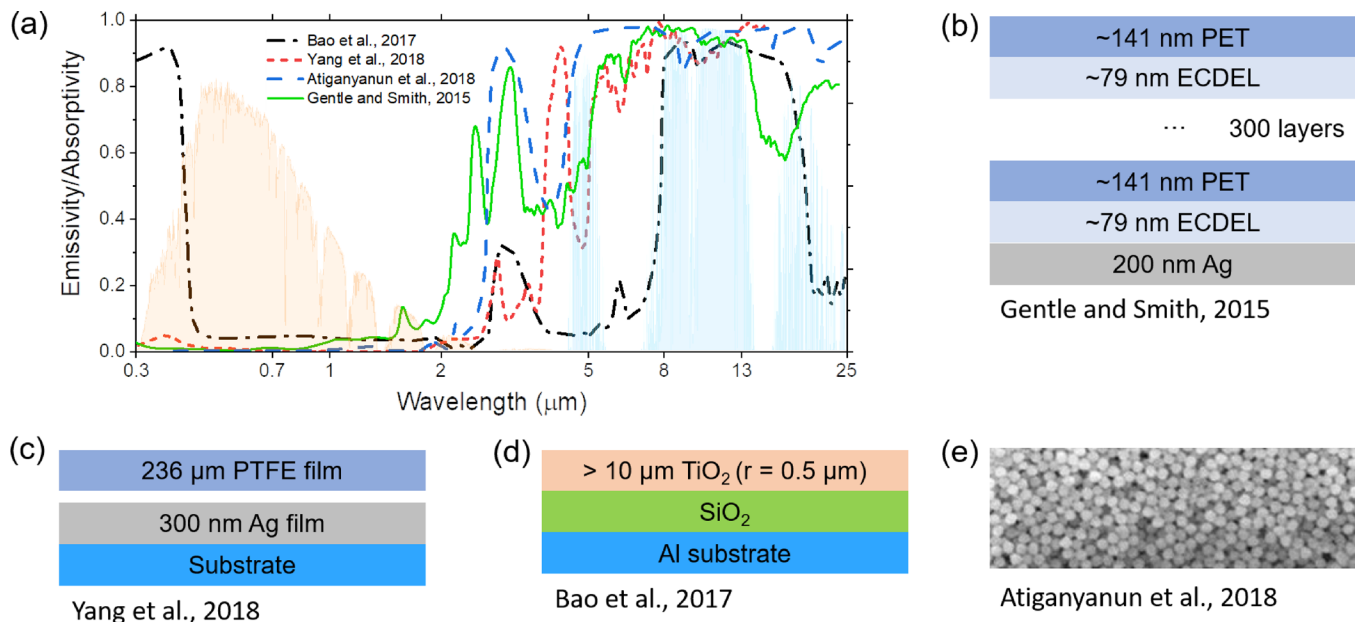


FIG. 21. Highlight of some polymeric daytime radiative sky cooling materials that can potentially be scalable-manufactured. (a) Measured emissivity/absorptivity of some daytime radiative sky cooling materials recently developed. The normalized solar irradiation of AM1.5 spectrum and clear sky transmittance in the infrared range are plotted for visualization. Adapted with permission from Bao *et al.*, *Sol. Energy Mater. Sol. Cells* **168**, 78–84 (2017). Copyright 2017 Elsevier. Atiganyanun *et al.*, *ACS Photonics* **5**, 1181–1187 (2018). Copyright 2018 American Chemical Society. Yang *et al.*, *Sol. Energy* **169**, 316–324 (2018). Copyright 2018 Elsevier. A. R. Gentle and G. B. Smith, *Adv. Sci.* **2**, 1500119 (2015). Copyright 2015 WILEY. (b) A polymer mirror that consists of 300 layers of Polyethylene terephthalate (PET)/ECDEL pairs. ECDEL is a copolyester using 1,4-cyclohexane dicarboxylic acid, 1,4-cyclohexane dimethanol, and polytetramethylene ether glycol. The bottom Ag layer is added to raise solar reflectance in the near-infrared region. (c) A dual-layer structure that consists of a PTFE sheet and a back reflector made of the Ag film. Note that the Ag film is coated on a substrate and there exists an air gap between the PTFE sheet and the Ag film. (d) Double layer coating composed of TiO_2 and SiO_2 on an Al substrate. The densely packed TiO_2 top layer is for solar reflection and the underlying SiO_2 layer has selective emissivity within the atmosphere window. (e) A paint-format microsphere-based photonic random media that can potentially be scalable-manufactured.

compared eight different passive techniques, such as thermal insulation on roof, roof pond, and evaporative cooling for building cooling. They found that white-colored roof (i.e., “cool roof”) is the best for thermal comfort in arid areas, especially when

considering the ease of operation and without consumption of water. Due to its special advantage in energy efficiency, cool roof is one of the major and prevailing passive cooling techniques identified for building applications.²¹⁹

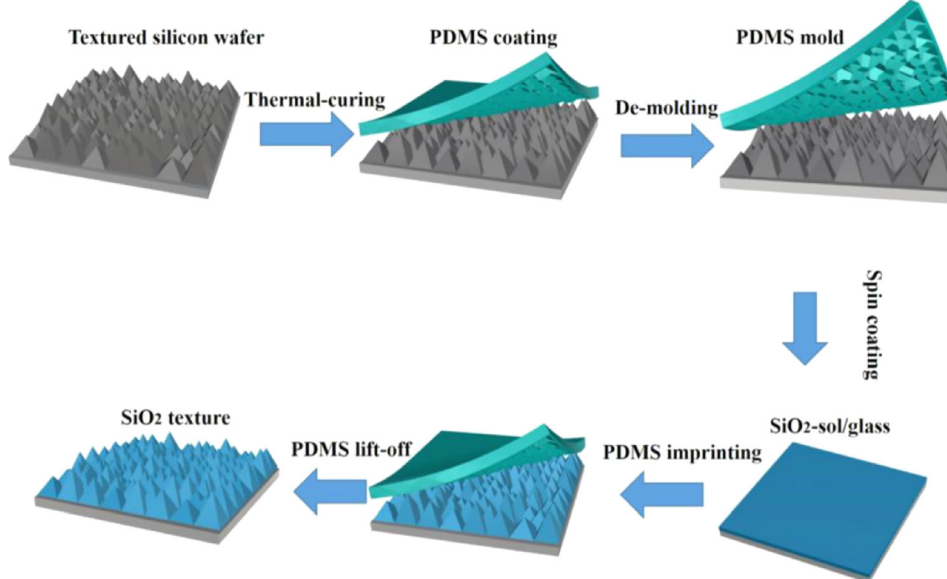


FIG. 22. Schematic illustration on the preparation of ultrabroadband versatile textures for radiative sky cooling and light management.²⁰⁵ Commercially available crystalline silicon wafer with the desired features was used as an original master. The original master was used to shape an intermediate PDMS mold, which was later imprinted onto a sol-gel silica layer to replicate the pyramidal textures. Figure reproduced with permission from Lu *et al.*, *Sol. RRL* **1**, 1700084 (2017). Copyright 2017 Wiley.

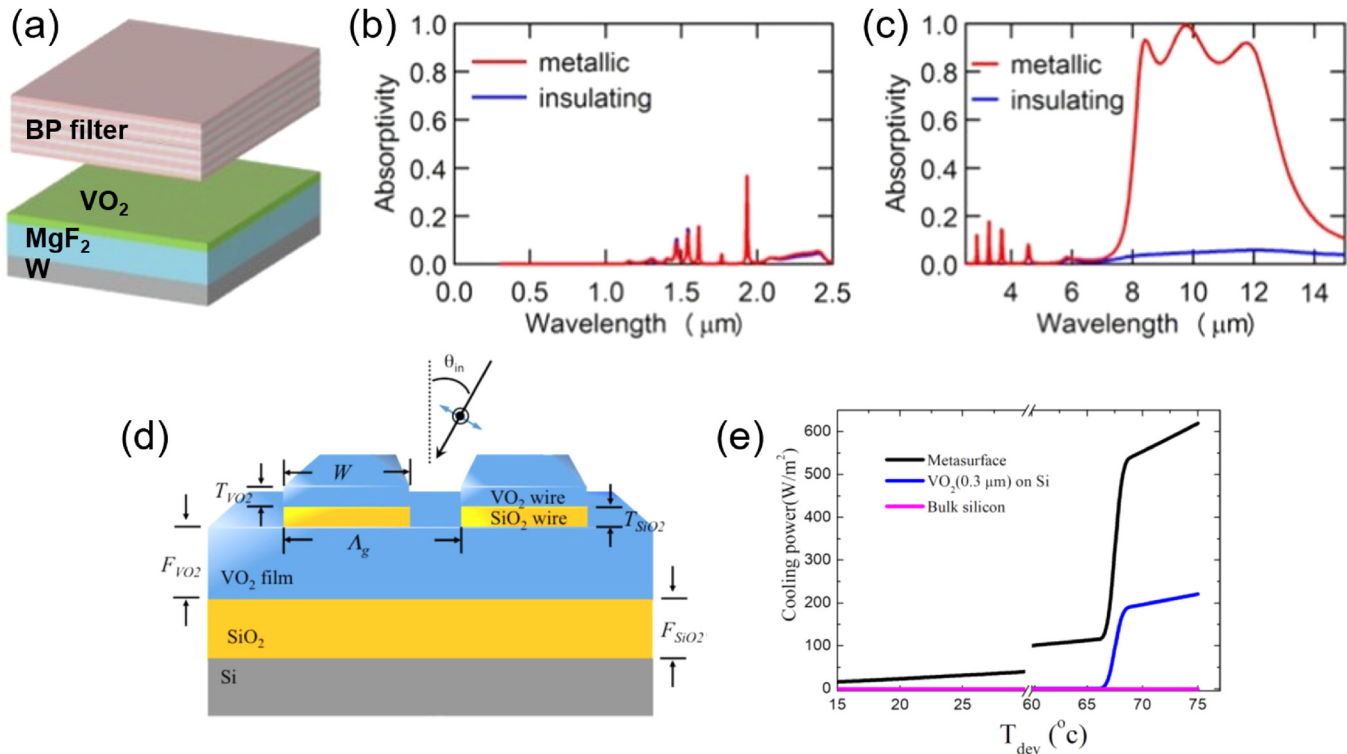


FIG. 23. Photonic structures to realize self-adaptive/switchable radiative sky cooling. (a) A two-layer photonic structure consists of a spectrally-selective filter (11 layers of Ge/MgF₂) as the top layer and a three layer VO₂/MgF₂/W structure as the bottom radiative cooler.²⁰⁷ (b) Solar (0.3–2.5 μm) absorptivity/emissivity of the photonic structure in metallic and insulating states. (c) Mid-infrared (2.5–15 μm) absorptivity/emissivity of the photonic structure in metallic and insulating states. Reproduced with permission from Ono *et al.*, Opt. Express **26**(18), A777–A787 (2018). Copyright 2018 The Optical Society. (d) A structure consisting of a VO₂/SiO₂ multilayer metasurface for passive temperature control. (e) Dramatic cooling power change after phase transition. T_{dev} is the temperature difference between the structure and ambient temperature, and ambient temperature is assumed to be 27 °C. Reproduced with permission from Wu *et al.*, Sci. Rep. **8**, 7684 (2018). Copyright 2018 Nature Publishing Group.

Cool roof refers to roof materials that have been designed to have high solar reflectance and high thermal emissivity (in mid-infrared regions) than a regular roof, which can lower roof temperatures and reduce heat transfer into a building, as shown in Figs. 24(a) and 24(b). The use of cool roof to increase albedo (i.e., solar reflectance) could reduce the building cooling load, lower peak electricity demand, improve indoor thermal comfort for unconditioned space, extend roof service life, and reduce building's contribution to the urban heat island [Fig. 24(c)].^{222–225} The solar reflectance (or albedo) and thermal emissivity are the two important performance indexes associated with a cool roof material. Cool roof products are versatile including tiles, paintings or coatings and can be found at the website of the cool roof rating council.²²⁶ The solar reflectance and thermal emissivity values of these products are usually also available via the cool roof rating council standard (CRRC-1).²²⁶ An optimized cool roof should have optimized thermal radiative properties (albedo and thermal emissivity) and roof R-value (i.e., thermal insulation).²²⁷ One common method to quantify cool roofs is the estimation of their solar reflectance index (SRI), which is calculated by using solar reflectance and thermal emissivity values adjusted with wind coefficients. According to the active standard ASTM E1980, SRI is defined by the equation

$$SRI = 123.97 - 141.35\chi + 9.655\chi^2, \quad (14)$$

where

$$\chi = \frac{(\alpha - 0.029\varepsilon)(8.797 + h_c)}{9.5205\varepsilon + h_c}. \quad (15)$$

Here, α is the solar absorptance, ε is the thermal emissivity, and h_c is the convective heat transfer coefficient. By definition, cool roofs should have an initial SRI value of at least 78.²²⁸ Table III gives a list of regular roofing materials and cool roof materials.

Energy saving benefits from installing a cool roof can be evaluated from both modeling and field tests, which is highly dependent on local weather and climate conditions, construction of building (e.g., roof insulation levels), and the use of the building (e.g., residential or commercial buildings). A study by the Lawrence Berkeley National Laboratory (LBNL) showed that raising the roof reflectivity from an existing 10%–20% to about 60% can reduce cooling-energy use in buildings for more than 20%.²³⁴ Even more capital benefits can come from the reduced size of air conditioners.²³⁵ A few field tests have been carried out to study the impact of cool roof on building energy consumption. Pisello and Cotana²³⁶ conducted a two-year long study in Italy to investigate the effect of an innovative cool roof tile (solar reflectance: 0.77, thermal emissivity: 0.89) on residential buildings. They showed that the proposed cool roof system can reduce the peak overheating of the external roof surface by 15–18 °C in summer, which

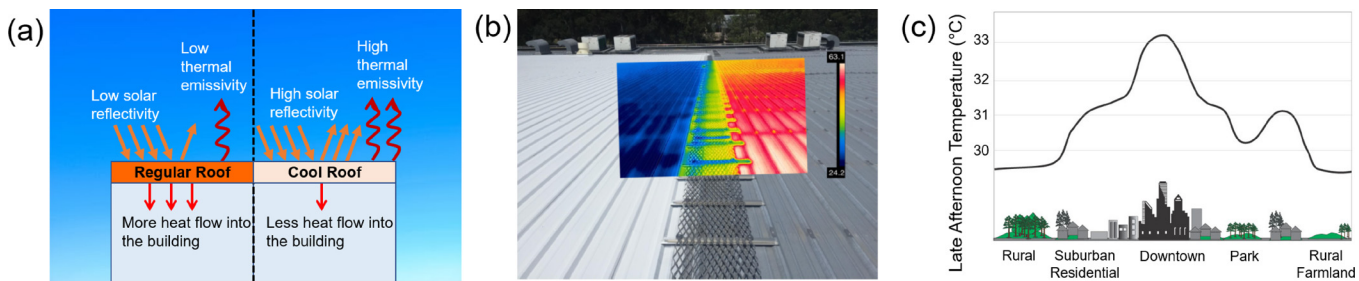


FIG. 24. Passive radiative sky cooling for buildings—cool roof application. (a) Cool roof reduces heat flow into buildings through enhanced solar reflection and infrared thermal emission. (b) A high albedo cool roof (left) compared to a galvanized low albedo roof (right). Much lower surface temperature is observed for the cool roof.²²⁰ Reproduced with permission from Smith *et al.*, Renewable Energy Environ. Sustainable **2**, 13 (2017). Copyright 2017 EDF Sciences. (c) The use of cool roof can reduce building's contribution to the urban heat island.²²¹ Reproduced with permission from Akbari *et al.*, *Cooling our Communities. A Guidebook on Tree Planting and Light-Colored Surfacing*. Copyright 1992 US Environmental Protection Agency. US Environmental Protection Agency.

produces a maximum decrease in peak indoor overheating of the attic by up to 4.7°C . Further analysis indicates the overall benefit corresponds to 14 kWh/m^2 cooling electricity saving per year for the southern Italian climate. Testa and Krarti⁵⁷ summarized both simulation studies and field tests in the literature and found that typical cooling energy savings from a cool roof with reflectance values of 0.3–0.4 for the US climates range from 0.1 to 8.6 kWh/m^2 for residential buildings, 1.1– 8.2 kWh/m^2 for office buildings, and 1.4– 10.9 kWh/m^2 for retail buildings.

Though most commercially available cool roof materials can lower the surface temperature of building roofs, none of those materials can reach subambient temperatures during the day under the sun. In 2015, Gentle and Smith¹⁴³ used a $67\text{-}\mu\text{m}$ -thick all-polyester material, which is a coextruded combinations of many bilayers of PET and ECDEL.²³⁷ By adding a 200-nm-thick silver coating at the bottom, the authors measured a solar reflectance of 0.97 and a thermal emissivity of 0.96 across the atmospheric window. 2°C subambient temperature under 1060 W/m^2 solar irradiance was demonstrated in a field test using a small piece of sample ($19 \text{ cm} \times 19 \text{ cm}$) mounted horizontally on a polystyrene block. Another field test, conducted by the authors of this paper, compared the glass-polymer hybrid metamaterial [see Fig. 20] roof and a regular gray-colored shingle roof. Two reduced-scale model rooms have been built and tested in Laramie, Wyoming, USA,

with dimensions of $2.4 \text{ m} \times 1.8 \text{ m} \times 2.4 \text{ m}$ (width \times length \times height) as shown in Fig. 25(a). Temperature comparison for the roof surface and the air inside the room are shown in Figs. 25(b) and 25(c), respectively. Solar irradiation and outdoor temperature change with time are given in Fig. 25(d). It is observed that the maximum temperature difference at the roof surface and indoor were 28.6°C and 11.2°C , respectively. The simulation results show that the cooling load reduction from utilizing the metamaterial cool roof could save as much as $91 \text{ kWh/(m}^2 \text{ yr)}$ of cooling electricity for the analyzed location of Orlando, Florida, USA, compared to the conventional shingle roof.

Cost and payback period are important factors when considering cool roof installation. Zhang *et al.*²³⁸ conducted life cycle analysis of using cool roof paint in the tropical country of Singapore. Annual cooling energy savings of $\$33/\text{m}^2$ can be achieved. The payback period is expected to be less than two months in unventilated roof and less than six months in a ventilated roof. Testa and Krarti⁵⁷ reviewed the benefits of cool roof and found that annual energy cost savings from cool roofs ranges from $\$0.16/\text{m}^2$ to $\$0.36/\text{m}^2$.

Even though the energy saving benefits are obvious, there are also challenges associated with cool roof applications including:

- (1) The use of a cool roof could increase heating energy in winter. This problem becomes more severe for those climates where heating seasons are longer than cooling seasons. For example, at high latitudes,

TABLE III. List of some regular roofing materials and some cool roof material properties.

	Materials	Solar reflectance	Thermal emittance	SRI	Reference
Regular roofing materials	Generic black shingle	0.05	0.91	1	57
	Shasta white shingle	0.26	0.91	27	57
	Light gravel	0.34	0.90	37	57
Cool roof materials	White coating on shingle	0.71	0.91	87	57
	United Coatings TM	0.87	0.87	110	229 and 230
	Kymax TM Coating				
	Miracool silicon acrylic emulsion paint	0.89	0.89	113	229 and 231
	Renolit Alkorbright polyester-reinforced roofing membrane	0.91	0.84	115	229 and 232
	APOC 256X coating	0.94	0.88	120	229 and 233

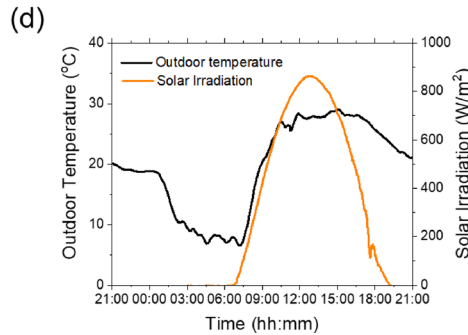
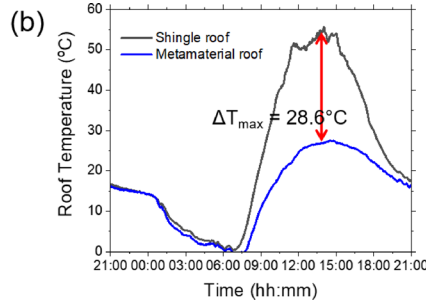
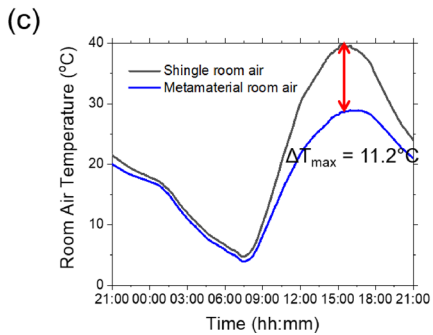


FIG. 25. Comparison study of a polymer-based metamaterial cool roof and a regular shingle roof. The polymer-based metamaterial developed at the University of Colorado is shown in Fig. 20. The test was conducted at Laramie, Wyoming, USA. (a) A picture shows the two rooms for comparison study. The sizes of both rooms are $2.4\text{ m} \times 1.8\text{ m} \times 2.4\text{ m}$ (width \times length \times height). (b) The temperatures change of the metamaterial cool roof and shingle roof during a 24-h testing period. The maximum roof temperature difference is 28.6°C . (c) Room temperature change during the testing period. The maximum room temperature difference is 11.2°C . (d) Ambient temperature and solar irradiation during the testing period.

the use of cool roof is not as effective for reducing the energy consumption due to low solar irradiation. For a year-round operation of cool roofs, one needs to make sure that the cool roof could produce substantial benefits in summer along with relatively small or negligible penalties in winter. The cool roof technique could easily find its application at low latitudes (*e.g.*, southeast Asia²³⁹), where cooling is a major concern for buildings. At high latitudes, one potential solution is to implement a switchable cool roof,^{57,207} which has the ability to change roof reflectance when buildings transition to the heating mode from the cooling mode (see Sec. III B—self-adaptive/switchable radiative sky cooling material).

- (2) Another challenge of cool roof is the visual discomfort caused by such highly reflective roofs. To solve this problem, researchers have been working on increasing solar reflectivity and thermal emissivity without affecting the existing color preference, which is a compromise between roof temperature reduction and visual aesthetics.^{240–243} For example, the cool-colored roofing technology, which can make solar-reflective roofing available in any color (dark or light) by selectively reflecting the invisible component of sunlight in the near-infrared spectrum, which accounts for 52% of total solar power.²³⁴ Figure 26 shows a few cool-colored roof tile coatings that has higher solar reflectance. In the visible spectrum between $0.4\text{ }\mu\text{m}$ and $0.7\text{ }\mu\text{m}$, the cool-colored roof tile does not have too much difference with the standard roof, as shown in Fig. 26(a). But in the near infrared between $0.7\text{ }\mu\text{m}$ and $2.5\text{ }\mu\text{m}$, the cool-colored roof has much higher reflectance. This result in higher solar reflectance without changing too much the color of the roof tile, as shown in Fig. 26(b).
- (3) The performance of the cool roof could degrade over time due to dust accumulation and material degradation. Soiling and accumulation of soot particles can reduce solar reflectance by about 0.15 with most degradation occurring in the first year.²⁴⁴ Even though the solar reflectance degradation due to soiling can be effectively restored by simply washing,²⁴⁵ the degradation due to material itself is usually more difficult to restore. Fortunately, the thermal emissivity of the cool roof material does not degrade significantly over time.²⁴⁴

Wide use of cool roofs can benefit not only buildings, but also cities by mitigating the global warming effect. Oleson *et al.*²⁴⁶ found that the use of white roofs could decrease urban daily maximum temperature by 0.6°C and daily minimum temperature by 0.3°C . A few

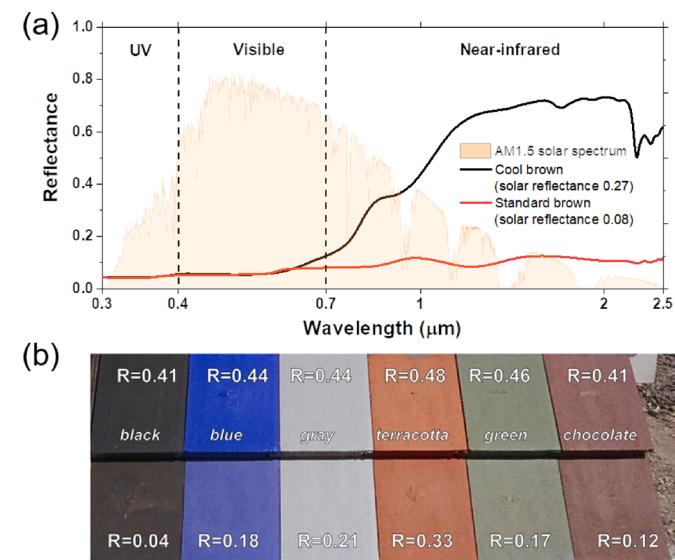


FIG. 26. Cool-colored roofing materials.²³⁴ (a) Solar spectrum reflectance of the cool and standard brown surface, as an example for demonstrating the principle of cool color roofing materials. Normalized AM 1.5 solar spectrum is shown for visualization. (b) Palette of color-matched cool (top row) and conventional (bottom row) roof tile coatings developed by American Roof Tile Coatings. Shown on each coated tile is its solar reflectance Adapted with permission from Akbari *et al.*, *Cool Color Roofing Materials*. Copyright 2006 Lawrence Berkeley National Laboratory. Lawrence Berkeley National Laboratory.

energy standards, such as ASHRAE 90.1–2016,²⁴⁷ ASHRAE 90.2–2007,²⁴⁸ and California Title 24²⁴⁹ have already implemented the cool roof standard. Other rating standards, such as LEED,²⁵⁰ also give incentive to the implementation of cool roof technology.

2. Active applications

Though cooling energy or cold harnessed through radiative sky cooling is totally free, some external energy sources (e.g., fan and pump) are needed to transfer and then to use the cooling energy. Active systems, including air-based,^{251–256} open or closed loop water-based,^{37,257–260} and hybrid systems, have been proposed to integrate nighttime radiative sky cooling with other energy systems (e.g., photovoltaic-thermal^{36,261}). The efficiency of those systems is usually determined by radiative cooling surface properties and climate conditions (e.g., ambient air temperature, humidity, wind speed). A typical air-based radiative system consists of a radiative cooling surface (e.g., roof-mounted radiator or a cool roof), an air circulating loop, and a fan to drive the air. Lu *et al.*³⁴ compared different system configurations of the nighttime radiative sky cooling system. Figure 27(a) shows a system that uses the roof as a radiator to lower the indoor temperature. Figures 27(b) and 27(c) show two schematic systems that combine the air-based system with building air conditioner for energy saving. The average net cooling power of air-based systems is usually low, between 20 and 30 W/m².^{253,262} The reason could possibly be due to the low heat transfer coefficient of the air. In general, air-based systems are simpler to implement without freezing concerns. They can provide instantaneous cooling during the nighttime for buildings.²⁵²

Water-based radiative cooling systems utilize water as a heat transfer fluid. Depending on whether there is a cold storage unit (e.g., a water tank²⁶⁴), water-based systems can serve either as an *in-situ* cooling source [Figs. 27(d) and 27(e)] or as a cold storage system [Fig. 27(f)]. The average net cooling power of water-based systems are usually between 40 and 80 W/m²,^{36,37,265} higher than that of the air-based systems. By using a radiative cooling system that consists of a 5.3 m² radiator and a 280-l water tank in Oslo, Norway, Meir *et al.*³⁷ concluded that except for midsummer with extremely high relative humidity, radiative sky cooling can cover the cooling need of single-family houses. Flat panels that are similar to typical solar collectors can be used for cold energy collection.^{37,265–267} The radiative cooling panels can be integrated as a roof component.²⁶⁸ The cooling energy (i.e., cold water) stored due to nighttime radiative cooling can provide cold water for daytime cooling. However, since the supply temperature of chilled water from the building air conditioning system is usually low (e.g., 7 °C), water from the radiative sky cooling system might not be sufficiently chilled for direct use. Possible solutions are to integrate the water-based cooling system with the radiant floor/ceiling system that do not need a very low supply temperature of water, e.g., 15–18 °C, or use radiative-cooled water to precool the heat transfer fluid before it enters the chiller. Integrating the water-based radiative sky cooling system with other energy systems has also been explored for energy saving and efficiency improvement. For example, hybrid systems can integrate nighttime radiative sky cooling with phase-change materials for effective cold storage,²⁵ with direct/indirect evaporative cooling units (e.g., cooling towers) to improve its efficiency,^{269,270} with desiccant systems to enhance cooling performance,²⁷¹ with solar collectors to obtain both solar heating and nighttime radiative sky cooling,^{272,273} with

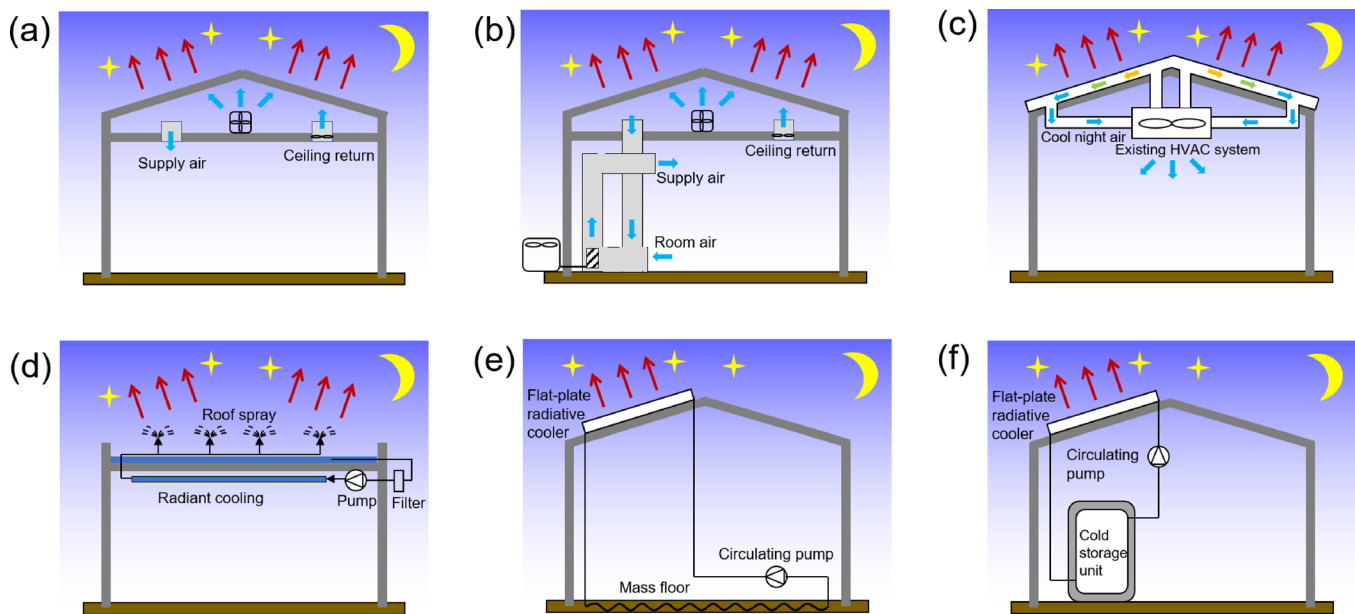


FIG. 27. Building-integrated nighttime radiative sky cooling systems. (a) Air-based radiative sky cooling system that uses the roof as a radiator. (b) Air-based radiative sky cooling system integrated with a building air conditioner. (c) NightSolar® system utilize a ventilation roof design to allow both space cooling in summer and solar space heating in winter.²⁶³ (d) A radiative cooling system that takes advantage of nighttime radiative sky cooling and convection cooling. (e) Nighttime radiative sky cooling system that pumps cooled water into slab floors at night, storing the cooling energy in the building's thermal mass. (f) Nighttime radiative sky cooling for cold water production. The cold water produced can be used in various applications.³⁷ For example, during the day, cool water stored in the tank can be pumped through interior fan-coil units to provide on-demand cooling.

photovoltaic-thermal panels to generate electricity and heating in the day, and cooling at night,^{36,261} and with ground source heat pumps to solve thermal accumulation problem in cooling dominated regions.²⁷⁴

Recent advancement of daytime radiative sky cooling has rendered this technology to new possibilities in buildings.^{38,51,275,276} The building attic usually has much higher temperatures than the indoor environment during the day,^{277,278} which inevitably increase the air conditioner load due to heat transfer from the attic to the conditioned living space. Current attic ventilation directly uses ambient air. With subambient radiative cooling of air during the day, the temperature of the ventilation air into the attic can be reduced, as shown in Fig. 28(a). Another application is to precool the fresh air intake from the outdoor,²⁷⁹ which can reduce the cooling load of air conditioning systems, as shown in Fig. 28(b). Based on a low-cost daytime radiative sky cooling metamaterial,³² the authors of this work have developed a radiative air cooler that has a surface area of $1.84 \text{ m} \times 0.58 \text{ m}$, as shown by a picture in Fig. 28(c). Results on a typical summer day with clear sky conditions are shown in Fig. 28(d). Subambient cooling of moving air with a decent flow rate was demonstrated for the first time during the day under the sunlight. It can be observed that the radiative air cooler can cool intake outdoor air by $2\text{--}3^\circ\text{C}$ at noon under a flow rate of $7.9 \text{ l}/(\text{m}^2 \text{ s})$.

Water-based daytime radiative sky cooling systems usually can produce more energy savings. Wang *et al.*²⁷⁶ introduced a nanophotonic radiative sky cooling system for office buildings, as shown in Fig. 29(a). The system has a radiative sky cooling loop and a space-cooling loop. The radiative sky cooling loop circulates water through a roof-mounted radiator whenever the temperature at the outlet of the radiator is lower than the temperature of water at the outlet of the tank. It was shown that the photonic radiative sky cooling system saved between 45% and 68% cooling electricity relative to the variable

air volume (VAV) system and between 9% and 23% relative to the nighttime radiative cooling system featured with the best commercially available coating in the market. Zhang *et al.*³⁸ proposed a hybrid radiative sky cooling system that stores cooling energy harnessed from the radiative cooling system in a cold storage tank, as shown in Fig. 29(b). The cooling energy is then used to precool the conditioned air to reduce the cooling load on the air conditioner for residential applications. In comparison with the electricity consumption of a split air conditioner alone, the hybrid radiative sky cooling system could save annual cooling electricity by 26% to 46% for the modeled locations (Orlando, San Diego, San Francisco, Denver).

It is important to note that the temperature at the outlet of the radiative sky cooling panels always varies with the ambient temperature, which means that temperature of the heat transfer fluid from the cooling panels is much lower at night than during the day. Therefore, for a 24-h cycle, the lowest temperature in the cold storage tank should always occur in the early morning before sunrises. After sunrise, the ambient temperature goes up and the temperature of heat transfer fluid from radiative sky cooling panels also increases and can be higher than the cold storage tank. Therefore, the radiative cooling loop would be forced to stop. The benefit from daytime radiative sky cooling is therefore reduced without a good operation strategy.

Goldstein *et al.*⁵¹ proposed to use daytime radiative sky cooling based on reducing the temperature of the air conditioner's condenser to improve the overall efficiency. It is estimated that the electricity consumption can be reduced by 3%–5% for every 1°C reduction of condenser temperature.²⁸¹ They built a circulated daytime radiative water cooling panels and showed that a temperature reduction of between 3 and 5°C under a water flow rate of $0.21 \text{ l}/(\text{min m}^2)$ can be achieved. The cooled water is then used to subcool the refrigerant from the condenser through a heat exchanger, as shown in Fig. 29(c). The modeling

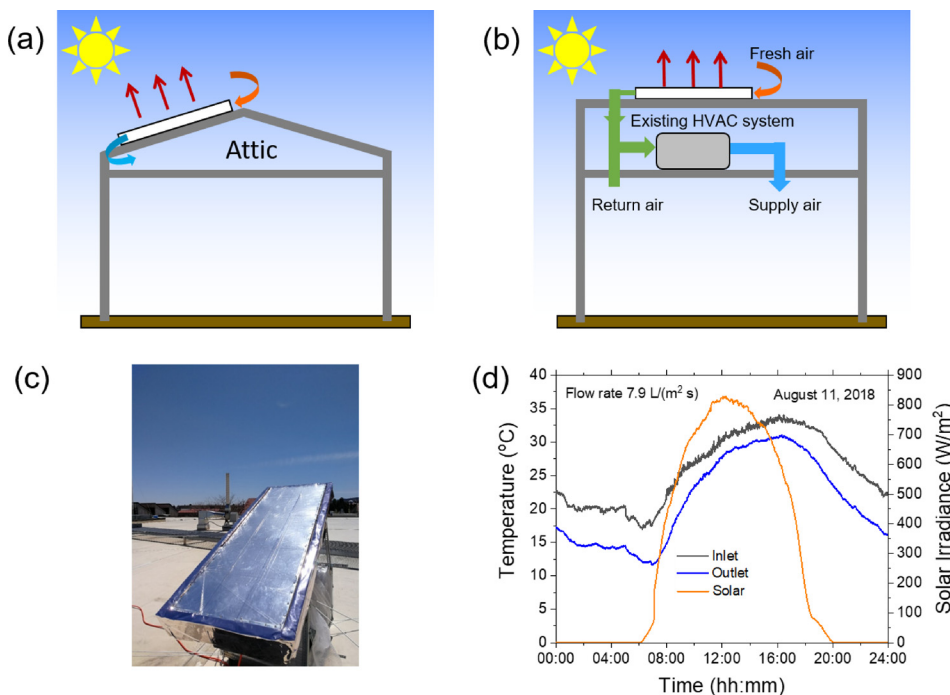


FIG. 28. Air-based daytime radiative sky cooling for buildings. (a) Air-based radiative sky cooling system to reduce the temperature in the building attics. (b) Air-based radiative sky cooling to precool the building intake air. (c) Photo of the daytime radiative air cooler developed at the University of Colorado Boulder. (d) Test of the radiative air cooler on August 11, 2018, at Boulder, Colorado, USA. At flow $7.9 \text{ l}/(\text{m}^2 \text{ s})$, intake outdoor air temperature can be reduced by $2\text{--}3^\circ\text{C}$ at noon. The benefit from using such a radiative air cooler comes from two aspects: (1) reduced solar absorption by roofing materials and (2) lower inlet air temperature for attic ventilation.

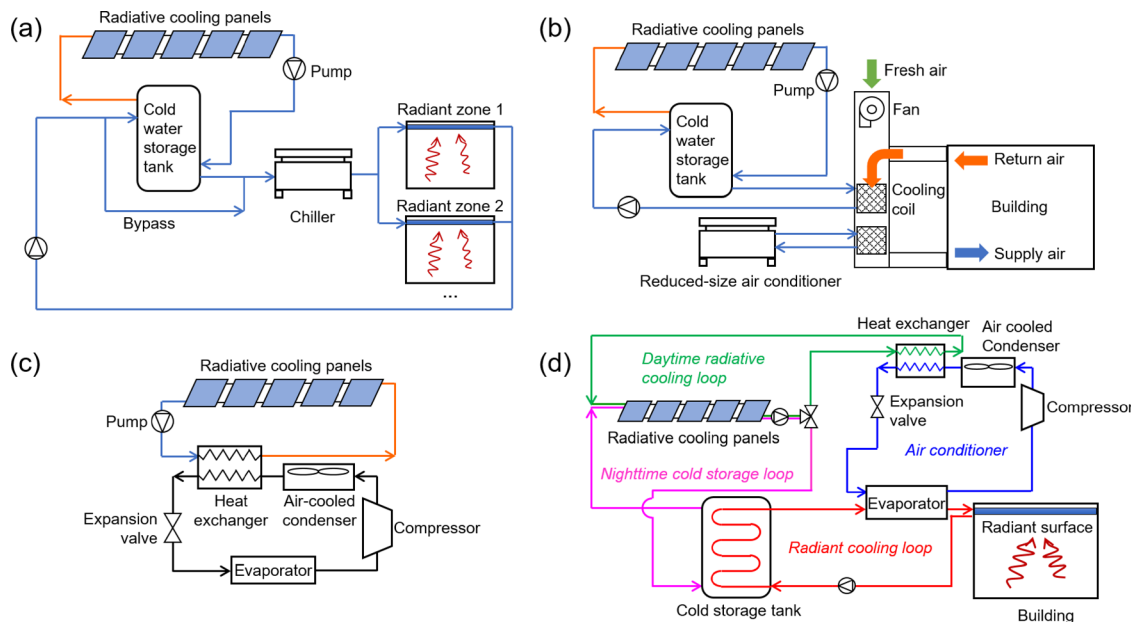


FIG. 29. Water-based daytime radiative sky cooling applications in buildings. (a) A photonic radiative cooling system.²⁷⁶ Adapted with permission from Wang *et al.*, Renewable Energy **118**, 265–277 (2018). Copyright 2017 Elsevier. (b) A hybrid radiative cooled-cold storage cooling system.^{38,280} Adapted with permission from Zhang *et al.*, Appl. Energy **224** 371–381 (2018). Copyright 2018 Elsevier. (c) A daytime radiative sky cooling system that is used to cool condenser to improve air-conditioner's efficiency.⁵¹ Adapted with permission from Goldstein *et al.*, Nat. Energy **2**, 17143 (2017). Copyright 2017 Macmillan Publishers Limited. (d) A radiative sky cooling system that uses both daytime and nighttime radiative sky cooling to maximize the system efficiency.⁵² Adapted with permission from Zhao *et al.*, Joule **3**, 111–123 (2019). Copyright 2018 Elsevier Inc.

results show a 21% reduction in cooling electricity use for buildings. However, this approach applies to daytime use only. Considering that there could be limited or even no cooling load at night, the integration of a cold storage unit is truly beneficial to taking advantage of the cooling effect 24 h a day. Recently, Zhao *et al.*⁵² introduced a radiative cooled cold collection and storage (RadiCold) system that can provide continuous day-and-night cooling. In this system, daytime and nighttime radiative sky cooling are used separately, as depicted in Fig. 29(d). During the day the subambient temperature heat transfer fluid generated is used to directly cool the condenser, while at night the RadiCold system stores the cooling energy in a storage unit, which is retrieved during the day to reduce the cooling load on air conditioners.

Zhao *et al.*⁵² built a kW-scale RadiCold system at the University of Colorado Boulder, USA. Figure 30(a) shows the schematic of the radiative sky cooling module. Figure 30(b) shows a picture of the radiative sky cooling system that consists of 10 radiative cooling modules arranged in a 2×5 array. Each module has a surface area of 1.35 m^2 , giving a total radiative cooling surface area of 13.5 m^2 . Figure 30(c) shows a typical test result of three consecutive days. The inlet water temperature tracks the ambient temperature throughout the test. The net cooling power is calculated from the inlet/outlet temperature difference by using the equation $q = \frac{cm\Delta T}{A}$, where A is 13.5 m^2 . Figure 30(d) shows that the net cooling power per square meter fluctuates between 40 and 100 W/m^2 during the testing period. The maximum net cooling power at night is 96 W/m^2 (1296 W for the 13.5 m^2 system) when the water was cooled to 3.1°C subambient on average, and the average cooling power at noon (12–2 pm) is 45 W/m^2 (607 W for the system) under an average of 952 W/m^2 solar irradiance on July 1. A modeling tool based on EnergyPlus and MATLAB has been

developed for evaluating the monthly electricity saving for cooling a 5000 m^2 commercial office building. Modeling results show that for three different subtropical locations (Phoenix, Houston, and Miami) in the United States, the RadiCold system (810 m^2 radiative cooling surface area) could potentially save 64%–82% of the electricity consumption for cooling in winter (from November to February), and save 32%–45% of the electricity consumption for cooling in summer (from May to August), as shown in Figs. 30(e) and 30(f).

B. Solar cells

Solar cells convert the solar energy directly into electricity through the photovoltaic effect. A commercial solar cell usually has an energy conversion efficiency between 12% and 20%.²⁸² For a solar cell material that has a specific band gap, such as 1.1 eV for Si, Fig. 31(a) shows that photons with energies below this band are not absorbed and converted to electricity, while photons with energies above the band gap are not fully converted to electrical energy.²⁸³ Therefore, a large portion of solar irradiation eventually becomes heat and heats up the solar cell. Unfortunately, solar cells are susceptible to the unwanted solar heating effect that both degrades their efficiency and shortens their lifetime.²⁸⁴ The operating temperature of commercially-available solar cells can easily exceed 60°C on a sunny summer day. The relative efficiency of crystalline silicon solar cells is estimated to drop at a rate of 0.45% every 1°C temperature increase.¹⁴⁹ The degradation rate of the solar cell can be doubled with every 10°C increase in the operating temperature.

Earlier works on cooling technologies for solar cells include surface water cooling,^{285,286} natural or forced air ventilation,^{42,287} heat pipes,²⁸⁸ thermoelectric modules,²⁸⁹ and phase change material.^{290,291}

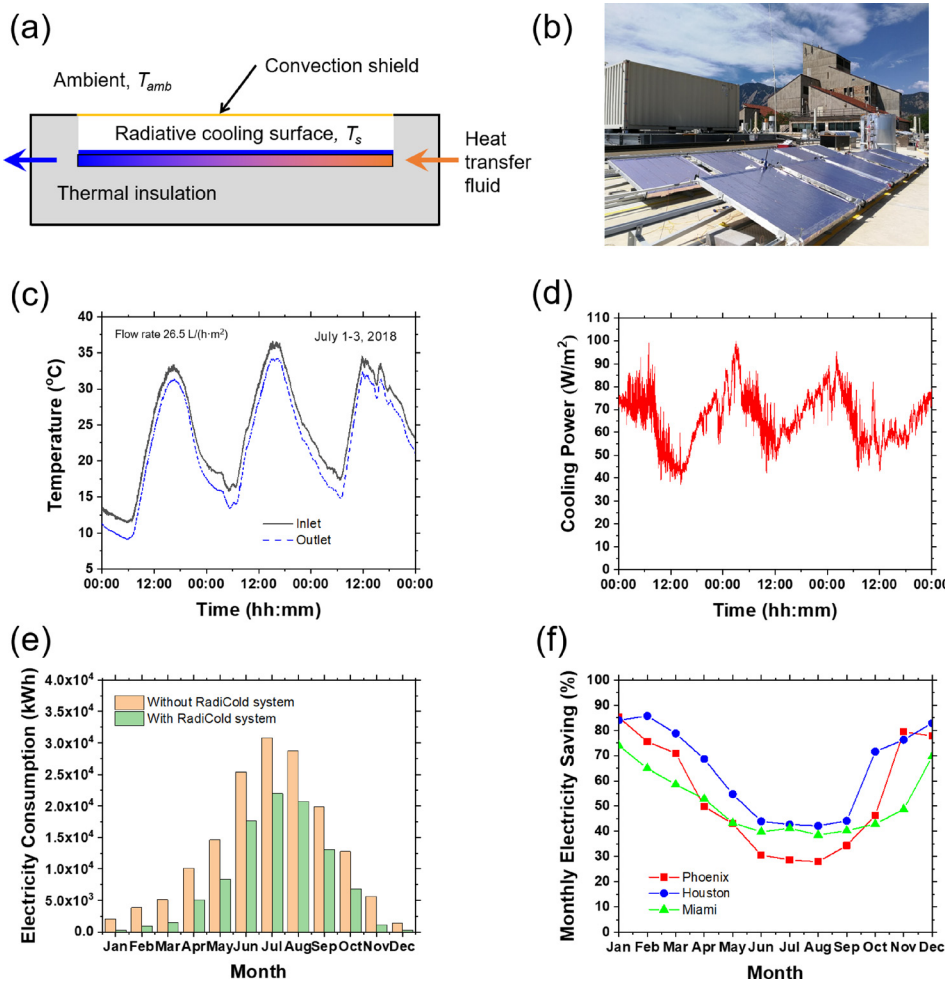


FIG. 30. Radiative sky cooling system coupled with heat transfer fluid for generating the continuous cooling effect.⁵² (a) Schematic of a radiative cooling device with the heat transfer fluid. (b) Picture of a radiative cooling system that has several radiative cooling panels connected in series. Water is used as the heat transfer fluid. The system has a total of 13.5 m² radiative cooling surface area. (c) Results of a 3-day continuous test. Inlet temperature tracks ambient temperature. The test was conducted at Boulder, Colorado, USA. (d) Net cooling power change during the 3-day test. (e) Monthly electricity consumption of a commercial office building located in Phoenix, Arizona with and without the RadiCold system. (f) Monthly electricity saving by the RadiCold system at three different locations, Phoenix, Houston, and Miami. Reproduced with permission from Zhao *et al.*, Joule 3, 111–123 (2019). Copyright 2018 Elsevier Inc.

Radiative sky cooling of solar cells could be a straightforward idea and can be made possible by placing a thin-layer material that has high transmittance in the solar spectrum and high emissivity over the infrared spectrum at the operating temperature. Different from building applications that seek to achieve subambient temperatures, the major objective of solar cell cooling is to lower its operating temperature as much as possible while maintaining its solar absorptance,²⁹² although Safi and Munday²⁹³ theoretically showed that solar cells can be cooled to subambient temperature with radiative sky cooling. Therefore, a wavelength-selective radiative emitter at the atmospheric window is not absolutely necessary. A broadband surface is instead preferred for solar cell cooling, especially when considering the cost benefits.²⁹⁴

Standard solar cells are typically covered with glass, which has a mid-infrared emissivity of 0.84. Riverola *et al.*²⁹⁵ deduced that the mid-infrared emissivity of a PV module is very high and almost independent of the underlying solar cell structure. Subedi *et al.*²⁹⁶ calculated emissivity from specular and diffuse reflectance measurements of three commercial low iron soda lime glasses commonly used in PV modules: SoliteTM, Diamant®, and Pilkington. The authors concluded that all three glasses have almost the same hemispherical emissivities

and are greater than 0.84. However, Gentle and Smith²⁹⁴ suggested that the emissivity value of glass (i.e., 0.84) could have been overestimated and suggested to hemispherical emissivity to be around 0.75. The higher the emissivity of glass cover, the more challenging to obtain the additional radiative sky cooling effect by enhancing mid-infrared thermal radiation. However, the thermal emissivity of typical glass is not optimized in terms of both wavelength and incident angle, which suggests that there still remain some rooms to enhance the radiative cooling power. Zhu *et al.*²⁹² showed theoretically that an ideal radiative emitter (emissivity equals to 1) on a solar cell could operate at a temperature 5.2 K below that with a 5-mm-thick fused silica glass (emissivity around 0.73). Then the same group of authors proposed a structure using silica nanophotonic crystal [Fig. 31(b)] that has near-unity emissivity across the mid-infrared wavelength range [Fig. 31(c)] on top of the silicon absorber.⁴⁰ The field temperature test showed that the silica absorber with the nanophotonic crystal structure is >1 °C cooler than with the planar silica layer at noon, as shown in Fig. 31(d). Even though this is not a big temperature reduction, the efficiency improvement is still worth pursuing if no extra infrastructure is needed and the nanophotonic structure can be manufactured in a cost-effective way.²⁹⁴

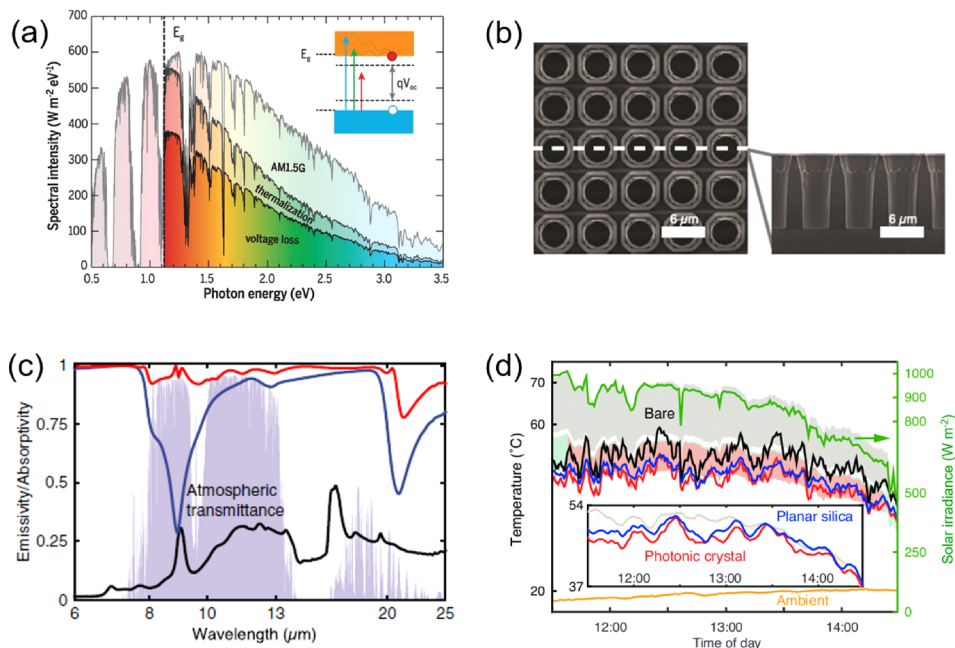


FIG. 31. Radiative sky cooling for solar cells. (a) Schematic showing that photons with energies below the band gap (E_g , denoted by the dashed black line) of the solar cell material are not absorbed and converted to electricity (left side of the dashed black line), and photons with energies above the band gap (right side of the dashed black line) are not fully converted into electrical energy with the excessive energy heating up the cell.²⁸³ Reproduced with permission from Polman *et al.*, Science **352**(6283), aad4424 (2016). Copyright 2016 American Association for the Advancement of Science. (b) Normal-view and side-view SEM images of the 2-dimensional silica photonic crystal structure. The photonic crystal consists of a square-lattice with a periodicity of 6 μm made by etching 10- μm -deep air holes into a 500- μm -thick double-side-polished fused silica wafer.⁴⁰ (c) Measured emissivity/absorptivity of solar absorbers at 10° angle of incidence between the wavelengths of 6 μm and 25 μm , averaged over both polarizations. The black, blue, and red curves show the measured emissivity/absorptivity for the bare absorber structure, the absorber structure with the planar silica layer, and the absorber structure with the silica photonic crystal, respectively. (d) Steady-state temperature measurement showing that the silica photonic crystal is on average 1.3 °C cooler than the absorber structure with the planar silica layer. (b)-(d) are reproduced with permission from Zhu *et al.*, PNAS **112**(40), 12282–12287 (2015). Copyright 2015 National Academy of Sciences.

Radiative sky cooling is more appealing for concentrated photovoltaic (CPV) systems which usually operates at even higher temperatures.⁷⁹ By using a 30- μm -thick radiative cooling layer consists of acrylate resin and inorganic fillers (coated on the aluminum chassis of a CPV module), Nishioka *et al.*²⁹⁷ experimentally demonstrated 10 °C temperature reduction (from 93.1 °C to 82.6 °C) of a CPV module compared to that without the radiative cooling layer. The employment of the radiative cooling coating also showed considerably improved uniformity of the temperature distribution in the CPV module. The open-circuit voltage of the CPV module with radiative cooling coating was 0.5 V higher than that of the module without the coating during the test period, which gives 0.5% higher conversion efficiency.

Published studies on radiative sky cooling for solar cells are limited to theoretical analysis,^{41,292} with a few field tests showing solar cell temperature reduction compared to that with no radiative sky cooling.^{40,297,298} There still lacks experimental investigation on the photocurrent-voltage (I-V) characteristics of solar cells.²⁰⁵ The other challenges are long-term durability and cost-effectiveness. Although some researchers claimed that their materials can be made on a large-scale and in a cost-effectively way,²⁹⁹ it is still unclear whether radiative sky cooling can be both technically feasible and economically viable.

Recently a combined approach to cool solar cells by simultaneously reflecting of sub-band-gap and ultraviolet solar irradiation, and enhancing radiative sky cooling was proposed, as shown in Fig. 32(a).

Li *et al.*⁴¹ proposed a multilayer dielectric stack coating on top of an existing encapsulated solar panel, which was designed to simultaneously reflect sub-band-gap solar irradiation and to enhance radiative sky cooling, as shown in Fig. 32(b). Based on calculated solar reflectivity [Fig. 32(c)] and thermal emissivity [Fig. 32(d)] spectra, the photonic coating structure can provide a temperature reduction of ~5.7 K as compared to the same solar cell without the coating. Another simulation study by Sun *et al.*³⁰⁰ shows that the combined technique would cool one-sun terrestrial solar modules up to 10 °C. This combined technique is very promising for reducing the solar cell temperature while further research should be focused on field testing.³⁰¹

C. Dew water harvesting

Dew forms on a surface when the surface temperature is below the local dew point temperature. Dew harvesting could generate a significant impact on water supply in certain climates/regions,^{302,303} for example, in many arid and semi-arid areas where traditional water sources are subject to depletion. The atmosphere air is a huge and renewable reservoir that contains 12 900 cubic kilometers of water.³⁰⁴ The availability of atmosphere water has no geographic dependence. Moreover, dew water is generally potable, especially in rural and isolated locations (e.g., islands), where it is most beneficial.^{47,305,306}

There are generally three ways to harvest water from air: adsorption technology based on using adsorbent,^{307–309} surface cooling by

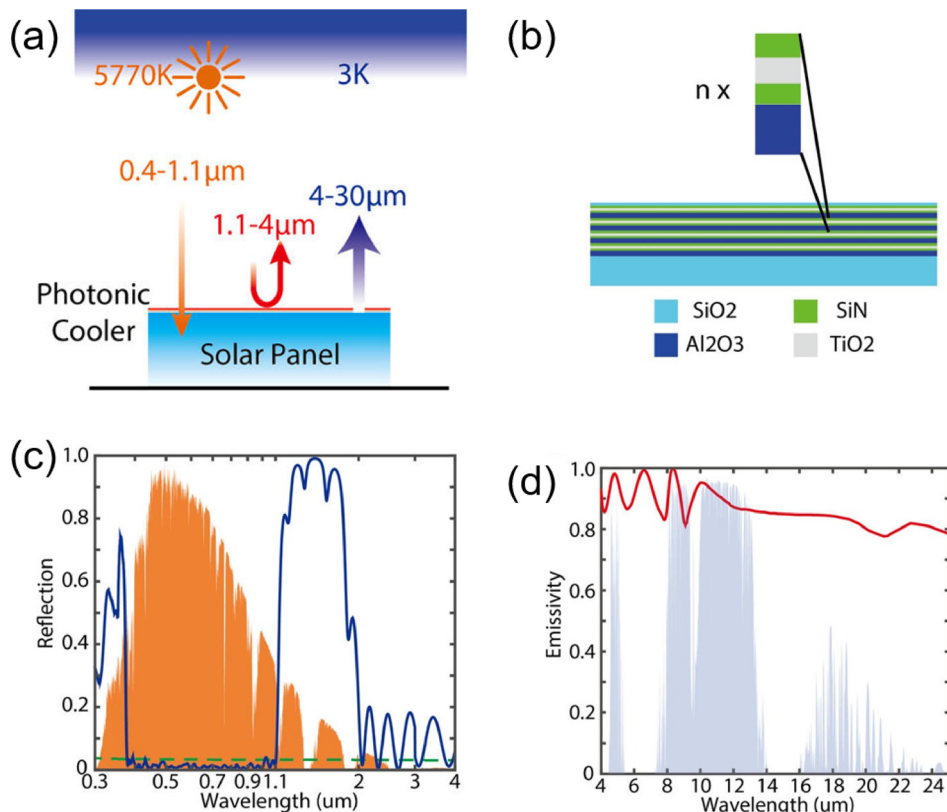


FIG. 32. Cooling of solar cells by both radiative sky cooling and sub-band-gap reflection.⁴¹ (a) A schematic showing that radiative sky cooling can be enhanced and the sub-band-gap solar radiation can be strongly reflected by using a nanophotonic cooler coated on top of an existing encapsulated solar panel. (b) A schematic of the nanophotonic cooler made of a multilayer dielectric stack that consists of alternating layers of $\text{Al}_2\text{O}_3/\text{SiN}/\text{TiO}_2/\text{SiN}$ with aperiodic arrangement of thickness. (c) Reflection spectrum of the photonic cooler (blue) with $n = 11$ sublayers. Near unity reflectivity is achieved in the wavelength range between 1.3 and 1.8 μm . (d) Emissivity spectra of the photonic cooler show broadband high emissivity over the infrared wavelength (4–25 μm). Reproduced with permission from Li *et al.*, ACS Photonics **4**, 774–782 (2017). Copyright 2017 American Chemical Society.

using heat pumps,³¹⁰ and radiative sky cooling. Research works on radiative sky cooling dew condensers can be traced back to the 1960s.³¹¹ Efforts have been devoted to analyze climate and weather conditions,^{312,313} to develop radiative cooling surface materials,^{171,314} to design dew collectors,¹⁶⁹ and to study operating conditions that affect the water production rate.^{46,315–317} The dilemma for the radiative sky cooling dew harvester is that the local atmosphere should have a large amount of water vapor (i.e., high humidity) that can be condensed, while the presence of a large amount of water vapor inevitably limits the radiative cooling power due to the infrared absorption of water. While the surface should allow easy condensate nucleation, the condensate needs to be removed promptly right after condensation happens on the surface.

The theoretical limit of the dew yield is about $0.8 \text{l}/(\text{m}^2 \cdot \text{day})$ which is restricted by the available cooling power ($\sim 100 \text{ W/m}^2$) with respect to the latent heat of water condensation (2260 kJ/kg).³¹³ Nevertheless, in practice the dew yield is much less than this limit due to the imperfect climate condition and system design. Table IV lists the performance of some dew water harvesting devices using nighttime radiative sky cooling. Atmospheric emissivity, relative humidity, and local wind speed all affect dew water condensation. It was found that dew yields dropped linearly with the increase in the cloud coverage.³¹³ However, a completely clear sky does not necessarily give highest dew yield because a clearer sky is usually associated with drier air, indicating that a certain level of absolute humidity is necessary for dew condensation to occur.³¹³ The relative humidity has to be high to reduce the required temperature difference (between ambient and dew

point temperatures) for condensation to occur. While a high wind speed is not favorable for dew formation because it reduces the net cooling power, and a gentle wind speed (less than 1 m/s) is necessary for bringing atmospheric water vapor to the condenser (i.e., radiative cooling surface).^{306,320} Researchers have been exploring the correlations between meteorological data (relative humidity, cloud cover, and wind speed) with dew water yields to predict the water production rate under different climate conditions.

D. Cooling of power plant condensers

Worldwide power production is rapidly increasing to meet the expanding needs of growing world population and technological advancements. Currently, water-cooled thermal power plants are the mainstream because of their high thermal efficiency, in which the waste heat is generally being removed by cooling towers and cooling ponds. In the US alone, more than 99% of thermal power plants utilize some form of water cooling technologies today,⁵⁰ and power plants use 41% of the freshwater draw with 3% of water lost to the air, which is a direct challenge to resolving widespread water scarcity and frequent droughts.³²¹ Globally, water scarcity is a serious issue, especially in those areas such as northern Africa, the Middle East, and India where electrification is also projected to grow rapidly. Air-cooled (i.e., dry-cooled) techniques, as an alternative to water cooling, trade the water consumption with plant efficiency, cost (accounting for up to a 9% increase in the leveled cost of electricity [LCOE]), and robustness (power plant efficiency derates 1% per 3°C increase in ambient

TABLE IV. Dew water harvesting enabled by nighttime radiative sky cooling.

Material	Location (climate condition)	Cooling Performance (condensation rate)	Reference
Thin foil (0.39 mm thick) made of polyethylene embedded with TiO_2 and BaSO_4 microspheres, and a polyvinyl chloride plastic sheet (4 mm)	Netherlands (marine climate)	Average $0.15 \pm 0.05 \text{ l}/(\text{m}^2 \text{ day})$ over a 1.5-year period	Jacobs <i>et al.</i> ¹⁶⁹
Thin foil (0.39 mm thick) made of small TiO_2 and BaSO_4 microspheres embedded in a matrix of low-density polyethylene (LDPE)	Croatia (Mediterranean coast)	Yearly average $0.055 \text{ l}/(\text{m}^2 \text{ day})$ in Zadar and $0.025 \text{ l}/(\text{m}^2 \text{ day})$ in Komiza	Muselli <i>et al.</i> ³¹³
Pigmented polyethylene foils (pigments are TiO_2 and BaSO_4 microspheres embedded in a $350 \mu\text{m}$ thickness polyethylene foil	Dhahran, Saudi Arabia (dry)	$0.22 \text{ l}/(\text{m}^2 \text{ day})$ during a single night of operation	Gandhidasan and Abualhamayel ³¹⁸
Galvanized iron roof	Kothara, India (hot and dry)	Average $0.098 \text{ l}/(\text{m}^2 \text{ day})$ during the dry season	Sharan <i>et al.</i> ⁴⁴
Pigmented polymer foils (pigments are the $\text{SiO}_2/\text{TiO}_2$ composite)	Dodoma, Tanzania (semi-arid)	Average $0.04 \text{ l}/(\text{m}^2 \text{ day})$ during a dry month	Nilsson <i>et al.</i> ³¹⁹

temperature above the design point), as shown in Fig. 33(a). In such circumstances, passive and enhanced cooling technologies are appealing. Recent studies propose that radiative sky cooling can be a supplemental cooling option for both wet-cooled and dry-cooled thermal power plants.^{150,322} Radiative sky cooling could potentially both reduce the amount of water to be evaporated by cooling towers and outperform air-cooled systems in terms of efficiency.

Though a great potential has been identified for power plant cooling, there is not much investigation on radiative sky cooling for power plant application yet. Olwi and Sabbagh^{323,324} presented a modeling study to show the potential of using covered ponds as a cooling system for power plants in arid areas. Numerical study shows that a total heat rejection of 150 W/m^2 could be obtained on average. The biggest challenge in utilizing radiative sky cooling for power plants is its intrinsically low energy density ($\sim 100 \text{ W/m}^2$), while the need for the cooling of the power plant condenser is on the order of 100 MW . This indicates the need of large area of land and high operational cost to circulate heat transfer fluid between the power plant condenser and radiative sky cooling panels. It is important to note that not all thermal power plants favor radiative sky cooling technology, such as those power plants located at water abundant areas. On the other hand, most of the concentrating solar power (CSP) plants are located in deserts where solar resource is abundant, and water is scarce. Coupling of radiative sky cooling with CSP seems a perfect match since radiative sky cooling prefers the low nighttime temperatures and clear skies.¹⁵⁰ Assuming the nighttime radiative sky cooling system has the same size as the solar collector field, Dyreson and Miller¹⁵⁰ performed simulations and showed that the system can provide over 90% of the required cooling. However, their feasibility study requires two massive storage tanks, and the working temperature of the water seems to be rather high ($39\text{--}63^\circ\text{C}$), which implies higher backpressure in the condenser and thus lower thermal efficiency. Zeyghami and Khalili³²² investigated daytime radiative sky cooling for an air-cooled CSP plant that uses supercritical carbon dioxide (CO_2) cycles. The results show that it is possible to overcome the efficiency loss due to air cooling by 3%–7.5% depending on the hot source temperature.

Zhang *et al.*³²⁵ recently introduced a two-stage radiative cooled-cold collection and storage system to overcome the energy density mismatch problem, as shown in Fig. 33(b). The first stage is radiative cooling modules for local cold collection and storage. The selective radiative cooling surface material is laminated on top of the module. The second stage is larger size cold water storage tanks, which connect to multiple radiative cooling modules. A tree-like pipe network was proposed to minimize the pumping energy input for cold collection. Modeling has been conducted to study the benefits after applying the radiative cooling system to a wet-cooled CSP power plant (Mojave solar project). With the field aperture of the radiative cooling system the same as the power plant's solar field, up to 83% of water use can be saved if the cooling system works during both daytime and nighttime [see Figs. 33(c) and 33(d)]. Note that for some CSP systems, for example, the parabolic trough system, there already exist a solar farm and a hydraulic system for transferring thermal energy. If the solar farm can be turned into a radiative sky cooling farm at night using dual functional panels, the initial and maintenance costs for radiative sky cooling power plant application can be greatly reduced. Future research studies are still needed to identify optimal designs and operation strategies to show water savings while improving (or at least not affecting) the power plant thermal efficiencies.

E. Other applications

With daytime subambient radiative sky cooling now demonstrated, many other possible applications can be explored, especially with a scalable-manufactured low-cost material. For example, radiative sky cooling can be used for the storage of some fruits, vegetables, or medicine in the decentralized community in off-grid remote areas or in developing countries. Ezekew³²⁶ developed a cooling box ($0.6 \times 0.3 \times 0.5 \text{ m}$) with a heat pipe assisted sky radiative cooler. During a 24-h experiment, the lowest temperature in the box was 12.8°C (ambient 20°C) and 15°C (ambient 32°C) at night and during the day, respectively. The radiative cooling box's passive mode of operation and its portable nature make it suitable for use in remote areas. Other researchers have attempted to use radiative sky cooling to

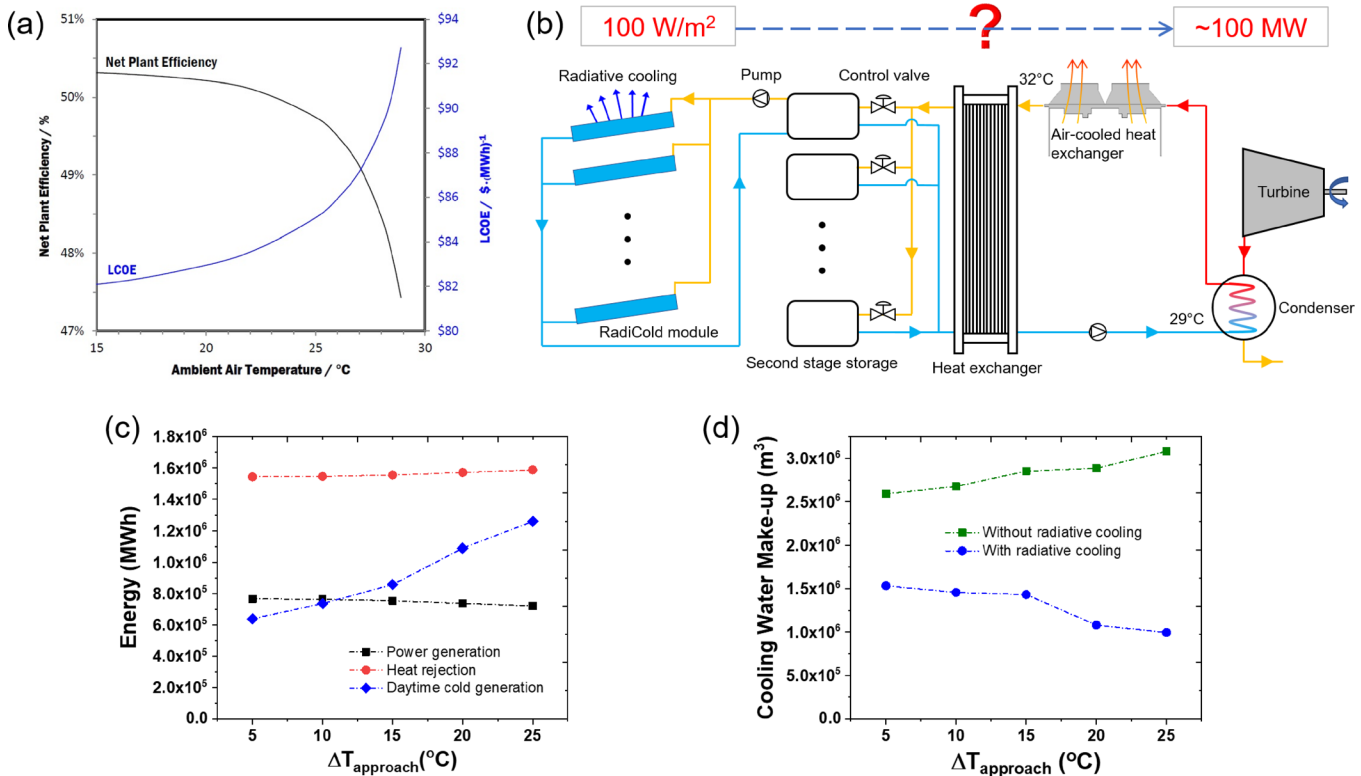


FIG. 33. Radiative sky cooling for power plant applications. (a) Variation in power plant energy conversion efficiency and leveled cost of electricity (LCOE) as a function of ambient air temperature for the air cooled heat exchanger. (b) Energy density mismatch is the biggest obstacle for implementing radiative sky cooling in power plants. A two-stage radiative cooled-cold collection and storage system was proposed to overcome the energy density mismatch problem for power plant supplementary cooling.^{52,325} The first stage is radiative cooling modules for local cold collection and storage. The selective surface structure is to be laminated on top of the module to provide cooling power. The second stage storage is a larger size cold water storage tank, which connects to multiple radiative cooling modules. (c) Power production and heat rejection by the power block and cold generation capacity of the radiative cooling system. $\Delta T_{\text{approach}}$ is the difference between the condenser inlet temperature and the web-bulb ambient temperature. The radiative sky cooling system is assumed to have the same size as and the CSP power plant solar field. The heat rejection by the power block and cold generation by the cooling system both increase, with the latter at a higher rate. (d) Annual cooling water make-up as a function of $\Delta T_{\text{approach}}$. Without the radiative sky cooling system, the cooling water make-up increases due to the increasing heat rejection. With the radiative sky cooling system, the cooling water make-up decreases because the system cold generation capacity goes up at a higher rate than the heat rejection.

enhance the performance of solar still. Haddad *et al.*³²⁷ proposed to store the nighttime radiative sky cooling energy in the solar still's packed bed condenser, then the cooling energy can be used during the day to condense vapor produced by the solar still. Recently, Mu *et al.*³²⁸ demonstrated an ultrathin thermoelectric generator that can directly convert heat from the environment into electricity by using radiative sky cooling. The idea is that electricity can be generated with zero energy input. With about 4 K temperature drop (across the thermoelectric generator) achieved by using the radiative cooling emitter, the output voltage of the thermoelectric generator reached up to 0.5 mV, and exhibited a continuous average 0.18 mV for 24 h operation.

In recent years, there have been significant advances in human body cooling by using visible-opaque, but infrared-transparent textiles in the indoor environment.^{329,330} There is also attempt to use radiative sky cooling for human body cooling in the outdoors, which requires the textile material to have both high reflection for solar irradiation and high transmission for human body thermal radiation. Cai *et al.*⁴⁹ developed a novel textile material by embedding zinc oxide nanoparticles (NPs) into nanoporous polyethylene (ZnO-PE), as shown in

Figs. 34(a) and 34(b). The reflection of solar irradiation is more than 90%, while the transmissivity of human body thermal radiation can be higher than 80% [Fig. 34(c)]. By covering the textile material on a simulated skin, the authors showed that the material can enable the simulated skin to avoid overheating by more than 10 °C, compared to cotton under typical outdoor environment with peak solar irradiation over 900 W/m², which has demonstrated radiative sky cooling for outdoor personal cooling. The nanoporous polyethylene can be potentially fabricated in large-scale for industrial fabric production.³³¹

V. SUMMARY

As the ultimate heat sink for the earth, the great potential of using radiative sky cooling without consuming external energy has been long recognized, but the practical applications have been largely fallen behind its potential for several decades. Recent advances on daytime radiative sky cooling materials have revived the interest world-wide in this field. In order to have the net cooling effect under the sunlight, the material should possess larger than 95% reflection of solar irradiation. As evidenced in this review, a list of nanophotonic materials,³¹

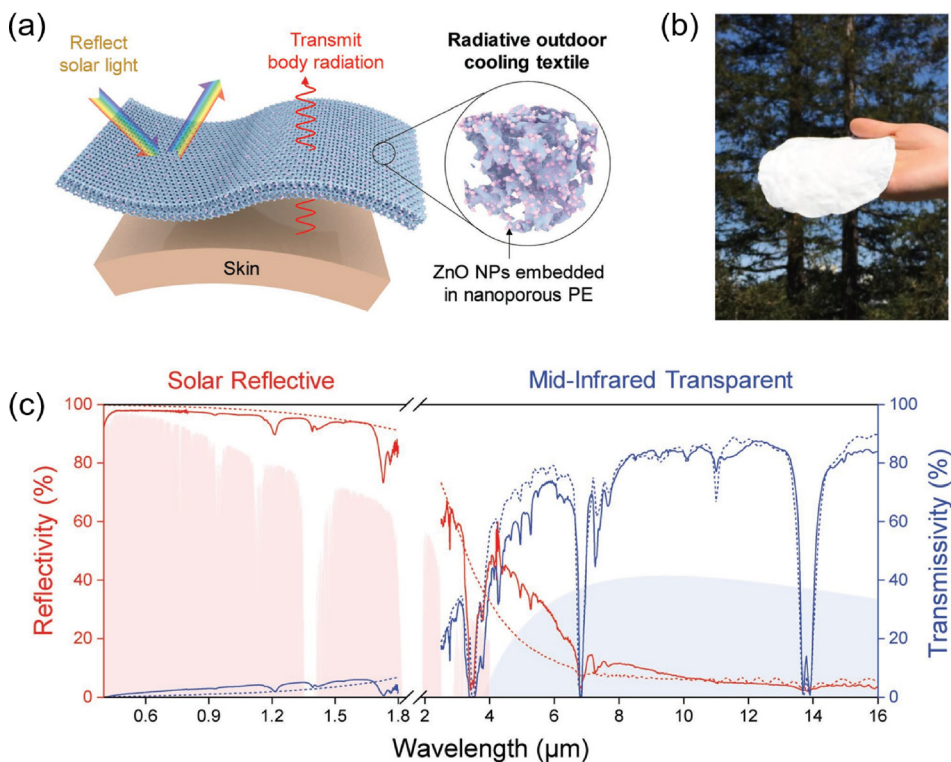


FIG. 34. Spectrally selective nanocomposite textile uses daytime radiative sky cooling for outdoor personal cooling.⁴⁹ (a) A novel textile material that has high reflection for solar irradiation and high transmission for human body thermal radiation enabled by embedding zinc oxide nanoparticles (ZnO-PE). (b) Photo of the ZnO-PE textile material under the sun. (c) Measured (solid curves) and simulated (dashed curves) reflectivity and transmissivity spectra of the ZnO-PE textile at the wavelength range between $0.3\text{ }\mu\text{m}$ and $16\text{ }\mu\text{m}$. Figures reproduced with permission from Cai *et al.* *Adv. Mater.* **30**, 1802512 (2018). Copyright 2018 Wiley.

metamaterials,³² paints, and coatings⁵⁸ have been developed. Great progresses have been made in terms of material fabrication. A scalable-manufactured polymer-based daytime radiative cooling material has been successfully demonstrated, which suggest that this technique can be applied on a large-scale at a low cost.³² The integration of daytime radiative sky cooling materials with new functionality, e.g., self-adaptive cooling,²⁰⁷ could play a significant role in improving the efficiency of this technique.

Great progresses have also been made in terms of demonstrating radiative sky cooling in real-world applications. The benefits of radiative sky cooling come from various aspects, including cooling electricity saving, downsizing the HVAC system in buildings, increase in solar cell power generation and efficiency gain, and water saving for power plants. For system integration, passive radiative sky cooling is currently the most promising approach due to its system simplicity, low cost, and low maintenance. Solar cell cooling by simultaneously reflecting the sub-band-gap and ultraviolet solar irradiation, and enhancing radiative sky cooling with a top layer on the existing solar cell structure is very appealing.⁴¹ For active radiative sky cooling systems, it is highly recommended to take advantage of the existing infrastructure, for example, the existing hydraulic loop and air ducts in the buildings. With daytime radiative sky cooling demonstrated, a radiative sky cooling system can be built to run 24 h continuously, which renders even larger energy savings from the system.⁵²

Performance of radiative sky cooling systems largely depends on the local meteorological conditions, such as the atmospheric constituents (primarily water vapor), sky conditions (i.e., clear or overcast), local wind speeds, and the constantly changing weather conditions (i.e., unstable). The effect of atmospheric water vapor on the radiative

sky cooling system efficiency can be detrimental. Though radiative sky cooling effect could still be available when the sky is partially or even completely covered (if the cloud base is high), the cooling power could be substantially reduced. As such, it is important to identify those locations (climates) that are most suitable for the deployment of radiative sky cooling technology. As the energy situation and environmental issues become more severe in the 21st century, radiative sky cooling is expected to play an important role in reducing energy consumption in buildings, mitigating the urban heat island effect, resolving water and environmental issues, and even fighting against the global warming effect³³² in the near future.

ACKNOWLEDGMENTS

The authors acknowledge the financial support of this work from the U.S. Department of Energy's Advanced Research Projects Agency—Energy (ARPA-E) under Contract No. DE-AR0000580.

REFERENCES

- ¹Cooling a Warming Planet: A Global Air Conditioning Surge, http://e360.yale.edu/features/cooling_a_warming_planet_a_global_air_conditioning_surge for Yale E360; accessed 11 November 2017.
- ²J. Steven Brown and P. A. Domanski, “Review of alternative cooling technologies,” *Appl. Therm. Eng.* **64**, 252–262 (2014).
- ³B. I. Cook, J. E. Smerdon, R. Seager, and S. Coats, “Global warming and 21st century drying,” *Clim. Dyn.* **43**, 2607–2627 (2014).
- ⁴J. Henley, “World set to use more energy for cooling than heating,” in *The Guardian* (2015).
- ⁵D. J. Fixsen, “The temperature of the cosmic microwave background,” *Astrophys. J.* **707**, 916 (2009).

- ⁶G. B. Smith and C.-G. S. Granqvist, *Green Nanotechnology: Solutions for Sustainability and Energy in the Built Environment* (CRC Press, 2010).
- ⁷K. Y. Kondrat'yev, *Radiative Heat Exchange Atmosphere* (Pergamon, 1965).
- ⁸S. Chu, Y. Cui, and N. Liu, "The path towards sustainable energy," *Nat. Mater.* **16**, 16–22 (2017).
- ⁹M. M. Hossain and M. Gu, "Radiative cooling: Principles, progress, and potentials," *Adv. Sci.* **3**, 1500360 (2016).
- ¹⁰J. L. Miller, "Passive cooling doesn't cost the planet," *Phys. Today* **70**(4), 16–18 (2017).
- ¹¹A. K. Stark, "Methods for rejecting daytime waste heat to outer space," *Natl. Sci. Rev.* **4**, 789–790 (2017).
- ¹²S. Buddhiraju, P. Santhanam, and S. Fan, "Thermodynamic limits of energy harvesting from outgoing thermal radiation," *Proc. Natl. Acad. Sci.* **115**, E3609–E3615 (2018).
- ¹³A. K. Head, "Method and means for producing refrigeration by selective radiation," U.S. patent US3043112A (10 July 1962).
- ¹⁴M. N. Bahadori, "Passive cooling systems in Iranian architecture," *Sci. Am.* **238**, 144–155 (1978).
- ¹⁵E. Clark and P. Berdahl, *Radiative Cooling: Resource and Applications* (Sponsor Development US Department of Energy, 1981), p. 219.
- ¹⁶C. G. Granqvist and A. Hjortsberg, "Surfaces for radiative cooling: Silicon monoxide films on aluminum," *Appl. Phys. Lett.* **36**, 139–141 (1980).
- ¹⁷P. Berdahl, "Radiative cooling with MgO and/or LiF layers," *Appl. Opt.* **23**, 370 (1984).
- ¹⁸C. D. Reid and E. D. McAlister, "Measurement of spectral emissivity from 2μ to 15μ ," *JOSA* **49**, 78–82 (1959).
- ¹⁹A. Ben-Shalom *et al.*, "Sky radiance at wavelengths between 7 and 14 μm : Measurement, calculation, and comparison with lowtran-4 predictions," *Appl. Opt.* **19**, 838 (1980).
- ²⁰E. E. Bell, L. Eisner, J. Young, and R. A. Oetjen, "Spectral radiance of sky and terrain at wavelengths between 1 and 20 microns II: sky measurements," *J. Opt. Soc. Am.* **50**, 1313 (1960).
- ²¹M. Hori *et al.*, "In-situ measured spectral directional emissivity of snow and ice in the 8–14 μm atmospheric window," *Remote Sens. Environ.* **100**, 486–502 (2006).
- ²²P. Berdahl and R. Fromberg, "The thermal radiance of clear skies," *Sol. Energy* **29**, 299–314 (1982).
- ²³M. Martin and P. Berdahl, "Summary of results from the spectral and angular sky radiation measurement program," *Sol. Energy* **33**, 241–252 (1984).
- ²⁴A. P. Tsoty, A. S. Granovskiy, A. V. Baranenko, and D. A. Tsoty, "Effectiveness of a night radiative cooling system in different geographical latitudes," *AIP Conf. Proc.* **1876**, 020060 (2017).
- ²⁵S. Zhang and J. Niu, "Cooling performance of nocturnal radiative cooling combined with microencapsulated phase change material (MPCM) slurry storage," *Energy Build.* **54**, 122–130 (2012).
- ²⁶A. Arigiriou, M. Santamouris, and D. N. Assimakopoulos, "Assessment of the radiative cooling potential of a collector using hourly weather data," *Energy* **19**, 879–888 (1994).
- ²⁷M. Martin and P. Berdahl, "Characteristics of infrared sky radiation in the United States," *Sol. Energy* **33**, 321–336 (1984).
- ²⁸T. S. Eriksson, E. M. Lushiku, and C. G. Granqvist, "Materials for radiative cooling to low temperature," *Sol. Energy Mater.* **11**, 149–161 (1984).
- ²⁹R. Family and M. P. Mengüç, "Materials for radiative cooling: A review," *Procedia Environ. Sci.* **38**, 752–759 (2017).
- ³⁰C. G. Granqvist, "Solar energy materials for thermal applications," in *Kirk-Othmer Encyclopedia of Chemical Technology* (John Wiley & Sons, Inc., 2017).
- ³¹A. P. Raman, M. A. Anoma, L. Zhu, E. Rephaeli, and S. Fan, "Passive radiative cooling below ambient air temperature under direct sunlight," *Nature* **515**, 540–544 (2014).
- ³²Y. Zhai *et al.*, "Scalable-manufactured randomized glass-polymer hybrid metamatteiral for daytime radiative cooling," *Science* **355**, 1062–1066 (2017).
- ³³S. Fan and A. Raman, "Metamaterials for radiative sky cooling," *Natl. Sci. Rev.* **5**, 132–133 (2018).
- ³⁴X. Lu, P. Xu, H. Wang, T. Yang, and J. Hou, "Cooling potential and applications prospects of passive radiative cooling in buildings: The current state-of-the-art," *Renewable Sustainable Energy Rev.* **65**, 1079–1097 (2016).
- ³⁵A. Royne, C. J. Dey, and D. R. Mills, "Cooling of photovoltaic cells under concentrated illumination: A critical review," *Sol. Energy Mater. Sol. Cells* **86**, 451–483 (2005).
- ³⁶U. Eicker and A. Dalibard, "Photovoltaic-thermal collectors for night radiative cooling of buildings," *Sol. Energy* **85**, 1322–1335 (2011).
- ³⁷M. G. Meir, J. B. Rekstad, and O. M. Løvvik, "A study of a polymer-based radiative cooling system," *Sol. Energy* **73**, 403–417 (2002).
- ³⁸K. Zhang, D. Zhao, X. Yin, R. Yang, and G. Tan, "Energy saving and economic analysis of a new hybrid radiative cooling system for single-family houses in the USA," *Appl. Energy* **224**, 371–381 (2018).
- ³⁹J. Yellott, "Utilization of sun and sky radiation for heating and cooling of buildings," *ASHRAE J. Am. Soc. Heat. Refrig. Air Cond. Eng.* **15**, 31–42 (1973).
- ⁴⁰L. Zhu, A. P. Raman, and S. Fan, "Radiative cooling of solar absorbers using a visibly transparent photonic crystal thermal blackbody," *Proc. Natl. Acad. Sci.* **112**, 12282–12287 (2015).
- ⁴¹W. Li, Y. Shi, K. Chen, L. Zhu, and S. Fan, "A comprehensive photonic approach for solar cell cooling," *ACS Photonics* **4**, 774–782 (2017).
- ⁴²D. Du, J. Darkwa, and G. Kokogiannakis, "Thermal management systems for photovoltaics (PV) installations: A critical review," *Sol. Energy* **97**, 238–254 (2013).
- ⁴³S.-H. Wu and M. L. Povinelli, "Solar heating of GaAs nanowire solar cells," *Opt. Express* **23**, A1363–A1372 (2015).
- ⁴⁴G. Sharan, D. Beysens, and I. Milimouk-Melnytchouk, "A study of dew water yields on Galvanized iron roofs in Kothara (North-West India)," *J. Arid Environ.* **69**, 259–269 (2007).
- ⁴⁵O. Clus *et al.*, "Comparison of various radiation-cooled dew condensers using computational fluid dynamics," *Desalination* **249**, 707–712 (2009).
- ⁴⁶J. F. Maestre-Valero, R. Ragab, V. Martínez-Alvarez, and A. Baille, "Estimation of dew yield from radiative condensers by means of an energy balance model," *J. Hydrol.* **460–461**, 103–109 (2012).
- ⁴⁷G. Sharan, "Harvesting dew with radiation cooled condensers to supplement drinking water supply in semi-arid," *Int. J. Serv. Learn. Eng. Humanit. Eng. Soc. Entrepreneur* **6**, 130–150 (2011).
- ⁴⁸D. Carvajal *et al.*, "Roof-integrated dew water harvesting in Combarbalá, Chile," *J. Water Supply Res. Technol. - Aqua* **67**, 357–374 (2018).
- ⁴⁹L. Cai *et al.*, "Spectrally selective nanocomposite textile for outdoor personal cooling," *Adv. Mater.* **30**, 1802152 (2018).
- ⁵⁰A. K. Stark and J. F. Klausner, "An R&D strategy to decouple energy from water," *Joule* **1**, 416–420 (2017).
- ⁵¹E. A. Goldstein, A. P. Raman, and S. Fan, "Sub-ambient non-evaporative fluid cooling with the sky," *Nat. Energy* **2**, 17143 (2017).
- ⁵²D. Zhao *et al.*, "Subambient cooling of water: Towards real-world applications of daytime radiative cooling," *Joule* **3**, 111–123 (2019).
- ⁵³E. du Marchie van Voorthuysen and R. Roes, "Blue sky cooling for parabolic trough plants," *Energy Procedia* **49**, 71–79 (2014).
- ⁵⁴C. G. Granqvist and A. Hjortsberg, "Radiative cooling to low temperatures: General considerations and application to selectively emitting SiO films," *J. Appl. Phys.* **52**, 4205–4220 (1981).
- ⁵⁵S. Catalanotti *et al.*, "The radiative cooling of selective surfaces," *Sol. Energy* **17**, 83–89 (1975).
- ⁵⁶M. Hanif, T. M. I. Mahlia, A. Zare, T. J. Saksahdan, and H. S. C. Metselaar, "Potential energy savings by radiative cooling system for a building in tropical climate," *Renewable Sustainable Energy Rev.* **32**, 642–650 (2014).
- ⁵⁷J. Testa and M. Krarti, "A review of benefits and limitations of static and switchable cool roof systems," *Renewable Sustainable Energy Rev.* **77**, 451–460 (2017).
- ⁵⁸J. Mandal *et al.*, "Hierarchically porous polymer coatings for highly efficient passive daytime radiative cooling," *Science* **362**, 315–319 (2018).
- ⁵⁹T. L. Bergman, F. P. Incropera, D. P. DeWitt, and A. S. Lavine, *Fundamentals of Heat and Mass Transfer* (John Wiley & Sons, 2011).
- ⁶⁰G. Olivetti, N. Arcuri, M. De Simone, and R. Bruno, "Experimental evaluations of the building shell radiant exchange in clear sky conditions," *Sol. Energy* **86**, 1785–1795 (2012).
- ⁶¹T. M. Crawford and C. E. Duchon, "An improved parameterization for estimating effective atmospheric emissivity for use in calculating daytime downwelling longwave radiation," *J. Appl. Meteorol.* **38**, 474–480 (1999).

- ⁶²J. A. Voogt and T. R. Oke, "Thermal remote sensing of urban climates," *Remote Sens. Environ.* **86**, 370–384 (2003).
- ⁶³N. G. Loeb *et al.*, "Observed changes in top-of-the-atmosphere radiation and upper-ocean heating consistent within uncertainty," *Nat. Geosci.* **5**, 110–113 (2012).
- ⁶⁴A. K. Ångström, *A Study of the Radiation of the Atmosphere: Based upon Observations of the Nocturnal Radiation during Expeditions to Algeria and to California* (Smithsonian Institution, 1915), Vol. 65.
- ⁶⁵D. Brunt, "Notes on radiation in the atmosphere. I," *Q. J. R. Meteorol. Soc.* **58**, 389–420 (1932).
- ⁶⁶H. E. Bennett, J. M. Bennett, and M. R. Nagel, "Distribution of infrared radiance over a clear sky," *JOSA* **50**, 100–106 (1960).
- ⁶⁷R. M. Goody, *Atmospheric Radiation Volume 1: Theoretical Basis* (Clarendon Press, Oxford, 1964).
- ⁶⁸R. W. Bliss, Jr., "Atmospheric radiation near the surface of the ground: A summary for engineers," *Sol. Energy* **5**, 103–120 (1961).
- ⁶⁹W. C. Swinbank, "Long-wave radiation from clear skies," *Q. J. R. Meteorol. Soc.* **89**, 339–348 (1963).
- ⁷⁰S. B. Idso and R. D. Jackson, "Thermal radiation from the atmosphere," *J. Geophys. Res.* **74**, 5397–5403, <https://doi.org/10.1029/JC074i023p05397> (1969).
- ⁷¹W. Brutsaert, "On a derivable formula for long-wave radiation from clear skies," *Water Resour. Res.* **11**, 742–744, <https://doi.org/10.1029/WR011i005p00742> (1975).
- ⁷²Cold Facts on Global Warming, <http://www.randombio.com/co2.html>, see Figure 4 for absorption of ultraviolet, visible, and infrared radiation by various gases in the atmosphere; accessed 7 August 2018.
- ⁷³J. P. Peixoto and A. H. Oort, *Physics of Climate* (AIP-Press, 1992).
- ⁷⁴E. M. Lushiku, A. Hjortsberg, and C. G. Granqvist, "Radiative cooling with selectively infrared-emitting ammonia gas," *J. Appl. Phys.* **53**, 5526–5530 (1982).
- ⁷⁵J. T. Kiehl and K. E. Trenberth, "Earth's annual global mean energy budget," *Bull. Am. Meteorol. Soc.* **78**, 197–208 (1997).
- ⁷⁶C. Riordan and R. Hulstrom, "What is an air mass 1.5 spectrum? (solar cell performance calculations)," in *IEEE Conference on Photovoltaic Specialists* (1990), Vol. 2, pp. 1085–1088.
- ⁷⁷Solar Spectral Irradiance: Air Mass 1.5, <https://rredc.nrel.gov/solar//spectra/am1.5/#about> for Air mass (AM) 1.5 direct solar spectrum; accessed 19 February 2019.
- ⁷⁸E. Rephaeli, A. Raman, and S. Fan, "Ultrabroadband photonic structures to achieve high-performance daytime radiative cooling," *Nano Lett.* **13**, 1457–1461 (2013).
- ⁷⁹X. Sun, Y. Sun, Z. Zhou, M. A. Alam, and P. Bermel, "Radiative sky cooling: Fundamental physics, materials, structures, and applications," *Nanophotonics* **6**, 997 (2017).
- ⁸⁰C. N. Awanou, "Clear sky emissivity as a function of the zenith direction," *Renewable Energy* **13**, 227–248 (1998).
- ⁸¹X. Berger and J. Bathiebo, "Directional spectral emissivities of clear skies," *Renewable Energy* **28**, 1925–1933 (2003).
- ⁸²A. W. Harrison, "Effect of atmospheric humidity on radiation cooling," *Sol. Energy* **26**, 243–247 (1981).
- ⁸³R. A. Oetjen, E. E. Bell, J. Young, and L. Eisner, "Spectral radiance of sky and terrain at wavelengths between 1 and 20 microns. I. Instrumentation," *JOSA* **50**, 1308–1313 (1960).
- ⁸⁴T. J. Garrett, L. F. Radke, and P. V. Hobbs, "Aerosol effects on cloud emissivity and surface longwave heating in the arctic," *J. Atmos. Sci.* **59**, 769–778 (2002).
- ⁸⁵X. Berger, J. Bathiebo, F. Kieno, and C. N. Awanou, "Clear sky radiation as a function of altitude," *Renewable Energy* **2**, 139–157 (1992).
- ⁸⁶X. Berger, B. Cubizolles, and I. Donet, "Radio-sounding data for the determination of the infra-red sky radiation," *Sol. Wind Technol.* **5**, 353–363 (1988).
- ⁸⁷L. Alados-Arboledas and J. I. Jimenez, "Day-night differences in the effective emissivity from clear skies," *Boundary-Layer Meteorol.* **45**, 93–101 (1988).
- ⁸⁸Y. Iijima and M. Shinoda, "The influence of seasonally varying atmospheric characteristics on the intensity of nocturnal cooling in a high mountain hollow," *J. Appl. Meteorol.* **41**, 734–743 (2002).
- ⁸⁹C. Ruckstuhl, R. Philipona, J. Morland, and A. Ohmura, "Observed relationship between surface specific humidity, integrated water vapor, and longwave downward radiation at different altitudes," *J. Geophys. Res. Atmos.* **112**, D03302, <https://doi.org/10.1029/2006JD007850> (2007).
- ⁹⁰W. B. Grant, "Water vapor absorption coefficients in the 8–13-μm spectral region: A critical review," *Appl. Opt.* **29**, 451–462 (1990).
- ⁹¹J. Duan *et al.*, "GPS meteorology: Direct estimation of the absolute value of precipitable water," *J. Appl. Meteorol.* **35**, 830–838 (1996).
- ⁹²A. W. Harrison and M. R. Walton, "Radiative cooling of TiO₂ white paint," *Sol. Energy* **20**, 185–188 (1978).
- ⁹³C. Y. Tso, K. C. Chan, and C. Y. H. Chao, "A field investigation of passive radiative cooling under Hong Kong's climate," *Renewable Energy* **106**, 52–61 (2017).
- ⁹⁴T. Suichi, A. Ishikawa, Y. Hayashi, and K. Tsuruta, "Performance limit of daytime radiative cooling in warm humid environment," *AIP Adv.* **8**, 055124 (2018).
- ⁹⁵P. Berdahl and M. Martin, "Emissivity of clear skies," *Sol. Energy* **32**, 663–664 (1984).
- ⁹⁶D. W. Deering and P. Leone, "A sphere-scanning radiometer for rapid directional measurements of sky and ground radiance," *Remote Sens. Environ.* **19**, 1–24 (1986).
- ⁹⁷E. M. Lushiku and C.-G. Granqvist, "Radiative cooling with selectively infrared-emitting gases," *Appl. Opt.* **23**, 1835–1843 (1984).
- ⁹⁸A. Skartveit, J. A. Olseth, G. Czeplak, and M. Rommel, "On the estimation of atmospheric radiation from surface meteorological data," *Sol. Energy* **56**, 349–359 (1996).
- ⁹⁹J. E. A. Selby and R. M. McClatchey, *Atmospheric Transmittance from 0.25 to 28.5/micrometers Computer Code LOWTRAN 2* (Air Force Cambridge Research Labs L G, Hanscom Field, MA, 1972).
- ¹⁰⁰J. E. Selby and R. A. McClatchey, *Atmospheric Transmittance from 0.25 to 28.5 Microns: Computer Code LOWTRAN 3* (Air Force Cambridge Research Labs, Hanscom AFB MA, 1975).
- ¹⁰¹O. P. Manley, H. J. P. Smith, Y. M. Treve, J. W. Carpenter, and T. C. Degges, *OPTIR II* (Visidyne Inc., Woburn, MA, 1971).
- ¹⁰²J. E. A. Selby, F. X. Kneizys, J. H. Chetwynd, and R. A. McClatchey, *Atmospheric Transmittance/Radiance: Computer Code LOWTRAN 4* (Air Force Geophysics Lab, Hanscom AFB, MA, 1978).
- ¹⁰³T. S. Eriksson and C. G. Granqvist, "Radiative cooling computed for model atmospheres," *Appl. Opt.* **21**, 4381 (1982).
- ¹⁰⁴F. X. Kneizys, E. P. Shettle, and W. O. Gallery, "Atmospheric transmittance and radiance: The LOWTRAN 5 code," in *Atmospheric Transmission* (International Society for Optics and Photonics, 1981), Vol. 0277, pp. 116–125.
- ¹⁰⁵X. Berger and J. Bathiebo, "From spectral clear sky emissivity to total clear sky emissivity," *Sol. Wind Technol.* **6**, 551–556 (1989).
- ¹⁰⁶A. J. Prata, "A new long-wave formula for estimating downward clear-sky radiation at the surface," *Q. J. R. Meteorol. Soc.* **122**, 1127–1151 (1996).
- ¹⁰⁷F. X. Kneizys, E. P. Shettle, L. W. Abreu, J. H. Chetwynd, and G. P. Anderson, *Users Guide to LOWTRAN 7* (Air Force Geophysics Lab, Hanscom AFB, MA, 1988).
- ¹⁰⁸A. Berk, L. S. Bernstein, and D. C. Robertson, *MODTRAN: A Moderate Resolution Model for LOWTRAN* (Spectral Sciences Inc., Burlington, MA, 1987).
- ¹⁰⁹MODTRAN®, <http://modtran.spectral.com/> for introduction about MODTRAN; accessed 30 September 2018.
- ¹¹⁰S. D. Lord, "A new software tool for computing Earth's atmospheric transmission of near- and far-infrared radiation," Report No. NASA-TM-103957 (1992).
- ¹¹¹S. A. Lord, <https://atran.sofia.usra.edu/cgi-bin/atran/atran.cgi> for introduction about ATRAN; accessed 4 April 2018 (1992).
- ¹¹²D. O. Staley and G. M. Jurica, "Effective atmospheric emissivity under clear skies," *J. Appl. Meteorol.* **11**, 349–356 (1972).
- ¹¹³M. Centeno, "New formulae for the equivalent night sky emissivity," *Sol. Energy* **28**, 489–498 (1982).
- ¹¹⁴R. Tang, Y. Etzion, and I. A. Meir, "Estimates of clear night sky emissivity in the Negev Highlands, Israel," *Energy Convers. Manage.* **45**, 1831–1843 (2004).
- ¹¹⁵P. Berdahl, M. Martin, and F. Sakkal, "Thermal performance of radiative cooling panels," *Int. J. Heat Mass Transfer* **26**, 871–880 (1983).

- ¹¹⁶M. Li, Y. Jiang, and C. F. M. Coimbra, "On the determination of atmospheric longwave irradiance under all-sky conditions," *Sol. Energy* **144**, 40–48 (2017).
- ¹¹⁷S. B. Idso, "A set of equations for full spectrum and 8- to 14- μm and 10.5- to 12.5- μm thermal radiation from cloudless skies," *Water Resour. Res.* **17**, 295–304, <https://doi.org/10.1029/WR017I002p00295> (1981).
- ¹¹⁸S. Vall and A. Castell, "Radiative cooling as low-grade energy source: A literature review," *Renewable Sustainable Energy Rev.* **77**, 803–820 (2017).
- ¹¹⁹M. Zeyghami, D. Y. Goswami, and E. Stefanakos, "A review of clear sky radiative cooling developments and applications in renewable power systems and passive building cooling," *Sol. Energy Mater. Sol. Cells* **178**, 115–128 (2018).
- ¹²⁰B. Zhao, M. Hu, X. Ao, N. Chen, and G. Pei, "Radiative cooling: A review of fundamentals, materials, applications, and prospects," *Appl. Energy* **236**, 489–513 (2019).
- ¹²¹L. Evangelisti, C. Guattari, and F. Asdrubali, "On the sky temperature models and their influence on buildings energy performance: A critical review," *Energy Build.* **183**, 607–625 (2019).
- ¹²²R. Vidhi, "A review of underground soil and night sky as passive heat sink: Design configurations and models," *Energies* **11**, 2941 (2018).
- ¹²³E. L. Andreas and S. F. Ackley, "On the differences in ablation seasons of arctic and Antarctic Sea ice," *J. Atmos. Sci.* **39**, 440–447 (1982).
- ¹²⁴X. Berger, D. Burriot, and F. Garnier, "About the equivalent radiative temperature for clear skies," *Sol. Energy* **32**, 725–733 (1984).
- ¹²⁵A. C. Dilley and D. M. O'brien, "Estimating downward clear sky long-wave irradiance at the surface from screen temperature and precipitable water," *Q. J. R. Meteorol. Soc.* **124**, 1391–1401 (1998).
- ¹²⁶S. Niemelä, P. Räisänen, and H. Savijärvi, "Comparison of surface radiative flux parameterizations: Part I: Longwave radiation," *Atmos. Res.* **58**, 1–18 (2001).
- ¹²⁷J. P. Lhomme, J. J. Vacher, and A. Rocheteau, "Estimating downward long-wave radiation on the Andean Altiplano," *Agric. Meteorol.* **145**, 139–148 (2007).
- ¹²⁸J. E. Sicart, R. Hock, P. Ribstein, and J. P. Chazarin, "Sky longwave radiation on tropical Andean glaciers: Parameterization and sensitivity to atmospheric variables," *J. Glaciol.* **56**, 854–860 (2010).
- ¹²⁹B. A. Kimball, S. B. Idso, and J. K. Aase, "A model of thermal radiation from partly cloudy and overcast skies," *Water Resour. Res.* **18**, 931–936, <https://doi.org/10.1029/WR018i004p00931> (1982).
- ¹³⁰F. Kasten and G. Czeplak, "Solar and terrestrial radiation dependent on the amount and type of cloud," *Sol. Energy* **24**, 177–189 (1980).
- ¹³¹J. Schmetz, "Towards a surface radiation climatology: Retrieval of downward irradiances from satellites," *Atmos. Res.* **23**, 287–321 (1989).
- ¹³²P. Schmetz, J. Schmetz, and E. Raschke, "Estimation of daytime downward longwave radiation at the surface from satellite and grid point data," *Theor. Appl. Climatol.* **37**, 136–149 (1986).
- ¹³³T. Saitoh and T. Ono, "Utilization of seasonal sky radiation energy for space cooling," *J. Sol. Energy Eng.* **106**, 403–407 (1984).
- ¹³⁴M. Sugita and W. Brutsaert, "Cloud effect in the estimation of instantaneous downward longwave radiation," *Water Resour. Res.* **29**, 599–605, <https://doi.org/10.1029/92WR02352> (1993).
- ¹³⁵P. Chylek and V. Ramaswamy, "Simple approximation for infrared emissivity of water clouds," *J. Atmos. Sci.* **39**, 171–177 (1982).
- ¹³⁶P. J. Robinson and J. A. Davies, "Laboratory determinations of water surface emissivity," *J. Appl. Meteorol.* **11**, 1391–1393 (1972).
- ¹³⁷M. Aubinet, "Longwave sky radiation parametrizations," *Sol. Energy* **53**, 147–154 (1994).
- ¹³⁸NSRDB: 1991–2005 Update: TMY3, https://rredc.nrel.gov/solar/old_data/nsrdb/1991-2005/tmy3/ for obtaining meteorological data; accessed 12 September 2018.
- ¹³⁹A. Dai, T. R. Karl, B. Sun, and K. E. Trenberth, "Recent trends in cloudiness over the United States: A tale of monitoring inadequacies," *Bull. Am. Meteorol. Soc.* **87**, 597–606 (2006).
- ¹⁴⁰J. R. Minder, P. W. Mote, and J. D. Lundquist, "Surface temperature lapse rates over complex terrain: Lessons from the Cascade Mountains," *J. Geophys. Res. Atmos.* **115**, D14122, <https://doi.org/10.1029/2009JD013493> (2010).
- ¹⁴¹J. W. Salisbury and D. M. D'Aria, "Emissivity of terrestrial materials in the 8–14 μm atmospheric window," *Remote Sens. Environ.* **42**, 83–106 (1992).
- ¹⁴²A. R. Gentle and G. B. Smith, "Radiative heat pumping from the earth using surface phonon resonant nanoparticles," *Nano Lett.* **10**, 373–379 (2010).
- ¹⁴³A. R. Gentle and G. B. Smith, "A subambient open roof surface under the mid-summer sun," *Adv. Sci.* **2**, 1500119 (2015).
- ¹⁴⁴Z. Chen, L. Zhu, A. Raman, and S. Fan, "Radiative cooling to deep sub-freezing temperatures through a 24-h day-night cycle," *Nat. Commun.* **7**, 13729 (2016).
- ¹⁴⁵D. Michell and K. L. Biggs, "Radiation cooling of buildings at night," *Appl. Energy* **5**, 263–275 (1979).
- ¹⁴⁶C. G. Granqvist, *Materials Science for Solar Energy Conversion Systems* (Elsevier, 2013).
- ¹⁴⁷F. L. Test, R. C. Lessmann, and A. Johary, "Heat transfer during wind flow over rectangular bodies in the natural environment," *J. Heat Transfer* **103**, 262 (1981).
- ¹⁴⁸S. Sharples and P. S. Charlesworth, "Full-scale measurements of wind-induced convective heat transfer from a roof-mounted flat plate solar collector," *Sol. Energy* **62**, 69–77 (1998).
- ¹⁴⁹E. Skoplaki and J. A. Palyvos, "On the temperature dependence of photovoltaic module electrical performance: A review of efficiency/power correlations," *Sol. Energy* **83**, 614–624 (2009).
- ¹⁵⁰A. Dyreson and F. Miller, "Night sky cooling for concentrating solar power plants," *Appl. Energy* **180**, 276–286 (2016).
- ¹⁵¹K. D. Dobson, G. Hodes, and Y. Mastai, "Thin semiconductor films for radiative cooling applications," *Sol. Energy Mater. Sol. Cells* **80**, 283–296 (2003).
- ¹⁵²T. M. J. Nilsson, G. A. Niklasson, and C. G. Granqvist, "A solar reflecting material for radiative cooling applications: ZnS pigmented polyethylene," *Sol. Energy Mater. Sol. Cells* **28**, 175–193 (1992).
- ¹⁵³B. Bartoli *et al.*, "Nocturnal and diurnal performances of selective radiators," *Appl. Energy* **3**, 267–286 (1977).
- ¹⁵⁴M. Mostrel and B. Givoni, "Windscreens in radiant cooling," *Passive Sol. J. U. S.* **1**(4), 229 (2018).
- ¹⁵⁵Y. Mastai, Y. Diamant, S. T. Aruna, and A. Zaban, " TiO_2 nanocrystalline pigmented polyethylene foils for radiative cooling applications: Synthesis and characterization," *Langmuir* **17**, 7118–7123 (2001).
- ¹⁵⁶A. Golaka and R. H. B. Exell, "An investigation into the use of a wind shield to reduce the convective heat flux to a nocturnal radiative cooling surface," *Renewable Energy* **32**, 593–608 (2007).
- ¹⁵⁷A. M. Parsons and K. Sharp, "The effects of multiple covers with condensation and optical degradation of a polyethylene windscreens on the performance of a sky cooling system," *Int. J. Sustainable Energy* **38**, 469–485 (2018).
- ¹⁵⁸T. E. Johnson, "Radiation cooling of structures with infrared transparent wind screens," *Sol. Energy* **17**, 173–178 (1975).
- ¹⁵⁹A. Addeo *et al.*, "Light selective structures for large scale natural air conditioning," *Sol. Energy* **24**, 93–98 (1980).
- ¹⁶⁰A. Hjortsberg and C. G. Granqvist, "Radiative cooling with selectively emitting ethylene gas," *Appl. Phys. Lett.* **39**, 507–509 (1981).
- ¹⁶¹Z. Chen, L. Zhu, W. Li, and S. Fan, "Simultaneously and synergistically harvest energy from the sun and outer space," *Joule* **3**, 101–110 (2019).
- ¹⁶²S. N. Bathgate and S. G. Bosi, "A robust convection cover material for selective radiative cooling applications," *Sol. Energy Mater. Sol. Cells* **95**, 2778–2785 (2011).
- ¹⁶³N. A. Nilsson, T. S. Eriksson, and C. G. Granqvist, "Infrared-transparent convection shields for radiative cooling: Initial results on corrugated polyethylene foils," *Sol. Energy Mater. Sol. Cells* **12**, 327–333 (1985).
- ¹⁶⁴A. R. Gentle, K. L. Dybdal, and G. B. Smith, "Polymeric mesh for durable infra-red transparent convection shields: Applications in cool roofs and sky cooling," *Sol. Energy Mater. Sol. Cells* **115**, 79–85 (2013).
- ¹⁶⁵R. C. Youngquist and M. A. Nurje, "Achieving cryogenic temperatures in deep space using a coating," *Opt. Lett.* **41**, 1086–1089 (2016).
- ¹⁶⁶G. B. Smith, "Amplified radiative cooling via optimised combinations of aperture geometry and spectral emittance profiles of surfaces and the atmosphere," *Sol. Energy Mater. Sol. Cells* **93**, 1696–1701 (2009).
- ¹⁶⁷J. A. Schuller, T. Taubner, and M. L. Brongersma, "Optical antenna thermal emitters," *Nat. Photonics* **3**, 658–661 (2009).
- ¹⁶⁸I. Celanovic, D. Perreault, and J. Kassakian, "Resonant-cavity enhanced thermal emission," *Phys. Rev. B* **72**, 075127 (2005).
- ¹⁶⁹A. F. G. Jacobs, B. G. Heusinkveld, and S. M. Berkowicz, "Passive dew collection in a grassland area, The Netherlands," *Atmos. Res.* **87**, 377–385 (2008).

- ¹⁷⁰F. Trombe, "Perspectives sur l'utilisation des rayonnements solaires et terrestres dans certaines régions du monde," *Rev. Gen. Therm.* **6**, 1285 (1967).
- ¹⁷¹M. Muselli *et al.*, "Dew water collector for portable water in Ajaccio (Corsica Island, France)," *Atmos. Res.* **64**, 297–312 (2002).
- ¹⁷²B. Orel, M. K. Gunde, and A. Krainer, "Radiative cooling efficiency of white pigmented paints," *Sol. Energy* **50**, 477–482 (1993).
- ¹⁷³T. S. Eriksson, S.-J. Jiang, and C. G. Granqvist, "Surface coatings for radiative cooling applications: Silicon dioxide and silicon nitride made by reactive rf-sputtering," *Sol. Energy Mater.* **12**, 319–325 (1985).
- ¹⁷⁴T. S. Eriksson and C. G. Granqvist, "Infrared optical properties of electron-beam evaporated silicon oxynitride films," *Appl. Opt.* **22**, 3204–3206 (1983).
- ¹⁷⁵M. Diatezua, P. Thiry, and R. Caudano, "Characterization of silicon oxynitride multilayered systems for passive radiative cooling application," *Vacuum* **46**, 1121–1124 (1995).
- ¹⁷⁶T. S. Eriksson and C. G. Granqvist, "Infrared optical properties of silicon oxynitride films: Experimental data and theoretical interpretation," *J. Appl. Phys.* **60**, 2081–2091 (1986).
- ¹⁷⁷P. Grenier, "Réfrigération radiative. Effet de serre inverse," *Rev. Phys. Appl.* **14**, 87–90 (1979).
- ¹⁷⁸H. Miyazaki, K. Okada, K. Jinno, and T. Ota, "Fabrication of radiative cooling devices using Si₂N₂O nano-particles," *J. Ceram. Soc. Jpn.* **124**, 1185–1187 (2016).
- ¹⁷⁹H. Miyazaki, S. Yoshida, Y. Sato, H. Suzuki, and T. Ota, "Fabrication of radiative cooling materials based on Si₂N₂O particles by the nitridation of mixtures of silicon and silicon dioxide powders," *J. Ceram. Soc. Jpn.* **121**, 242–245 (2013).
- ¹⁸⁰C. N. Suryawanshi and C.-T. Lin, "Radiative cooling: Lattice quantization and surface emissivity in thin coatings," *ACS Appl. Mater. Interfaces* **1**, 1334–1338 (2009).
- ¹⁸¹E. A. Taft, "Characterization of silicon nitride films," *J. Electrochem. Soc.* **118**, 1341–1346 (1971).
- ¹⁸²T. Mouhib *et al.*, "Stainless steel/tin/glass coating as spectrally selective material for passive radiative cooling applications," *Opt. Mater.* **31**, 673–677 (2009).
- ¹⁸³A. Addeo *et al.*, "Selective covers for natural cooling devices," *Il Nuovo Cimento C* **1**, 419–429 (1978).
- ¹⁸⁴T. M. Nilsson and G. A. Niklasson, "Radiative cooling during the day: Simulations and experiments on pigmented polyethylene cover foils," *Sol. Energy Mater. Sol. Cells* **37**, 93–118 (1995).
- ¹⁸⁵B. Bhatia *et al.*, "Passive directional sub-ambient daytime radiative cooling," *Nat. Commun.* **9**, 5001 (2018).
- ¹⁸⁶N. N. Shi *et al.*, "Keeping cool: Enhanced optical reflection and radiative heat dissipation in Saharan silver ants," *Science* **349**, 298–301 (2015).
- ¹⁸⁷C. C. Tsai, N. Shi, J. Pelaez, N. Pierce, and N. Yu, "Butterflies regulate wing temperatures using radiative cooling," in *2017 Conference on Lasers and Electro-Optics (CLEO)* (2017), pp. 1–2.
- ¹⁸⁸N. N. Shi, C. C. Tsai, C. Craig, and N. Yu, "Nano-structured wild moth cocoon fibers as radiative cooling and waveguiding optical materials," in *2017 Conference on Lasers and Electro-Optics (CLEO)* (2017), pp. 1–2.
- ¹⁸⁹W. Li and S. Fan, "Nanophotonic control of thermal radiation for energy applications [invited]," *Opt. Express* **26**, 15995 (2018).
- ¹⁹⁰M. M. Hossain, B. Jia, and M. Gu, "A metamaterial emitter for highly efficient radiative cooling," *Adv. Opt. Mater.* **3**, 1047–1051 (2015).
- ¹⁹¹C. Zou *et al.*, "Metal-loaded dielectric resonator metasurfaces for radiative cooling," *Adv. Opt. Mater.* **5**, 1700460 (2017).
- ¹⁹²T. Liu and J. Takahara, "Ultrabroadband absorber based on single-sized embedded metal-dielectric-metal structures and application of radiative cooling," *Opt. Express* **25**, A612–A627 (2017).
- ¹⁹³D. Wu *et al.*, "The design of ultra-broadband selective near-perfect absorber based on photonic structures to achieve near-ideal daytime radiative cooling," *Mater. Des.* **139**, 104–111 (2018).
- ¹⁹⁴Z. Huang and X. Ruan, "Nanoparticle embedded double-layer coating for daytime radiative cooling," *Int. J. Heat Mass Transfer* **104**, 890–896 (2017).
- ¹⁹⁵Y. Zhai *et al.*, "Large scale random metamaterial for effective day-time radiative cooling," in *2017 Conference on Lasers and Electro-Optics (CLEO)* (2017), pp. 1–2.
- ¹⁹⁶R. Yang, X. Yin, G. Tan, D. Zhao, Y. Ma, and Y. Zhai, "Radiative cooling structures and systems," U.S. Patent No. US20170248381A1 (31 August 2017).
- ¹⁹⁷R. Y. M. Wong, C. Y. Tso, C. Y. H. Chao, B. Huang, and M. P. Wan, "Ultra-broadband asymmetric transmission metallic gratings for subtropical passive daytime radiative cooling," *Sol. Energy Mater. Sol. Cells* **186**, 330–339 (2018).
- ¹⁹⁸M. A. Kecebas, M. P. Menguc, A. Kosar, and K. Sendur, "Passive radiative cooling design with broadband optical thin-film filters," *J. Quant. Spectrosc. Radiat. Transfer* **198**, 179–186 (2017).
- ¹⁹⁹S. Atiganyanun *et al.*, "Effective radiative cooling by paint-format microsphere-based photonic random media," *ACS Photonics* **5**, 1181–1187 (2018).
- ²⁰⁰H. Kim and A. Lenert, "Optical and thermal filtering nanoporous materials for sub-ambient radiative cooling," *J. Opt.* **20**, 084002 (2018).
- ²⁰¹H. Yuan *et al.*, "Effective, angle-independent radiative cooler based on one-dimensional photonic crystal," *Opt. Express* **26**, 27885–27893 (2018).
- ²⁰²J. Kou, Z. Jurado, Z. Chen, S. Fan, and A. J. Minnich, "Daytime radiative cooling using near-black infrared emitters," *ACS Photonics* **4**, 626–630 (2017).
- ²⁰³P. Yang, C. Chen, and Z. M. Zhang, "A dual-layer structure with record-high solar reflectance for daytime radiative cooling," *Sol. Energy* **169**, 316–324 (2018).
- ²⁰⁴H. Bao *et al.*, "Double-layer nanoparticle-based coatings for efficient terrestrial radiative cooling," *Sol. Energy Mater. Sol. Cells* **168**, 78–84 (2017).
- ²⁰⁵Y. Lu *et al.*, "A universal route to realize radiative cooling and light management in photovoltaic modules," *Sol. RRL* **1**, 1700084 (2017).
- ²⁰⁶M. Santamouris and J. Feng, "Recent progress in daytime radiative cooling: Is it the air conditioner of the future?," *Buildings* **8**, 168 (2018).
- ²⁰⁷M. Ono, K. Chen, W. Li, and S. Fan, "Self-adaptive radiative cooling based on phase change materials," *Opt. Express* **26**, A777–A787 (2018).
- ²⁰⁸S.-R. Wu, K.-L. Lai, and C.-M. Wang, "Passive temperature control based on a phase change metasurface," *Sci. Rep.* **8**, 7684 (2018).
- ²⁰⁹A. Gentle *et al.*, "Design, control, and characterisation of switchable radiative cooling," in *New Concepts in Solar and Thermal Radiation Conversion and Reliability* (International Society for Optics and Photonics, 2018), Vol. 10759, p. 107590L.
- ²¹⁰G. McKay, "It's not rocket science #5: Night sky radiant cooling," in *Misfits' Architecture* (2013).
- ²¹¹G. Nebbia and G. N. Menozzi, "Early experiments on water desalination by freezing," *Desalination* **5**, 49–54 (1968).
- ²¹²L. Pérez-Lombard, J. Ortiz, and C. Pout, "A review on buildings energy consumption information," *Energy Build.* **40**, 394–398 (2008).
- ²¹³H. Zhao and F. Magoulès, "A review on the prediction of building energy consumption," *Renewable Sustainable Energy Rev.* **16**, 3586–3592 (2012).
- ²¹⁴U.S. Energy Information Administration (EIA) - Total Energy Monthly Data, <https://www.eia.gov/totalenergy/data/monthly/> for building cooling energy consumption data; 19 October 2018.
- ²¹⁵K. Nwaigwe, O. Anthony, N. Ogueke, and E. Anyanwu, "Review of nocturnal cooling systems," *Int. J. Energy Clean Environ.* **11**, 117–143 (2010).
- ²¹⁶R. Pacheco, J. Ordóñez, and G. Martínez, "Energy efficient design of building: A review," *Renewable Sustainable Energy Rev.* **16**, 3559–3573 (2012).
- ²¹⁷R. Kumar and S. C. Kaushik, "Performance evaluation of green roof and shading for thermal protection of buildings," *Build. Environ.* **40**, 1505–1511 (2005).
- ²¹⁸N. M. Nahar, P. Sharma, and M. M. Purohit, "Performance of different passive techniques for cooling of buildings in arid regions," *Build. Environ.* **38**, 109–116 (2003).
- ²¹⁹D. Asimakopoulos, *Passive Cooling of Buildings* (Routledge, 2013).
- ²²⁰G. B. Smith, A. R. Gentle, M. D. Arnold, M. A. Gali, and M. B. Cortie, "The importance of surface finish to energy performance," *Renewable Energy Environ. Sustainable* **2**, 13 (2017).
- ²²¹H. Akbari, S. Davis, S. Dorsano, J. Huang, and S. Winnett, *Cooling Our Communities. A Guidebook on Tree Planting and Light-Colored Surfacing* (US Environmental Protection Agency, 1992), p. 246.
- ²²²A. Synnefa, M. Santamouris, and K. Apostolakis, "On the development, optical properties and thermal performance of cool colored coatings for the urban environment," *Sol. Energy* **81**, 488–497 (2007).
- ²²³A. M. Rizwan, L. Y. C. Dennis, and C. Liu, "A review on the generation, determination and mitigation of Urban Heat Island," *J. Environ. Sci.* **20**, 120–128 (2008).
- ²²⁴M. Zinzi and S. Agnoli, "Cool and green roofs. An energy and comfort comparison between passive cooling and mitigation urban heat island techniques for residential buildings in the Mediterranean region," *Energy Build.* **55**, 66–76 (2012).

- ²²⁵M. Muselli, "Passive cooling for air-conditioning energy savings with new radiative low-cost coatings," *Energy Build.* **42**, 945–954 (2010).
- ²²⁶Cool Roof Rating Council, <http://coolroofs.org/> for introduction to The Cool Roof Rating Council; accessed 25 July 2018.
- ²²⁷A. R. Gentle, J. L. C. Aguilar, and G. B. Smith, "Optimized cool roofs: Integrating albedo and thermal emittance with R-value," *Sol. Energy Mater. Sol. Cells* **95**, 3207–3215 (2011).
- ²²⁸ASHRAE. *Advanced Energy Design Guide for Small to Medium Office Buildings: Achieving 50% Energy Savings toward a Net Zero Energy Building* (American Society of Heating, Refrigerating and Air-Conditioning Engineers, 2011).
- ²²⁹Find rated products - Cool Roof Rating Council, <https://coolroofs.org/directory> for searching commercial cool roof products; accessed 27 July 2018.
- ²³⁰GAF | United CoatingsTM KymaxTM Coating, <https://www.gaf.com/en-us/roofing-products/commercial-roofing-products/liquid-applied/roof-coatings/pvdf/united-coatings-kymax-coating> for information on United Coatings Kymax Coating product; accessed 25 October 2018.
- ²³¹Miracool, MIRACOOL high reflective coating product datasheet.
- ²³²The white roofing membrane that keeps the roof cool RENOLIT ALKORBRIGHT, <https://www.renolit.com/waterproofing-roofing/oc/products/renolit-alkorbright/> for information on Renolit Alkorbright Membrane product; accessed 25 October 2018.
- ²³³APOC® 256 Elastomeric One® PVDF Premium Fluropolymer Coating, <https://www.apoc.com/products/apoc-256-elastomeric-one-pvdf-premium-fluropolymer-coating> for APOC; accessed 25 October 2018.
- ²³⁴H. Akbari, P. Berdahl, R. Levinson, and S. Wiel, *Cool Color Roofing Materials* (Lawrence Berkeley National Laboratory, 2006), p. 73.
- ²³⁵H. Akbari, M. Pomerantz, and H. Taha, "Cool surfaces and shade trees to reduce energy use and improve air quality in urban areas," *Sol. Energy* **70**, 295–310 (2001).
- ²³⁶A. L. Pisello and F. Cotana, "The thermal effect of an innovative cool roof on residential buildings in Italy: Results from two years of continuous monitoring," *Energy Build.* **69**, 154–164 (2014).
- ²³⁷3MTM Enhanced Specular Reflector (3M ESR), https://www.3m.com/3M/en_US/company-us/all-3m-products/~/3M-Enhanced-Specular-Reflector-3M-ESR-/?N=5002385+3293061534&rt=rud for information on 3M ESR film; accessed 26 July 2018.
- ²³⁸Z. Zhang, S. Tong, and H. Yu, "Life cycle analysis of cool roof in tropical areas," *Procedia Eng.* **169**, 392–399 (2016).
- ²³⁹K. M. Al-Obaidi, M. Ismail, and A. M. Abdul Rahman, "Passive cooling techniques through reflective and radiative roofs in tropical houses in Southeast Asia: A literature review," *Front. Archit. Res.* **3**, 283–297 (2014).
- ²⁴⁰L. Zhu, A. Raman, and S. Fan, "Color-preserving daytime radiative cooling," *Appl. Phys. Lett.* **103**, 223902 (2013).
- ²⁴¹G. J. Lee, Y. J. Kim, H. M. Kim, Y. J. Yoo, and Y. M. Song, "Colored, daytime radiative coolers with thin-film resonators for aesthetic purposes," *Adv. Opt. Mater.* **6**, 1800707 (2018).
- ²⁴²J. Song *et al.*, "The effects of particle size distribution on the optical properties of titanium dioxide rutile pigments and their applications in cool non-white coatings," *Sol. Energy Mater. Sol. Cells* **130**, 42–50 (2014).
- ²⁴³W. Li, Y. Shi, Z. Chen, and S. Fan, "Photonic thermal management of coloured objects," *Nat. Commun.* **9**, 4240 (2018).
- ²⁴⁴S. E. Bretz and H. Akbari, "Long-term performance of high-albedo roof coatings," *Energy Build.* **25**, 159–167 (1997).
- ²⁴⁵H. Akbari *et al.*, "Aging and weathering of cool roofing membranes," Report No. LBNL-58055 (2005).
- ²⁴⁶K. W. Oleson, G. B. Bonan, and J. Feddema, "Effects of white roofs on urban temperature in a global climate model," *Geophys. Res. Lett.* **37**, L03701, <https://doi.org/10.1029/2009GL042194> (2010).
- ²⁴⁷Standard 90.1, <https://www.ashrae.org/technical-resources/bookstore/standard-90-1> for ASHRAE Standard 90.1-2016; accessed 26 September 2018.
- ²⁴⁸ASHRAE 90.2-2007, https://www.techstreet.com/standards/ashrae-90-2-2007?product_id=1509386 for ASHRAE Standard 90.2-2007; accessed 26th September 2018.
- ²⁴⁹Building Energy Efficiency Program - California Energy Commission, <https://www.energy.ca.gov/title24/> for introduction of building energy efficiency program; accessed 26 September 2018.
- ²⁵⁰LEED | USGBC, <https://new.usgbc.org/leed> for information on building rating system LEED; accessed 26 September 2018.
- ²⁵¹M. Fiorentini, P. Cooper, and Z. Ma, "Development and optimization of an innovative HVAC system with integrated PVT and PCM thermal storage for a net-zero energy retrofitted house," *Energy Build.* **94**, 21–32 (2015).
- ²⁵²H. S. Bagiorgas and G. Mihalakakou, "Experimental and theoretical investigation of a nocturnal radiator for space cooling," *Renewable Energy* **33**, 1220–1227 (2008).
- ²⁵³Z. Liu, H. Tam, and G. Ma, "Experimental investigation on night sky radiant cooling performance of duct-type heat exchanger," *Int. J. Vent.* **16**, 255–267 (2017).
- ²⁵⁴G. Mihalakakou, A. Ferrante, and J. O. Lewis, "The cooling potential of a metallic nocturnal radiator," *Energy Build.* **28**, 251–256 (1998).
- ²⁵⁵M. Al-Nimir, M. Tahat, and M. Al-Rashdan, "A night cold storage system enhanced by radiative cooling—a modified Australian cooling system," *Appl. Therm. Eng.* **19**, 1013–1026 (1999).
- ²⁵⁶J. Khedari, J. Waewsak, S. Thepa, and J. Hirunlabh, "Field investigation of night radiation cooling under tropical climate," *Renewable Energy* **20**, 183–193 (2000).
- ²⁵⁷D. Zhao *et al.*, "Development of a single-phase thermosiphon for cold collection and storage of radiative cooling," *Appl. Energy* **205**, 1260–1269 (2017).
- ²⁵⁸A. Hamza, H. Ali, I. M. S. Taha, and I. M. Ismail, "Cooling of water flowing through a night sky radiator," *Sol. Energy* **55**, 235–253 (1995).
- ²⁵⁹A. Zuazua-Ros, C. Martín Gómez, J. C. Ramos, and J. Bermejo-Busto, "Towards cooling systems integration in buildings: Experimental analysis of a heat dissipation panel," *Renewable Sustainable Energy Rev.* **72**, 73–82 (2017).
- ²⁶⁰J. A. F. Tevar, S. Castaño, A. G. Marijuán, M. R. Heras, and J. Pistono, "Modelling and experimental analysis of three radioconvective panels for night cooling," *Energy Build.* **107**, 37–48 (2015).
- ²⁶¹M. Hu, B. Zhao, J. Li, Y. Wang, and G. Pei, "Preliminary thermal analysis of a combined photovoltaic-photothermic-nocturnal radiative cooling system," *Energy* **137**, 419–430 (2017).
- ²⁶²Parker, D. S. Sherwin, J. R. Hermelink, A. H. Center, and F. S. E. NightCool, "A nocturnal radiation cooling concept," in *2008 ACEEE Summer Study Energy Efficiency in Buildings* (2008), pp. 209–222.
- ²⁶³NightSolar Air Cooling - from the makers of SolarWall, <http://solarwall.com/en/products/nightSolar-air-cooling.php> for introduction of NightSolar air cooling system accessed 29 September 2018.
- ²⁶⁴S. Ito and N. Miura, "Studies of radiative cooling systems for storing thermal energy," *J. Sol. Energy Eng.* **111**, 251–256 (1989).
- ²⁶⁵E. Erell and Y. Etzion, "A radiative cooling system using water as a heat exchange medium," *Archit. Sci. Rev.* **35**, 39–49 (1992).
- ²⁶⁶M. A. Al-Nimir, Z. Kodah, and B. Nassar, "A theoretical and experimental investigation of a radiative cooling system," *Sol. Energy* **63**, 367–373 (1998).
- ²⁶⁷E. Erell and Y. Etzion, "Radiative cooling of buildings with flat-plate solar collectors," *Build. Environ.* **35**, 297–305 (2000).
- ²⁶⁸A. Dimoudi and A. Androutsopoulos, "The cooling performance of a radiator based roof component," *Sol. Energy* **80**, 1039–1047 (2006).
- ²⁶⁹M. Farmahini Farahani and G. Heidarinejad, "Increasing effectiveness of evaporative cooling by pre-cooling using nocturnally stored water," *Appl. Therm. Eng.* **38**, 117–123 (2012).
- ²⁷⁰M. Farmahini Farahani, G. Heidarinejad, and S. Delfani, "A two-stage system of nocturnal radiative and indirect evaporative cooling for conditions in Tehran," *Energy Build.* **42**, 2131–2138 (2010).
- ²⁷¹A. H. H. Ali, "Desiccant enhanced nocturnal radiative cooling-solar collector system for air comfort application in hot arid areas," *Sustainable Energy Technol. Assess.* **1**, 54–62 (2013).
- ²⁷²C. Yong, W. Yiping, and Z. Li, "Performance analysis on a building-integrated solar heating and cooling panel," *Renewable Energy* **74**, 627–632 (2015).
- ²⁷³M. Matsuta, S. Terada, and H. Ito, "Solar heating and radiative cooling using a solar collector-sky radiator with a spectrally selective surface," *Sol. Energy* **39**, 183–186 (1987).
- ²⁷⁴Y. Man, H. Yang, J. D. Spitler, and Z. Fang, "Feasibility study on novel hybrid ground coupled heat pump system with nocturnal cooling radiator for cooling load dominated buildings," *Appl. Energy* **88**, 4160–4171 (2011).
- ²⁷⁵T. L. Bergman, "Active daytime radiative cooling using spectrally selective surfaces for air conditioning and refrigeration systems," *Sol. Energy* **174**, 16–23 (2018).

- ²⁷⁶W. Wang, N. Fernandez, S. Katipamula, and K. Alvine, "Performance assessment of a photonic radiative cooling system for office buildings," *Renewable Energy* **118**, 265–277 (2018).
- ²⁷⁷M. C. Yew *et al.*, "Integration of thermal insulation coating and moving-air-cavity in a cool roof system for attic temperature reduction," *Energy Convers. Manage.* **75**, 241–248 (2013).
- ²⁷⁸K. S. Ong, "Temperature reduction in attic and ceiling via insulation of several passive roof designs," *Energy Convers. Manage.* **52**, 2405–2411 (2011).
- ²⁷⁹B. F. Yu *et al.*, "Review of research on air-conditioning systems and indoor air quality control for human health," *Int. J. Refrig.* **32**, 3–20 (2009).
- ²⁸⁰S. Y. Jeong, C. Y. Tso, M. Zouaqui, Y. M. Wong, and C. Y. H. Chao, "A numerical study of daytime passive radiative coolers for space cooling in buildings," *Build. Simul.* **11**, 1011–1028 (2018).
- ²⁸¹T. Facius and B. Aircoil, in *CTI Sponsored Educational Program* (2011), p. 50.
- ²⁸²M. A. Green *et al.*, "Solar cell efficiency tables (version 50)," *Prog. Photovoltaic Res. Appl.* **25**, 668–676 (2017).
- ²⁸³A. Polman, M. Knight, E. C. Garnett, B. Ehrler, and W. C. Sinke, "Photovoltaic materials: Present efficiencies and future challenges," *Science* **352**, aad4424 (2016).
- ²⁸⁴J. Siecker, K. Kusakana, and B. P. Numbi, "A review of solar photovoltaic systems cooling technologies," *Renewable Sustainable Energy Rev.* **79**, 192–203 (2017).
- ²⁸⁵M. Abdolzadeh and M. Ameri, "Improving the effectiveness of a photovoltaic water pumping system by spraying water over the front of photovoltaic cells," *Renewable Energy* **34**, 91–96 (2009).
- ²⁸⁶H. Bahaidarah, A. Subhan, P. Gandhidasan, and S. Rehman, "Performance evaluation of a PV (photovoltaic) module by back surface water cooling for hot climatic conditions," *Energy* **59**, 445–453 (2013).
- ²⁸⁷E. Cuce, T. Bali, and S. A. Sekucoglu, "Effects of passive cooling on performance of silicon photovoltaic cells," *Int. J. Low-Carbon Technol.* **6**, 299–308 (2011).
- ²⁸⁸A. Akbarzadeh and T. Wadowski, "Heat pipe-based cooling systems for photovoltaic cells under concentrated solar radiation," *Appl. Therm. Eng.* **16**, 81–87 (1996).
- ²⁸⁹A. G. Lupu, V. M. Homutescu, D. T. Balanescu, and A. Popescu, "A review of solar photovoltaic systems cooling technologies," *IOP Conf. Ser. Mater. Sci. Eng.* **444**, 082016 (2018).
- ²⁹⁰M. J. Huang, P. C. Eames, B. Norton, and N. J. Hewitt, "Natural convection in an internally finned phase change material heat sink for the thermal management of photovoltaics," *Sol. Energy Mater. Sol. Cells* **95**, 1598–1603 (2011).
- ²⁹¹M. C. Browne, B. Norton, and S. J. McCormack, "Phase change materials for photovoltaic thermal management," *Renewable Sustainable Energy Rev.* **47**, 762–782 (2015).
- ²⁹²L. Zhu, A. Raman, K. X. Wang, M. A. Anoma, and S. Fan, "Radiative cooling of solar cells," *Optica* **1**, 32–38 (2014).
- ²⁹³T. S. Safi and J. N. Munday, "Improving photovoltaic performance through radiative cooling in both terrestrial and extraterrestrial environments," *Opt. Express* **23**, A1120–A1128 (2015).
- ²⁹⁴A. R. Gentle and G. B. Smith, "Is enhanced radiative cooling of solar cell modules worth pursuing?," *Sol. Energy Mater. Sol. Cells* **150**, 39–42 (2016).
- ²⁹⁵A. Riverola *et al.*, "Mid-infrared emissivity of crystalline silicon solar cells," *Sol. Energy Mater. Sol. Cells* **174**, 607–615 (2018).
- ²⁹⁶I. Subedi, T. J. Silverman, M. G. Deceglie, and N. J. Podraza, "Emissivity of solar cell cover glass calculated from infrared reflectance measurements," *Sol. Energy Mater. Sol. Cells* **190**, 98–102 (2019).
- ²⁹⁷K. Nishioka, Y. Ota, K. Tamura, and K. Araki, "Heat reduction of concentrator photovoltaic module using high radiation coating," *Surf. Coat. Technol.* **215**, 472–475 (2013).
- ²⁹⁸B. Zhao, M. Hu, X. Ao, and G. Pei, "Performance analysis of enhanced radiative cooling of solar cells based on a commercial silicon photovoltaic module," *Sol. Energy* **176**, 248–255 (2018).
- ²⁹⁹Y. Huang *et al.*, "Ultra-broadband large-scale infrared perfect absorber with optical transparency," *Appl. Phys. Express* **10**, 112601 (2017).
- ³⁰⁰X. Sun *et al.*, "Optics-based approach to thermal management of photovoltaics: Selective-spectral and radiative cooling," *IEEE J. Photovoltaics* **7**, 566–574 (2017).
- ³⁰¹R. Vaillon, O. Dupré, R. B. Cal, and M. Calaf, "Pathways for mitigating thermal losses in solar photovoltaics," *Sci. Rep.* **8**, 13163 (2018).
- ³⁰²Y. Tu, R. Wang, Y. Zhang, and J. Wang, "Progress and expectation of atmospheric water harvesting," *Joule* **2**, 1452–1475 (2018).
- ³⁰³J. Y. Wang, R. Z. Wang, L. W. Wang, and J. Y. Liu, "A high efficient semi-open system for fresh water production from atmosphere," *Energy* **138**, 542–551 (2017).
- ³⁰⁴Inner Earth May Hold More Water Than the Seas, https://news.nationalgeographic.com/news/2002/03/0307_0307_waterworld.html for information on water in the atmosphere; accessed 10 November 2017.
- ³⁰⁵M. Tomaszkiewicz, M. Abou Najm, D. Beysens, I. Alameddine, and M. El-Fadel, "Dew as a sustainable non-conventional water resource: A critical review," *Environ. Rev.* **23**, 425–442 (2015).
- ³⁰⁶B. Khalil *et al.*, "A review: Dew water collection from radiative passive collectors to recent developments of active collectors," *Sustainable Water Resour. Manage.* **2**, 71–86 (2016).
- ³⁰⁷Y. D. Tu, R. Z. Wang, T. S. Ge, and X. Zheng, "Comfortable, high-efficiency heat pump with desiccant-coated, water-sorbing heat exchangers," *Sci. Rep.* **7**, 40437 (2017).
- ³⁰⁸Y. Liu and R. Wang, "Pore structure of new composite adsorbent $\text{SiO}_2 \cdot \text{xH}_2\text{O} \cdot \text{yCaC}_{12}$ with high uptake of water from air," *Sci. China Ser. E Technol. Sci.* **46**, 551–559 (2003).
- ³⁰⁹X. Zheng, T. S. Ge, and R. Z. Wang, "Recent progress on desiccant materials for solid desiccant cooling systems," *Energy* **74**, 280–294 (2014).
- ³¹⁰D. Bergmair, S. J. Metz, H. C. de Lange, and A. van Steenhoven, "A System analysis of membrane facilitated water generation from air humidity," *Desalination* **339**, 26–33 (2014).
- ³¹¹I. Gindel, "Irrigation of plants with atmospheric water within the desert," *Nature* **207**, 1173–1175 (1965).
- ³¹²D. Beysens *et al.*, "Application of passive radiative cooling for dew condensation," *Energy* **31**, 2303–2315 (2006).
- ³¹³M. Muselli, D. Beysens, M. Mileta, and I. Milimouk, "Dew and rain water collection in the Dalmatian Coast, Croatia," *Atmos. Res.* **92**, 455–463 (2009).
- ³¹⁴M. Muselli, D. Beysens, and I. Milimouk, "A comparative study of two large radiative dew water condensers," *J. Arid Environ.* **64**, 54–76 (2006).
- ³¹⁵D. Beysens, I. Milimouk, V. Nikolayev, M. Muselli, and J. Marcillat, "Using radiative cooling to condense atmospheric vapor: A study to improve water yield," *J. Hydrol.* **276**, 1–11 (2003).
- ³¹⁶S. M. Berkowicz *et al.*, "Urban dew collection under Semi-arid conditions: Jerusalem," in *Proceedings of the Third International Conference on Fog, Fog Collection and Dew* (2004).
- ³¹⁷T. Nilsson, "Initial experiments on dew collection in Sweden and Tanzania," *Sol. Energy Mater. Sol. Cells* **40**, 23–32 (1996).
- ³¹⁸P. Gandhidasan and H. I. Abualhamayel, "Modeling and testing of a dew collection system," *Desalination* **180**, 47–51 (2005).
- ³¹⁹T. M. J. Nilsson, W. E. Vargas, G. A. Niklasson, and C. G. Granqvist, "Condensation of water by radiative cooling," *Renewable Energy* **5**, 310–317 (1994).
- ³²⁰I. Lekouch *et al.*, "Rooftop dew, fog and rain collection in southwest Morocco and predictive dew modeling using neural networks," *J. Hydrol.* **448–449**, 60–72 (2012).
- ³²¹M. T. H. v. Vliet, D. Wiberg, S. Leduc, and K. Riahi, "Power-generation system vulnerability and adaptation to changes in climate and water resources," *Nat. Clim. Change* **6**, 375–380 (2016).
- ³²²M. Zeyghami and F. Khalili, "Performance improvement of dry cooled advanced concentrating solar power plants using daytime radiative cooling," *Energy Convers. Manage.* **106**, 10–20 (2015).
- ³²³I. A. Olwi, J. A. Sabbagh, and A. M. A. Khalifa, "Mathematical modeling of passive dry cooling for power plants in arid land," *Sol. Energy* **48**, 279–286 (1992).
- ³²⁴J. A. Sabbagh, A. M. A. Khalifa, and I. A. Olwi, "Development of passive dry cooling system for power plants in arid land," *Sol. Energy* **51**, 431–447 (1993).
- ³²⁵K. Zhang *et al.*, "Modelling study of the low-pump-power demand constructal T-shaped pipe network for a large scale radiative cooled cold storage system," *Appl. Therm. Eng.* **127**, 1564–1573 (2017).
- ³²⁶C. I. Ezekwe, "Performance of a heat pipe assisted night sky radiative cooler," *Energy Convers. Manage.* **30**, 403–408 (1990).

- ³²⁷O. M. Haddad, M. A. Al-Nimr, and A. Maqableh, "Enhanced solar still performance using a radiative cooling system," *Renewable Energy* **21**, 459–469 (2000).
- ³²⁸E. Mu *et al.*, "A novel self-powering ultrathin TEG device based on micro/nano emitter for radiative cooling," *Nano Energy* **55**, 494–500 (2019).
- ³²⁹P.-C. Hsu *et al.*, "Personal thermal management by metallic nanowire-coated textile," *Nano Lett.* **15**, 365–371 (2015).
- ³³⁰P.-C. Hsu *et al.*, "Radiative human body cooling by nanoporous polyethylene textile," *Science* **353**, 1019–1023 (2016).
- ³³¹Y. Peng *et al.*, "Nanoporous polyethylene microfibres for large-scale radiative cooling fabric," *Nat. Sustainable* **1**, 105 (2018).
- ³³²T. Ming, R. de_Richter, W. Liu, and S. Caillol, "Fighting global warming by climate engineering: Is the Earth radiation management and the solar radiation management any option for fighting climate change?," *Renewable Sustainable Energy Rev.* **31**, 792–834 (2014).